UCRL-17472

University of California

Ernest O. Lawrence Radiation Laboratory

NUCLEAR SPIN AND HYPERFINE STRUCTURE MEASUREMENTS ON THE RADIOACTIVE ISOTOPES ^{110}In, ^{121}Sn, AND ^{88}Rb

TWO-WEEK LOAN COPY

This is a Library Circulating Copy which may be borrowed for two weeks. For a personal retention copy, call Tech. Info. Division, Ext. 5545

Berkeley, California

DISCLAIMER

This document was prepared as an account of work sponsored by the United States Government. While this document is believed to contain correct information, neither the United States Government nor any agency thereof, nor the Regents of the University of California, nor any of their employees, makes any warranty, express or implied, or assumes any legal responsibility for the accuracy, completeness, or usefulness of any information, apparatus, product, or process disclosed, or represents that its use would not infringe privately owned rights. Reference herein to any specific commercial product, process, or service by its trade name, trademark, manufacturer, or otherwise, does not necessarily constitute or imply its endorsement, recommendation, or favoring by the United States Government or any agency thereof, or the Regents of the University of California. The views and opinions of authors expressed herein do not necessarily state or reflect those of the United States Government or any agency thereof or the Regents of the University of California.

UCRL-17472

UNIVERSITY OF CALIFORNIA

Lawrence Radiation Laboratory
Berkeley, California

AEC Contract No. W-7405-eng-48

NUCLEAR SPIN AND HYPERFINE STRUCTURE MEASUREMENTS ON THE RADIOACTIVE ISOTOPES ^{110}In, ^{121}Sn, AND ^{88}Rb

Michael Herbert Prior

(Ph. D. Thesis)

March 25, 1967

Contents

Abstract v
I. Atomic Theory 1
II. The Hyperfine-Structure Interaction
A. First-Order Theory 5
B. Evaluation of Electronic Matrix Elements 11
C. J-Mixing Corrections to hfs 13
D. Effect of an External Magnetic Field 14
E. Relativistic Effects on hfs 18
III. Nuclear Theory 21
IV. The Atomic Beam Method 30
V. Research on ^{110}In
A. Production of the Isotope 37
B. Formation of the Atomic Beam 39
C. Measurement and Results 40
D. Interpretation of Results 48
VI. Research on ^{121}Sn
A. Production of the Isotope 49
B. Properties of the Atomic Beam 49
C. Spin Measurement 50
D. hfs Measurements and Results 52
E. Origin of the a Constant 70
F. J-Mixing Corrections to the hfs Constants . . . 72
G. The Nuclear Quadrupole Moment 72
H. Interpretation of the Nuclear Spin and Moments . . 73
VII. Research on ^{88}Rb
A. Production of the Isotope 75
B. Formation of the Atomic Beam 77
C. hfs Measurements and Results 77
D. Interpretation of the Nuclear Magnetic Moment . . 83
Acknowledgments 85
Appendices 86
1. Relativistic Correction Factors 86
2. Constants Used in Analysis of Measurements 88
References 89

NUCLEAR SPIN AND HYPERFINE STRUCTURE MEASUREMENTS ON THE RADIOACTIVE ISOTOPES ^{110}In, ^{121}Sn, AND ^{88}Rb

Michael Herbert Prior

Lawrence Radiation Laboratory
University of California
Berkeley, California

March 25, 1967

ABSTRACT

The atomic-beam magnetic-resonance technique has been used to measure the nuclear spin of 66 min ^{110}In, the spin and hyperfine structure interaction constants a and b for 27 hr ^{121}Sn in the $^3P_1$ electronic state, and the a constant for 18 min ^{88}Rb (I = 2). Values of the nuclear moments are inferred from the measured interaction constants. The results are:

Isotope	Spin, hfs constants	Moments	χ^2	Number of observations
^{110}In	I = 2			3
^{121}Sn	I = 3/2			
	a = + 128.726(8) MHz b = + 32.373(12) MHz	μ_I = - 0.699(7) nm Q = + 0.08(4) barn	4.72	32
	a = - 128.726(8) MHz b = - 32.374(12) MHz	μ_I = + 0.699(7) nm Q = - 0.08(4) barn	4.06	32
^{88}Rb	a = + 474.432(6) MHz	μ_I = + 0.506(5) nm	1.00	14
	a = - 474.432(6) MHz	μ_I = - 0.506(5) nm	2.50	14

The χ^2 of the least-squares computer fit to the observations is listed for the two possible signs of the interaction constants. The figures in parentheses represent the error in the last figure quoted. For the hfs constants this is one standard deviation from the computer mean. For μ_I the error is 1% to allow for effects of a possible hyperfine structure anomaly. For Q the error is 50% to allow for inaccuracies in the calculation of $\langle r^{-3} \rangle$ and the effects of Sternheimer shielding.

A relativistic calculation accounts for $\approx 1/3$ of the a for ^{121}Sn and the remainder is attributed to the effects of configuration interaction. Second-order corrections to the hfs constants are shown to be negligible for ^{121}Sn.

The nuclear quantities, except for Q, are in reasonable agreement with values calculated by using the shell model with an appropriate residual interaction, provided one takes the negative sign for the interaction constants. The quadrupole moment of ^{121}Sn may arise from polarization of the proton core.

I. ATOMIC THEORY

The electronic state of an atom can be represented to a very good approximation as a solution to the Schrödinger equation,

$$\mathcal{H}\psi = E\psi,$$

where E is the energy of state ψ and $\mathcal{H}$ is the atomic Hamiltonian. This Hamiltonian can be written as the sum of a number of parts,

$$\mathcal{H} = \mathcal{H}_0 + \mathcal{H}_1 + \mathcal{H}_{fs} + \mathcal{H}_{hfs} . \tag{I. 1}$$

The first three of the above have the form[1]

$$\mathcal{H}_0 = \sum_i \left[\frac{p_i^2}{2m} + U(r_i) \right], \tag{I. 2a}$$

$$\mathcal{H}_1 = - \sum_i \left[\frac{Ze^2}{r_i} + U(r_i) \right] + \sum_{i>j} \frac{e^2}{r_{ij}}, \tag{I. 2b}$$

$$\mathcal{H}_{fs} = \sum_i \xi(r_i)\, \bar{l}_i \cdot \bar{s}_i . \tag{I. 2c}$$

In $\mathcal{H}$ each term contributes to the atomic energy E an amount which is less than or approximately equal to the term on its left. That is,

$$E_0 > E_1 \gtrapprox E_{fs} > E_{hfs} .$$

The major portion of this work concerns the form and effect of the smallest term $\mathcal{H}_{hfs}$. Before entering into a detailed discussion of $\mathcal{H}_{hfs}$, however, a brief examination of the larger terms is in order.

The term $\mathcal{H}_0$ includes the kinetic energy of the electrons and their interaction with some general spherical potential $U(r_i)$. Because $U(r_i)$ is spherical and depends only on the coordinates of one electron, the orbital angular momentum quantum number l for each electron is a constant of the motion, as is the principal quantum number n, which determines the energy of a single electronic state. Thus the state of the entire atom can be specified by listing the n's and l's of all the electrons. Such a listing is called a configuration; for each configuration the total energy of the atom is different. The Pauli exclusion principle and the fact that electrons have spin $s = 1/2$ limit to $2l+2$ the number of electrons with the same nl. All states of different total

orbital L and total spin S angular momenta arising from the same configuration have the same energy E_0.

The term $\mathcal{H}_1$ removes the L, S degeneracy of the configurations. The first portion of $\mathcal{H}_1$ merely shifts the level of a configuration, but the second part, which represents the electrostatic repulsion of the electrons, splits the configuration into a number of different levels which are eigenfunctions of total spin and orbital angular momentum. These different levels, characterized by their values of L and S, are called terms.

The fine-structure Hamiltonian, $\mathcal{H}_{fs}$, is not diagonal with respect to eigenfunctions of $\overline{L}^2$ and $\overline{S}^2$, but is diagonal with respect to eigenfunctions of $\overline{J}^2$, where $\overline{J} = \overline{L} + \overline{S}$ is the total electronic angular momentum operator. Thus each term which is (2L+1)(2S+1)-fold degenerate breaks up under the influence of $\mathcal{H}_{fs}$ into a further set of levels which can be characterized by their eigenvalues of $\overline{J}^2$. These levels are termed multiplets and are (2J+1)-fold degenerate.

Finally, the $\mathcal{H}_{hfs}$ Hamiltonian, as is discussed later in more detail, couples the nuclear spin $\overline{I}$ to the electronic angular momentum $\overline{J}$ to split each multiplet into a number of hyperfine-structure levels characterized by different eigenvalues of $\overline{F}^2$, where $\overline{F}$ is the total atomic angular momentum $\overline{F} = \overline{I} + \overline{J}$. Figure I-1 shows in schematic form how a single configuration is affected by each of the terms in $\mathcal{H}$.

It should be emphasized that the action of each term in $\mathcal{H}$ is such as to reduce further the number of good quantum numbers available to describe a state. Thus, even though one often describes a given hyperfine level, F, as belonging to the J multiplet of the LS term of the nl^k configuration, it is not strictly true that J, L, S, **n**, and l are all quantum numbers of the system. In fact, for the complete Hamiltonian $\mathcal{H}$ the only good quantum numbers are F and the energy E. Thus the operator e^2/r_{12} in $\mathcal{H}_1$ can mix different configurations n_1l_1 and n_2l_2 provided they have the same parity. The operator $\mathcal{H}_{fs}$ can mix terms of different S and L provided ΔS, $\Delta L = 0, \pm 1$; and $\mathcal{H}_{hfs}$ can mix multiplets differing in J by $\Delta J = 0, \pm 1$. However, as is often the case, each term in $\mathcal{H}$ contributes to E_0 a small amount compared with those terms to its left in Eq. I.1, and it is then possible

to treat a given term in $\mathcal{H}$ as a small perturbation. This perturbation approximation is what is depicted schematically in Fig. I.1. This approach is particularly valid for light elements ($Z \lesssim 50$), where typically one has

$$E_0 \approx 10 \text{ eV},$$

$$E_1 \approx 1 \text{ eV},$$

$$E_{fs} \approx 0.05 \text{ eV},$$

$$E_{hfs} \approx 0.00005 \text{ eV}.$$

For heavier elements ($Z \gtrsim 50$) E_{fs} often becomes an appreciable fraction of E_1, and in this case one must consider the possibility of LS mixing by $\mathcal{H}_{fs}$. Such mixing may be made apparent by large deviations of the atomic g factor, g_J, from the value predicted for a pure LS state.

Despite the smallness of E_{hfs}, the high-precision radio-frequency atomic resonance experiments sometimes detect the effects of the mixing of different J states by $\mathcal{H}_{hfs}$. The effects of this J mixing on the hfs energy levels are considered in more detail later.

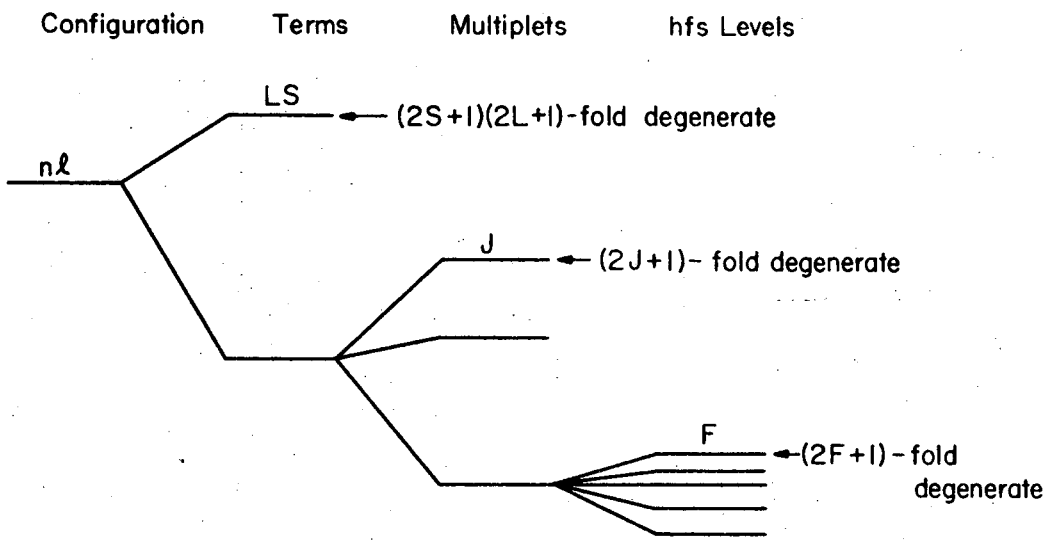

$$\mathcal{H}_0 = \sum_i \left[\frac{p_i^2}{2m} + U(r_i)\right] \qquad \mathcal{H}_1 = -\sum_i \left[\frac{Ze^2}{r_i} + U(r_i)\right] + \sum_{i>j} \frac{e^2}{r_{ij}} \qquad \mathcal{H}_{fs} = \sum_i \xi(r_i)\,\underline{\ell}_i \cdot \underline{s}_i \qquad \mathcal{H}_{hfs}$$

MU-32345

Fig. I-1. The effect of the inclusion of different terms in the atomic Hamiltonian.

II. THE HYPERFINE-STRUCTURE INTERACTION

A. First-Order Theory

Classically, the hyperfine-structure interaction (hfs) between the nucleus and the atomic electrons may be written as the interaction between the nuclear and electronic charge and current distributions. That is,

$$E_{hfs} = \left[\int d\tau_n \int d\tau_e \frac{\rho_n \rho_e}{r_{ne}} - Ze \int d\tau_e \frac{\rho_e}{r_e}\right] + \left[-\frac{1}{2c^2}\int d\tau_n \int d\tau_e \frac{\bar{j}_n \cdot \bar{j}_e}{r_{ne}}\right], \tag{II.1}$$

$$E_{hfs} = E_E + E_M ,$$

where E_{hfs} is the hfs energy; ρ_n, $\bar{j}_n$ and ρ_e, $\bar{j}_e$ are the nuclear and electronic charge and current densities separated in distance by r_{ne}; and $d\tau_n$, $d\tau_e$ are differential elements of nuclear and electronic volume. The second term in E_E is the large interaction of the electrons with the central potential due to a point nucleus of charge Ze; it is included in the first term and so must be subtracted to leave only the small hfs energy.

It is convenient to modify the form of the third term of Eq. II.1 by introducing the nuclear and electronic magnetizations $\bar{M}_n$ and $\bar{M}_e$ so that

$$\bar{j}_{n,e} = \bar{\nabla} \times \bar{M}_{n,e} .$$

This can be done because the two charge distributions do not depend on time, and hence by the equation of continuity, one has

$$\bar{\nabla} \cdot \bar{j}_{n,e} = -\frac{\partial \rho_{n,e}}{\partial t} = 0 .$$

Substituting for $\bar{j}_n$ and $\bar{j}_e$ and performing some transformations with the aid of the theorems of vector calculus and the fact that $\bar{M}_n$ and $\bar{M}_e$ vanish at infinity, one obtains

$$E_M = \frac{1}{c^2}\int d\tau_n \int d\tau_e \frac{(\bar{\nabla} \cdot \bar{M}_n)(\bar{\nabla} \cdot \bar{M}_e)}{r_{ne}} - \frac{4\pi}{c^2}\int d\tau_n \, \bar{M}_n \cdot \bar{M}_e .$$

One may now make the substitution

$$\frac{1}{r_{ne}} = \sum_k \frac{r_<^k}{r_>^{k+1}} \; C^k(n) \cdot C^k(e) \; ,$$

where $r_<$ and $r_>$ are the lesser and greater of r_n and r_e and the C^k are tensor operators of rank k related to the spherical harmonics Y_{kq} by

$$C_q^k = \sqrt{\frac{4\pi}{2k+1}} \; Y_{kq} \; .$$

The quantity $C^k \cdot C^k$ is the tensor dot product,

$$C^k \cdot C^k = \sum_q (-1)^q \, C_{-q}^k \, C_q^k \; ;$$

it will not be distinguished from the normal vector dot product, as the context in which the dot symbol appears usually indicates whether the quantities are to be treated as spherical tensors or Cartesian vectors. Thus one has

$$E_E = \sum_{k=1} \int d\tau_n \int d\tau_e \; \rho_n \rho_e \; \frac{r_<^k}{r_>^{k+1}} \; C^k(n) \cdot C^k(e) \; ,$$

$$E_M = \sum_{k=1} \frac{1}{c^2} \int d\tau_n \int d\tau_e \; (\nabla \cdot M_n)\,(\nabla \cdot M_e) \; \frac{r_<^k}{r_>^{k+1}} \; C^k(n) \cdot C^k(e)$$

$$- \frac{4\pi}{c^2} \int d\tau_n \; \overline{M}_n \cdot \overline{M}_e \; .$$

The important point about these two expressions is that they are of the general form

$$E_{hfs} = \sum_k T^k(n) \cdot T^k(e) \; , \qquad \text{(II.2)}$$

where $T^k(n)$ and $T^k(e)$ are tensor operators of rank k operating on the nuclear and electronic coordinates respectively. Because the hfs interaction may be written in this form, one may apply the powerful techniques of tensor calculus, developed first by Racah, for the evaluation of matrix elements of such operators. Before doing so, however, one must make the transformation to quantum mechanics by substituting

the appropriate operators for ρ and $\bar{M}$ in order to make explicit the form of the T^k.

Schwartz[2] has shown that the correct quantum mechanical expressions for the T^k are, for the electric terms,

$$T^k(n) = e\sum g_l \, r^k \, C^k(n) \, ,$$
$$T^k(e) = e\sum g_l \, \frac{C^k(e)}{r^{k+1}} \, , \qquad \text{(II.3)}$$

and for the magnetic terms,

$$T^k(n) = \mu_N \sum (\bar{\nabla} \, r^k \, C^k(n) \cdot \left(\frac{-2}{k} \, g_l \, \bar{l} + g_s \bar{s} \right) \, ,$$
$$T^k(e) = \mu_0 \sum \left[\bar{\nabla} \, r^{-k-1} \, C^k(e) \right] \cdot \left[\frac{2}{k+1} \, g_l \, \bar{l} + g_s \bar{s} \right] . \qquad \text{(II.4)}$$

Here $\bar{l}$ and $\bar{s}$ are the orbital and spin angular momentum operators and g_l and g_s are the orbital and spin g factors ($g_l = -1$ for an electron, $+1$ for a proton, 0 for a neutron); μ_0 and μ_N are the Bohr and nuclear magnetons $e\hbar/2m_e c$ and $e\hbar/2M_p c$.

It should be pointed out that these formulas were derived under the assumption that there is no overlap of the electronic and nuclear wave functions. This is not the case for an electron in an s state ($l = 0$), and the magnetic dipole ($k = 1$) tensors must be modified to

$$T^1(n) = -\frac{\mu_I}{I} \, \bar{I} \, , \qquad T^1(e) = \frac{8\pi}{3} \, \mu_0 \sum_s g_s \, \bar{s} \, \psi^2(0) \, . \qquad \text{(II.5)}$$

The summation $\sum_s$ extends only over s electrons, and $\psi^2(0)$ is the square of the electron's wave function at the origin. This form includes the assumption that the nucleus is a point with angular momentum $\bar{I}$ and magnetic moment μ_I. That the nucleus is not strictly a point magnetic dipole accounts for the fact that for different isotopes of the same element the magnetic dipole interaction is not exactly proportional to the nuclear magnetic moment. The extent to which this proportionality between two isotopes is not preserved is measured by the so-called hfs anomaly Δ. This quantity is largest for atoms with unpaired s electrons, and is rarely larger than an effective 1% change in the nuclear magnetic moment.

Putting aside for the moment the evaluation of the T^k, one can see that the noncentral nature of the hfs interaction will lead to a coupling of the nuclear and electronic angular moment I and J to a resultant total angular momentum F of the entire atom. Thus to the extent that the hfs mixes nuclear states of different I and electronic states of different J, I and J are no longer good quantum numbers. In the nucleus, states of differing I are separated in energy by thousands to millions of electron volts, and hence are little mixed by the hfs, which rarely exceeds 2×10^{-4} electron volt ($1.7\ \mathrm{cm}^{-1}$). On the other hand, electronic states of differing J separated by $1000\ \mathrm{cm}^{-1}$ (0.12 eV) can be measurably mixed by a normal hfs of $0.033\ \mathrm{cm}^{-1}$ (4.1×10^{-6} eV). This corresponds to a shift in energy of one part in 10^6 easily within reach of the atomic beam magnetic resonance technique, which can measure energy differences to one part in 10^8 or 10^9. Nonetheless, the J mixing effect is small albeit measurable in some cases, and it is for most purposes sufficient to calculate the first-order hfs energy for a state $|\,I\ J\ F\rangle$, though one must remember that higher-order corrections may be necessary. The first-order hfs energy is then

$$E_{hfs} = \sum_k \langle\, I\ J\ F \,|\, T(e)^k \cdot T(n)^k \,|\, I\ J\ F \,\rangle\ . \qquad \text{(II.6)}$$

By use of a theorem from tensor calculus,[1] the F dependence may be separated out to yield

$$E_{hfs} = \sum_k (-1)^{I+J+F} \begin{Bmatrix} I & J & F \\ J & I & k \end{Bmatrix} (J\,||\,T(e)^k\,||\,J)\ (I\,||\,T(n)^k\,||\,I)\ . \qquad \text{(II.7)}$$

Inspection of the explicit forms of the T^k shows that the magnetic tensors have parity $(-1)^{k-1}$ and the electric tensors $(-1)^k$. Since the nuclear and electronic states are to a very good approximation, states of definite parity, contributions to E_{hfs} from even magnetic and odd electric tensors must vanish. Henceforth terms with k odd will be understood to be magnetic and those with k even electric. Furthermore the 6-j symbol vanishes unless k is less than or equal to the lesser of 2I or 2J. Thus, one has 2(min I, J) terms in $E_{hfs}(F)$ and the same number of independent energy intervals $E_{hfs}(F) - E_{hfs}(F')$. Hence measurement of all the hfs intervals should allow determination of all the terms in

Eq. II.7. For the work to be treated here only the terms with $k = 1$ and $k = 2$ need be considered.

The double-barred quantities in Eq. II.7 are the so-called reduced matrix elements, and may be evaluated by using the Wigner-Eckart theorem of tensor calculus,[1]

$$\langle J\, M_J \mid T_q^k \mid J\, M_J \rangle = (-1)^{J-M_J} \begin{pmatrix} J & k & J \\ -M_J & q & M_J \end{pmatrix} (J \| T^k \| J). \quad \text{(II.8)}$$

This is an important theorem because it shows that the matrix elements of any two tensors of the same rank operating on the same system are proportional to each other. Thus $T^1(e)$ may be written as

$$T^1(e) = \frac{-H_e \bar{J}}{J},$$

where H_e is determined from

$$H_e = -J \frac{(J \| T^1(e) \| J)}{(J \| \bar{J} \| J)}. \quad \text{(II.9)}$$

Similarly, $T^1(n)$ may be written as

$$T^1(n) = \frac{\mu_I}{I} \bar{I},$$

with

$$\mu_I = I \frac{(I \| T^1(n) \| I)}{(I \| \bar{I} \| I)}. \quad \text{(II.10)}$$

For $k = 2$ one can proceed in a similar manner to write

$$T^2(n) = t_n K^2,$$
$$T^2(e) = t_e P^2,$$

where K^2 and P^2 are second-rank tensors made up from components of the nuclear and electronic angular momenta $\mathbf{I}$ and $\mathbf{J}$ respectively; that is,

$$K_0^2 = \frac{1}{2}\left[3I_z^2 - I(I+1)\right],$$

$$K_{\pm 1}^2 = \mp \left(\frac{3}{8}\right)^{1/2} (I_z I_\pm + I_\pm I_z),$$

$$K_{\pm 2}^2 = \left(\frac{3}{8}\right)^{1/2} I_\pm^2,$$

$$I_\pm = \mp \frac{I_x \pm i I_y}{\sqrt{2}},$$

with a similar expression for P^2 in terms of J. The t_n and t_e are constants of proportionality easily determined from

$$\langle II \mid T_0^2(n) \mid II \rangle = t_n \langle II \mid K_0^2 \mid II \rangle$$

and

$$\langle JJ \mid T_0^2(e) \mid JJ \rangle = t_e \langle JJ \mid P_0^2 \mid JJ \rangle .$$

For the nuclear part it is customary to define

$$Q = 2 \langle II \mid r^2 C_0^2(n) \mid II \rangle \tag{II.11}$$

where Q is the nuclear quadrupole moment. Thus

$$t_n = \frac{eQ}{2I(2I-1)} .$$

For the electronic part the customary definition is

$$q_J = \langle JJ \mid T_0^2(e) \mid JJ \rangle \tag{II.12}$$

q_J is a measure of the electric field gradient at the nucleus due to the electrons. Then t_e is

$$t_e = \frac{g_J}{J(2J-1)} .$$

It is customary to define the hfs magnetic dipole and electric quadrupole constants a and b as

$$a = -\frac{\mu_I H_e}{h I J} , \tag{II.13}$$

$$b = \frac{e Q q_J}{h} . \tag{II.14}$$

The constants are normally expressed in units of 1 MHz (10^6 cps). Thus the effective hfs Hamiltonian including k = 1 and k = 2 terms is

$$\mathcal{H}(\text{hfs}) = ha\, \bar{I} \cdot \bar{J} + \frac{hb}{2I(2I-1)\, J(2J-1)} \left[3(\bar{I} \cdot \bar{J})^2 + \frac{3}{2}(\bar{I} \cdot \bar{J}) - I(I+1)J(J+1) \right] . \tag{II. 15}$$

Because $\mathcal{H}(\text{hfs})$ is diagonal in F it is easy to calculate the hfs energies $E_{hfs}(F)$; one simply substitutes $\bar{I} \cdot \bar{J} = \left[F(F+1) - I(I+1) - J(J+1) \right]/2$.

B. Evaluation of the Electronic Matrix Elements

To determine the nuclear quantities μ_I and Q from the measured hfs constants a and b it is necessary to evaluate H_e and q_J in terms of the electronic wave functions. For H_e one has Eq. II.9,

$$H_e = \frac{-J\,(J \,||\, T^1(e) \,||\, J)}{(J \,||\, \bar{J} \,||\, J)} .$$

Using Eq. II.8, it is easy to show

$$(J \,||\, \bar{J} \,||\, J) = [\,J(J+1)\,(2J+1)\,]^{1/2} .$$

From Eqs. II.4 and II.5 one has

$$T^1(e) = \mu_0 \sum_{ns} \left[\bar{\nabla}\, r^{-2}\, C^1(e)\right] \cdot \left[-2g_l\, \bar{l} + g_s\, \bar{s}\right] + \frac{8\pi}{3}\, \mu_0 \sum_s g_s\, \bar{s}\, \psi^2(0),$$

where ns and s indicate summation over non-s and s electrons. Because $C^1 = \frac{\bar{r}}{r}$, $T^1(e)$ may be written as

$$T^1(e) = 2\mu_0 \sum_{ns} (r^{-3}) \left[\bar{l} - \bar{s} + \frac{3(\bar{s}\cdot\bar{r})\bar{r}}{r^2}\right] - \frac{16\pi}{3}\, \mu_0 \sum_s \bar{s}\, \psi^2(0), \tag{II.16}$$

where g_s and g_l have been replaced by -2 and -1.

To facilitate calculation of matrix elements, $T^1(e)$ must be written as the sum of tensor operators which transform under rotations as do the spherical harmonics. All terms in $T^1(e)$ are first-rank tensors (vectors), but the third term is not in the appropriate tensor form. With some manipulation, using the coupling rules[1] for the C^k, one can rewrite the third term as

$$3\,\frac{(\bar{s}\cdot\bar{r})\,\bar{r}}{r^2} = \bar{s} - (10)^{1/2}\,(\bar{s}\, C^2)^1 ,$$

so that $T^1(e)$ becomes

$$T^1(e) = 2\,\mu_0 \sum_{ns} (r^{-3}) \left[\bar{l} - (10)^{1/2}\,(\bar{s}\, C^2)^1\right] - \frac{16\pi}{3} \sum_s \bar{s}\, \psi^2(0) . \tag{II.17}$$

For the quadrupole constant q_J one must evaluate the matrix element $\langle JJ \,|\, T^2_0(e) \,|\, JJ \rangle$. Using the Wigner-Eckart theorem II.8 and the explicit form for $T^2_0(e)$,

$$T_0^2(e) = e \sum g_l \frac{C_0^2(e)}{r^3} ,$$

one obtains

$$q_J = - e \left[\frac{J(2J-1)}{(2J+3)(J+1)(2J+1)}\right]^{1/2} (J \| T^2(e) \| J) . \qquad \text{(II.18)}$$

By use of the theorems of tensor calculus and the explicit forms for $T^1(e)$ and $T^2(e)$, it is a relatively straightforward problem to calculate the angular parts of the reduced matrix elements $(J \| T^1(e) \| J)$ and $(J \| T^2(e) \| J)$ for any electronic state $|S\,L\,J\rangle$ arising from a configuration of one or two electrons or electron holes. For configurations of more than two electrons (or holes) it is necessary to consider the various ways the electrons may couple their l and s angular momenta to the resultant L and S. This requires knowledge of the so-called coefficients of fractional parentage for the particular case under study. The atomic states studied here arise from one- or two-electron configurations and hence do not require this more general treatment.

Evaluation of the radial integral $\langle r^{-3}\rangle$ in the reduced matrix elements $(J \| T^1(e) \| J)$ and $(J \| T^2(e) \| J)$ is not so easy as the angular part since, in general, precise radial wave functions are not available for the particular state under study. Fortunately, one may often avoid use of approximate radial wave functions by obtaining a value for $\langle r^{-3}\rangle$ by one or both of two methods.

The first method relies on the fact that the magnetic hfs constant a is proportional to the product of $\langle r^{-3}\rangle$ and g_I. Thus, if one has independent knowledge of a and g_I, one can calculate $\langle r^{-3}\rangle$. Often the proportionality of a and g_I is used to calculate the g_I for one isotope from its a value and the independent a and g_I values of another isotope of the same element. Thus

$$g_I(1) = g_I(2) \frac{a(1)}{a(2)} . \qquad \text{(II.19)}$$

This formula depends on the assumption that the constant of proportionality between a and g_I is the same for every isotope. That this is not always true gives rise to the small hfs anomaly effect mentioned earlier.

The second method utilizes the fact that the spin orbit constant ξ is proportional to $\langle r^{-3} \rangle$; that is,

$$\langle r^{-3} \rangle = \frac{\xi}{2 \mu_0^2 Z_{eff} H}, \tag{II.20}$$

where Z_{eff} is an effective Z value seen by the electron in question and takes into account shielding of the nuclear charge by the inner electrons. Judd suggests[3] that one take $Z_{eff} = Z - 4$ for p electrons, $Z - 11$ for d electrons, $Z - 30$ for f electrons. The quantity H is a relativistic correction factor and may be obtained from a table in the appendix of Ref. 4. Because of the uncertainty in choosing Z_{eff}, this second method is less accurate than the first.

C. J-Mixing Corrections to hfs

It has been mentioned previously that $\mathcal{H}_{hfs}$ mixes electronic states of different J. In fact, for the general matrix element $\langle I\ J\ F\ |\mathcal{H}_{hfs}|\ I\ J'\ F \rangle$, one has

$$\langle I\ J\ F\ |\mathcal{H}_{hfs}|\ I\ J'\ F \rangle = \sum_k (-1)^{I+J+F} \begin{Bmatrix} I & J' & F \\ J & I & k \end{Bmatrix} \langle I\ ||\ T^k(n)\ ||\ I \rangle$$

$$\times \langle J\ ||\ T^k(e)\ ||\ J' \rangle .$$

The 6-j symbol shows that for $k = 1$, J states differing by $\Delta J = 0, \pm 1$ are mixed and for $k = 2$ those differing by $\Delta J = 0, \pm 1, \pm 2$.

Woodgate[5] has considered the second-order correction δE_{hfs} to the hfs energy, where

$$\delta E_{hfs}(F) = \sum_{J'} \frac{\langle I\ J\ F\ |\mathcal{H}_{hfs}|\ I\ J'\ F \rangle \langle I\ J'\ F\ |\mathcal{H}_{hfs}|\ I\ J\ F \rangle}{E_J - E_{J'}} ;$$

$E_J - E_{J'}$ is the energy separation of the F level in states J and J'. He has shown that the corrections to be added to the magnetic dipole and electric quadrupole constants a and b are given by

$$\delta a(J) = \frac{\delta A_1(J)}{IJ}, \tag{II.21}$$

$$\delta b(J) = 4\ \delta A_2(J) ,$$

where

$$\delta A_k(J) = \sum_{k_1 k_2} \begin{pmatrix} I & K & I \\ -I & 0 & I \end{pmatrix} \cdot \begin{pmatrix} J & K & J \\ -J & 0 & J \end{pmatrix} \langle I || X^K(n) || I \rangle \langle J || X^K(e) || J \rangle \qquad \text{(II.22)}$$

and

$$\langle I || X^K(n) || I \rangle \langle J || X^K(e) || J \rangle = (-1)^{2I+2J+k_1+k_2+K} (2K+1) \begin{Bmatrix} k_1 & k_2 & K \\ I & I & I \end{Bmatrix}$$

$$\times \langle I || T^{k_1}(n) || I \rangle \langle I || T^{k_2}(n) || I \rangle$$

$$\times \sum_{J'} \begin{Bmatrix} k_1 & k_2 & K \\ J & J & J \end{Bmatrix} \frac{\langle J || T^{k_1}(e) || J' \rangle \langle J' || T^{k_2}(e) || J \rangle}{E_J - E_{J'}} .$$

Thus in second order an electric quadrupole interaction contributes a term to $\delta a(J)$ and a magnetic dipole interaction contributes to $\delta b(J)$.

Due to the large energy denominator $E_J - E_{J'}$ these corrections will be small, but in precise experiments they may be greater than the experimental error in measurement of a and b.

D. Effect of an External Magnetic Field

A magnetic field $\overline{H}$ will add to the atomic Hamiltonian two terms,

$$\mathcal{H}_{mag} = - g_I \mu_0 \overline{I} \cdot \overline{H} - g_J \mu_0 \overline{J} \cdot \overline{H} .$$

Because these two terms depend on the relative orientation of $\overline{I}$ and $\overline{J}$ with respect to the external field, each (2F+1)-fold degenerate hyperfine level F will be split into 2F+1 levels specified by the values of M_F which run over the range -F to F. However, since the field exerts an external torque on the atom its total angular momentum is no longer a constant; that is, F is no longer a "good" quantum number. This can be seen formally from the Wigner-Eckart theorem Eq. II.8, where J, M_J are replaced by F, M_F and T^k_q by I_z or J_z; the magnetic field direction has been chosen as the z axis. The properties of the 3-j symbol show that M_F remains a good quantum number but that F levels differing by unity are mixed provided they contain a common M_F value.

The extent to which different F levels are mixed by $\mathcal{H}_{mag}$ depends on its strength relative to the hfs Hamiltonian $\mathcal{H}_{hfs}$. Clearly two limiting cases exist; namely, $\mathcal{H}_{mag} << \mathcal{H}_{hfs}$ and $\mathcal{H}_{mag} >> \mathcal{H}_{hfs}$. By varying the magnetic field it is usually possible to put the atom into either of these limiting situations. In the first case one may treat $\mathcal{H}_{mag}$ as a small perturbation acting on the states $|F\ M_F\rangle$. Thus $\bar{I}$ and $\bar{J}$ are still strongly coupled together and may be thought of as precessing about the direction of $\bar{F}$ (Fig. II-1a.) Only the component of $\bar{H}$ along the direction of $\bar{F}$ then contributes to the splitting by $\mathcal{H}_{mag}$. This component $\bar{H}_F$ may be expressed as

$$\bar{H}_F = \frac{(\bar{H} \cdot \bar{F})}{F(F+1)}\ \bar{F}\ .$$

Substituting this into $\mathcal{H}_{mag}$ and using the relations

$$\bar{I} \cdot \bar{F} = \frac{F(F+1) + I(I+1) - J(J+1)}{2}\ ,$$

$$\bar{J} \cdot \bar{F} = \frac{F(F+1) + J(J+1) - I(I+1)}{2}\ ,$$

one obtains

$$\mathcal{H}_{mag} = -\ g_F \mu_0\ \bar{F} \cdot \bar{H}\ , \tag{II.23}$$

where

$$g_F = g_J\ \frac{F(F+1) + J(J+1) - I(I+1)}{2} + g_I\ \frac{F(F+1) + I(I+1) - J(J+1)}{2} \tag{II.24}$$

Thus at small magnetic fields the states $|F\ M_F\rangle$ are separated by equal intervals $g_F\ \mu_0\ H$.

In the limiting second case one uses states $|m_I\ m_J\rangle$, which diagonalize $\mathcal{H}_{mag}$. In this limit $\bar{I}$ and $\bar{J}$ precess independently about the strong external field $\bar{H}$ (Fig. II.1b). Thus quantities $\bar{I} \cdot \bar{J}$ in $\mathcal{H}_{hfs}$ are replaced by $m_I\ m_J$. One has then

$$\mathcal{H}_{mag} = -\ g_I\ \mu_0\ m_I H - g_J\ \mu_0\ m_J\ H, \tag{II.25}$$

$$\mathcal{H}_{hfs} = a\ m_I m_J + \frac{b}{2I(2I-1)\ J(2J-1)}\ [\,3\ m_I^{\ 2}\ m_J^{\ 2} + (3/2) m_I\ m_J - I(I+1)\ J(J+1)]\ . \tag{II.26}$$

When $\mathcal{H}_{hfs}$ and $\mathcal{H}_{mag}$ contribute approximately equally to the atomic energy one may not use either of the approximations above, but must treat the problem exactly and diagonalize the complete Hamiltonian

$$\mathcal{H} = \mathcal{H}_{hfs} + \mathcal{H}_{mag} .$$

As a set of basis states one may use either the $|F\, m_F\rangle$ or the $|\, m_I m_J\rangle$. Using the $|\, F\, m_F\rangle$ set one must diagonalize the (2I+1) (2J+1) - order matrix of the form shown in Fig. (II.2). This can be done in closed form for the case I = 1/2 or J = 1/2, yielding the famous Breit-Rabi formula,[6] but for the general case one uses numerical methods and a digital computer to solve for the eigenvalues.[7]

E. Relativistic Effects on hfs

The atomic Hamiltonian $\mathcal{H}$, Eq. I.1, includes the effects of relativity only through the fine-structure operator $\mathcal{H}_{fs}$. This operator is an effective operator which reproduces in the Schrödinger formalism the largest effect of relativity on the electronic state. A better approximation to $\mathcal{H}$ (excluding the hfs) is the many-electron relativistic Hamiltonian

$$\mathcal{H}_{rel} = \sum_i \left\{ \beta_i\, mc^2 + \bar{a}_i \cdot c\bar{p}_i - Z\frac{e^2}{r_i} \right\} + \sum_{i<j} \frac{e^2}{r_{ij}} \left\{ 1 - \bar{a}_i \cdot \bar{a}_j \right\} ,$$

where $\bar{a}$ and β are the Dirac operators. Grant[8] has developed a self-consistent field theory for solution of

$$\mathcal{H}_{rel}\, \psi = E\, \psi .$$

The four-component wave function ψ is constructued from antisymmetric products of single-particle functions of the form

$$\Theta^R_{nljm} = \begin{pmatrix} \chi_{ljm}\; P(r)/r \\ \chi_{ljm}\; iQ(r)/r \end{pmatrix} ,$$

where

$$\chi_{ljm} = \sum_\sigma \langle \tfrac{1}{2} ljm \,|\, \tfrac{1}{2} l\sigma m{-}\sigma \rangle\, \phi^\sigma Y_{lm-\sigma} ,$$

$Y_{lm-\sigma}$ is a spherical harmonic, ϕ^σ a spin function with $s_z = \sigma$ and

$\langle \frac{1}{2} ljm \mid \frac{1}{2} l\sigma\ m\text{-}\sigma \rangle$, the Clebsch-Gordan coefficient; l and l' are related by $l = j \pm \frac{1}{2}$ when $l' = j \mp \frac{1}{2}$; $P(r)$ and $Q(r)$ are radial wave functions, and in the nonrelativistic limit $P(r)$ remains finite while $Q(r) \to 0$.

One may now distinguish two different corrections to nonrelativistic hfs caused by inclusion of relativity. One arises from the breakdown of LS coupling (BDLSC) which occurs when $\mathcal{H}_{fs}$ mixes different nonrelativistic LS terms. The second arises from the neglect of the four-component nature of the relativistic wave function when hfs matrix elements are calculated. BDLSC can be allowed for by including different LS terms in the wave function; the amount of each can often be determined by fitting the calculated g_J's, and term and multiplet spacings to the observed values.

Recently Sandars and Beck[9] have developed a technique which allows one to take into account the second effect of relativity while using nonrelativistic LS-type wave functions. They constructed effective operators for magnetic dipole and electric quadrupole hfs which, when matrix elements are taken between LS wave functions, yield correct relativistic expressions. These effective operators are of the form

$$\mathcal{H}^{k}_{\text{hfs eff}} = T^{k}(n) \cdot T^{k}(e)_{\text{eff}}, \tag{II.27}$$

where

$$T^{k}_{\text{eff}}(e) = \sum_{k_s k_l} P^{(k_s k_l)k} U^{(k_s k_l)k} . \tag{II.28}$$

The $P^{(k_s k_l)k}$ are coefficients involving radial integrals and are included in Appendix (1). The $U^{(k_s k_l)k}$ are tensors of rank k made up from a tensor t^{k_s} of rank k_s in spin space and a tensor v^{k_l} of rank k_l in orbital space; t^{k_s} and v^{k_l} are unit tensors; that is,

$$\langle \tfrac{1}{2} \| t^{k_s} \| \tfrac{1}{2} \rangle = 1 ,$$
$$\langle 1 \| v^{k_l} \| 1 \rangle = 1 .$$

With k_s restricted to 0 or 1 for the magnetic dipole hfs, there are three terms in $T^{1}_{\text{eff}}(e)$ containing $U^{(01)1}$, $U^{(12)1}$, and $U^{(10)1}$. Sandars and Beck point out that these are proportional to $\bar{l}$, $(\bar{s}\, C^{2})^{1}$ and $\bar{s}$ respectively. Thus one can write

$$\mathcal{H}^{1}_{\text{hfs eff}} = 2\,\mu_0 \frac{\mu_I}{I}\,\bar{I}\cdot\sum\Big\{\bar{I}\,\langle r^{-3}\rangle_{01} - (10)^{1/2}(\bar{s}\,C^2)^1\,\langle r^{-3}\rangle_{12} + \bar{s}\,\langle r^{-3}\rangle_{10}\Big\}. \qquad \text{(II.29)}$$

The various $\langle r^{-3}\rangle$ expressions involve relativistic radial integrals, and they are listed in Appendix 1. Equation II.29 is of the same form as the nonrelativistic $\mathcal{H}^{1}_{\text{hfs}}$ (see Eq. II.17 with the exception that here different radial quantities multiply the first two terms, and the last term is present regardless of whether or not there are unpaired s electrons in the configuration. In the nonrelativistic limit, $\langle r^{-3}\rangle_{10} = \langle r^{-3}\rangle_{12}$ and $\langle r^{-3}\rangle_{10} = 0$.

There are three terms in $T^{2}_{\text{eff}}(e)$ involving $U^{(02)2}$, $U^{(11)2}$ and $U^{(12)2}$. The first is proportional to C^2, which is the only form found in the nonrelativistic $T^2(e)$. The two remaining are peculiar to the relativistic formula, and in the nonrelativistic limit they vanish.

III. NUCLEAR THEORY

The present theory of the nucleus is in many ways similar to that for the atomic electrons. The theory is not, however, so successful in calculating nuclear properties as the atomic theory is in calculating electronic properties. The comparatively poor performance of nuclear theory is due to (a) a lack of knowledge of the nuclear Hamiltonian and (b) inability to solve, to a comparable degree of approximation, the many-body problem. In the atomic case, the overwhelming force holding the electrons to the nucleus is the simple Coulomb attraction; this is a long-range force and it is easy to see how it can account for the binding of the electrons. The force between nucleons, however, is a very short-range one, falling off very rapidly as nucleons are separated by more than a few nucleon diameters. It is not obvious how such a force can hold a nucleus containing many nucleons together and still account for the fact that, to a large extent, individual nucleons seem to move independently within the nucleus. Since it is not possible at present to derive a successful nuclear Hamiltonian from first principles starting with the internucleon force, one uses an effective Hamiltonian which can account empirically for many of the observed nuclear properties. This Hamiltonian takes the form

$$\mathcal{H}_{nuc} = \sum_i (T_i + U_i) - \sum_i C_i \, \bar{s}_i \cdot \bar{l}_i + \sum_{i<j} V_{ij} \; ; \qquad \text{(III.1)}$$

T_i is the kinetic energy of the ith nucleon and U_i is a central potential. The second term is the famous spin-orbit term; it must be included in order that the observed nuclear shell structure will be reproduced. The last term is the residual interaction between nucleons, and presumably includes all terms left out in the first two. The similarity of $\mathcal{H}_{nuc}$ to the atomic Hamiltonian, Eq. I.1, is apparent. The difference contributing to (b) is that the spin-orbit term is not small compared with the first two terms, nor is the residual interaction always small enough to yield to a simple first-order perturbation treatment.

If one neglects for a moment the residual interaction term in $\mathcal{H}_{nuc}$, one sees that Schrödinger's equation, just as in the atomic case, leads to a set of individual nucleon eigenfunctions and eigenvalues which can be specified by a principal quantum number n, an orbital quantum

number l, and a total individual angular momentum quantum number j; there is a (2j+1)-fold degeneracy in the energy of such a state corresponding to different projections m_j of $\bar{j}$ on some z axis. Thus, each nlj subshell will hold 2j+1 protons or 2j+1 neutrons. The energy of an nlj subshell depends on the form of U_i and C_i; by picking these quantities properly it is possible to obtain nlj eigenvalues which, to a large extent, reproduce the experimentally observed single-particle energy levels. Figure III-1 shows these shell-model levels for protons and neutrons; the small effect of Coulomb repulsion between protons has been included. (The usual convention of identifying l values by the letters s, p, d, f, g, h, and i for 0, 1, 2, 3, 4, 5, 6, and 7 is used.) One sees that large energy gaps occur after 2, 8, 20, 28, 50, 82, 126 neutrons or protons have been added; these are the so-called "magic numbers." Nuclei with a magic number of nucleons are especially stable; those with two magic numbers exceptionally so. The existence of magic numbers is analogous to the closing of major shells in an atom, yielding the special stability of the noble gases. Many nuclear properties exhibit pronounced changes as the N or Z passes over a magic number.

It is important to emphasize the role of the spin-orbit term in giving the proper level ordering. Examination of the figure shows that the splitting between the j = l+1/2 and the j = l-1/2 levels is decisive for the pairs $1f_{7/2}$, $1f_{5/2}$; $1g_{9/2}$, $1g_{7/2}$; $1h_{11/2}$, $1h_{9/2}$; and $1i_{13/2}$, $1i_{11/2}$. Each member of these pairs is in a different major shell; this is required to give the observed magic numbers. The level ordering shown in Fig. III-1 is not necessarily correct within a given major shell (between magic numbers); however, the division into major shells is correctly given by the $\mathcal{H}_{nuc}$ with zero residual interaction.

There are two ways of dealing with the effects of V_{ij} in $\mathcal{H}_{nuc}$. The simplest describes its effect in terms of a set of coupling rules which are based on the large body of empirical data on nuclear ground states. Thus it has been observed that all nuclei with even N and Z have nuclear spin (total angular momentum quantum number) I = 0. Furthermore, a great many nuclei with N or Z odd have I and parity equal to the j and parity of "last-odd nucleon," a single nucleon

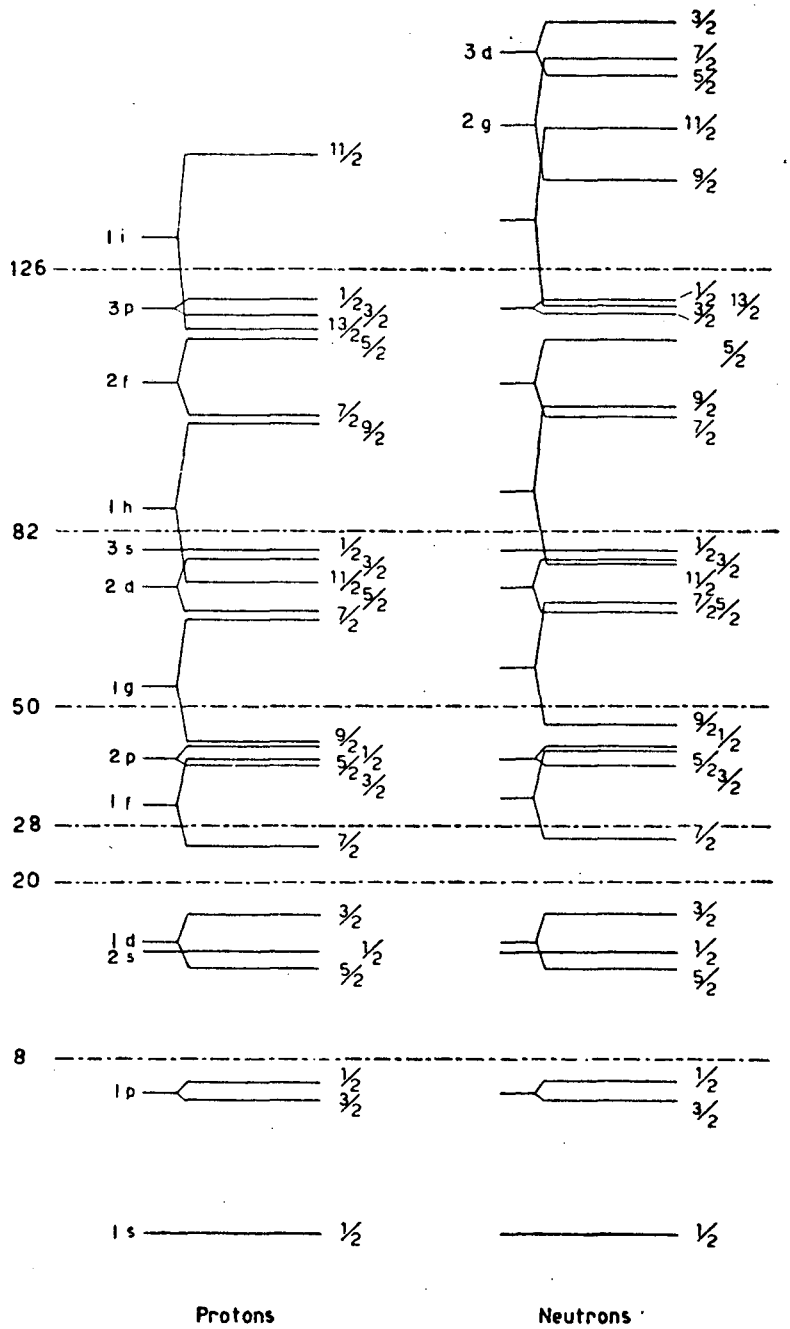

MU-21466A

Fig. III-1. Shell-model single-particle energy levels (spin-orbit and Coulomb energy terms included).

in the highest occupied level. On this basis, the extreme single-particle shell model (ESM) postulates that all nuclear properties are due to the last odd particles (one or two at most), all others coupling to an inert core with zero angular momentum. When both N and Z are odd, the nuclear spin I may take on the values $(j_p + j_n) \geq I \geq |j_p - j_n|$, where j_p and j_n are the angular momenta of the last odd proton and neutron. The exact value of I in any one case depends sharply on the effects of V_{ij}. On the basis of the empirical observation that in odd-odd nuclei the odd-nucleon spins tend to line up, Nordheim[10] proposed two coupling rules:

$$\text{if} \quad j_p = l_p \pm \frac{1}{2} \quad \text{and} \quad j_n = l_n \mp \frac{1}{2}, \quad \text{then} \quad I = |j_p - j_n| \; ;$$

$$\text{if} \quad j_p = l_p \pm \frac{1}{2} \quad \text{and} \quad j_n = l_n \pm \frac{1}{2}, \quad \text{then} \quad I > |j_p - j_n| \; .$$

In order for the ESM to account for the large number of nuclei with $I = 1/2$ in regions where high-spin subshells are being filled (e.g., $1h_{11/2}$) the pairing energy rule is postulated; it states that two nucleons paired to zero angular momentum in a subshell with large orbital angular momentum l' may have lower energy than 2 coupled to zero in a subshell with $l < l'$, even though the single-particle level for l' is higher than that for l. Thus for ^{119}Sn $I = 1/2$ and the configuration $(3s_{1/2})^1 (1h_{11/2})^4$ is lower in energy than $(3s_{1/2})^2 (1h_{11/2})^3$, even though for a single particle $(3s_{1/2})^1$ is lower than $(1h_{11/2})^1$.

The magnetic dipole moment of a nucleus in the ESM is easily calculated by use of the free proton and neutron magnetic moments. For odd-N or odd-Z nuclei it is given by

$$\mu = \frac{\mu_{nm}}{2(I+1)} \left\{ g_l \left[I(I+1) + l(l+1) - 3/4 \right] + g_s \left[I(I+1) - l(l+1) + \frac{3}{4} \right] \right\}, \qquad \text{(III.2)}$$

where $g_l = +1$ for a proton, $g_l = 0$ for a neutron, and $g_s = 5.5856$ for a proton and -3.8263 for a neutron; μ_{nm} is the nuclear magneton, $\mu_{nm} = e\hbar/2M_p c$, where M_p = mass of proton. This formula yields the

Schmidt values for the magnetic moments; these differ from the measured values for odd-mass nuclei by as much as 400%. However, virtually all the measured magnetic moments lie within the two Schmidt limits calculated with $I = l+1/2$ and $I = l-1/2$. For odd-odd nuclei one can calculate the expected magnetic moment from the equation

$$\frac{\mu}{I}\,\bar{I} = \frac{\mu_p}{I_p}\,\bar{I}_p + \frac{\mu_n}{I_n}\,\bar{I}_n\,; \tag{III.3}$$

this yields

$$\mu = \frac{1}{2(I+1)}\left\{\frac{\mu_p}{I_p}\left[I(I+1) + I_p(I_p+1) - I_n(I_n+1)\right] + \frac{\mu_n}{I_n}\left[I(I+1) + I_n(I_n+1) - I_p(I_p+1)\right]\right\}, \tag{III.4}$$

where I_p, μ_p, I_n, μ_n are spins and moments of neighboring odd-Z and odd-N isotopes.

The electric quadrupole moments for an odd-proton nucleus is given in the ESM by[11]

$$Q_p = \frac{-(2j-1)}{2(j+1)}\,\langle r^2\rangle \cdot \left[1 - \frac{2n-2}{2j-1}\right], \tag{III.5}$$

where n is the number of nucleons in the j subshell. For an odd-neutron nucleus in the ESM, the quadrupole moment is due to recoil of the charged core and is given approximately by[11]

$$Q_n = \frac{Z}{(A-1)^2}\,Q_p\,. \tag{III.6}$$

Observed quadrupole moments differ from those calculated in the ESM by as much as a factor of 20 or 30. Furthermore, it appears that odd-neutron nuclei have quadrupole moments equal in magnitude to odd-proton nuclei. There seems also to be a preponderance of positive quadrupole moments, whereas ESM predicts equal numbers of positive and negative moments.

The deficiencies of the ESM theory lie in its neglect of the effects of the V_{ij} term in $\mathcal{H}_{nuc}$. V_{ij} is represented only through the empirical coupling rules, which do a good job of predicting spins of odd nuclei, but do not contribute to the calculation of moments. V_{ij} has much the same

effect on nuclear configurations as e^2/r_{ij} has on atomic ones, that is, V_{ij} can mix different ESM configurations. This can be an important effect when one is considering matrix elements of any Hermitian operator O, such as the moment operators. Thus, if ψ_0 is the ESM state and V_{ij} mixes in a state ψ_1 in first order, the new state is

$$\psi = \psi_0 + a\psi_1 ,$$

where

$$a = \frac{\langle \psi_1 | V_{ij} | \psi_0 \rangle}{\Delta E_{10}} ;$$

here ΔE_{10} is the zero-order (ESM) energy difference between states ψ_1 and ψ_0. Neglecting second-order terms in a, one has

$$\langle \psi | O | \psi \rangle \approx \langle \psi_0 | O | \psi_0 \rangle + 2a \langle \psi_1 | O | \psi_0 \rangle ;$$

thus if ψ_1 is admixed only 1%, this corresponds to $a = 0.1$, and if

$$\langle \psi_1 | O | \psi_0 \rangle \approx \langle \psi_0 | O | \psi_0 \rangle ,$$

then a 20% change will result in the expectation value of O.

It is important to pick the correct form for V_{ij}. This form must be consistent with the empirical coupling rules, since they are postulated to arise from its effect. V_{ij} is expected to have a large short-range part, since the free-nucleon scattering force is observed to be short-range. Noya, Arima, and Horie[12] have carried out calculations for odd-mass nuclei using this first-order mixing of ESM configurations. The V_{ij} they used was

$$V_{ij} = [V_s(1-4\bar{s}_i \cdot \bar{s}_j)/4 + V_t(3 + 4\bar{s}_i \cdot \bar{s}_j)/4] \delta(r_{ij}) ;$$

V_s and V_t are the singlet and triplet strengths and $\bar{s}_i$ and $\bar{s}_j$ are the spin angular momentum operators for the ith and jth nucleon. V_{ij} has zero range due to the delta function. Noya et al. used ψ_0 functions derived from both a square-well form for U_i and an isotropic harmonic oscillator potential $U_i \propto r_i^2$. From free-nucleon scattering they obtained $V_t/V_s = 1.5$, and determined V_s by fitting calculated to observed pairing energies. Magnetic moments calculated agreed with experiment to within $\approx 30\%$, except for the heavy nuclei ($A \gtrsim 150$). Quadrupole moments

were less successfully reproduced, agreeing to $\approx 50\%$, except for the heavy nuclei, for which the observed Q's are as much as ten times those calculated. This is considered good agreement for the Q's in the light nuclei because of the large uncertainties in the measured Q's.

Another treatment of V_{ij} is that carried out in the individual-particle model (IPM). Here the matrix of V_{ij} of the form used by Noya et al. is diagonalized when one uses as basis states all antisymmetrized wave functions arising from the unfilled configurations beyond a major closed shell. This treatment does not include the configuration interaction effects treated by Noya et al., and hence is not so successful at predicting moments. It does, however, predict more precisely than ESM the ground-state spins of odd-odd nuclei. Several authors[13, 14] have derived coupling rules which predict the spin I of odd-odd nuclei in terms of the spins of the odd nucleons. These are summarized:[15]

	j_p	j_n	Particle-particle	Particle-hole	One midshell
strong	$l_p \pm \frac{1}{2}$	$l_n \mp \frac{1}{2}$	$I = \lvert j_p - j_n \rvert$	$I = \lvert j_p + j_n - 1 \rvert$	$I = \lvert j_p - j_n \rvert$
weak	$l_p \pm \frac{1}{2}$	$l_n \pm \frac{1}{2}$	$I = \lvert j_p + j_n \rvert$ or $\lvert j_p - j_n \rvert$	$I = \lvert j_p + j_n - 1 \rvert$ or $\lvert j_p + j_n - 2 \rvert$	$I = \lvert j_p + j_n \rvert$

Here "particle-particle" refers to the case in which the proton and neutron subshells are both less than half filled or both more than half filled. "Particle-hole" refers to the case in which either of the shells is more than half filled and the other is less than half filled. "One midshell" is for the case in which either the proton or the neutron subshell is exactly half full.

It has been mentioned that in the region of heavy nuclei ($A \approx 150$), far from closed shells, the observed quadrupole moments differ as much as one order of magnitude from those predicted by the ESM augmented by the configuration mixing of the short-range V_{ij}. For example, for ${}_{71}Lu^{175}$ Noya et al. calculate $Q = 0.44$ barn(1 barn $= 10^{-24}$ cm^2), whereas experimentally $Q = 5.1$ barns. The difference cannot be remedied by extending the short-range configuration interaction treatment to higher order,

or by extending it to include the interaction between nucleons inside and outside closed shells. Present theory seems to indicate that an additional long-range part must be added to V_{ij} in order to account for the large quadrupole moments. In addition, one must consider the long-range interaction between the closed-shell core nucleons and those outside the core. The long-range portion of V_{ij} is usually taken as proportional to $P^2(\cos \theta_{ij})$, the second-order Legendre polynomial. In the regions far from closed shells such a long-range interaction leads to a static ellipsoidal deformation of the entire nucleus. Thus all protons may contribute to the observed quadrupole moment, not just those beyond closed shells. Furthermore, odd-neutron nuclei have cores just as strongly deformed as odd-proton nuclei, and since there are far more protons in the core than outside, one expects equally large quadrupole moments for odd-neutron nuclei. This is indeed the case, as exemplified by ${}_{68}Er^{167}$ with $Q \approx 10$ barns. Because of the long-range portion of the residual interaction and the consequent possible ellipsoidal deformation of the entire nucleus, it is possible for the nucleus to possess rotational and vibrational as well as single-particle modes of excitation. The collective model (CM) concerns itself with the region between major shells where these collective excitations are most pronounced. It makes the assumption that the rotational and vibrational excitations are much lower in energy than the single-particle excitations. This allows a separation of the nuclear wave function,

$$\psi = \chi \cdot \phi_{vib} \cdot D_{rot} ,$$

where χ is the wave function for intrinsic motion of the nucleons within a coordinate system fixed to the deformed nucleus, ϕ_{vib} is the wave function describing vibrations about the equilibrium nuclear shape, and D_{rot} is the wave function describing rotation of the deformed nucleus. For the calculation of magnetic moments in the collective model, one must include the rotational magnetic moment as well as the single-particle contributions. This is expressed in terms of a rotation g factor, g_R. For a nucleus with uniform distribution of neutrons and protons, one should have $g_R = Z/A$; no nucleus is perfectly uniform throughout and one usually must regard g_R as a parameter. This work does not require extensive application of the CM and hence is not dealt with in detail.

There are a great many nuclei which are not so near closed major shells that the collective effects can be ignored [that is, $P^2(\cos\theta_{ij})$ left out of V_{ij}] or so far from closed shells that the collective-model assumptions are valid. In this region one can turn to the so-called unified model (UM). In this model the V_{ij} is expanded

$$V_{ij} = V(r_i, r_j) = \sum_l v_l(r_i, r_j)\, P_l(\cos\theta_{ij}) .$$

It is assumed that the isotropic $l = 0$ term is incorporated in the central self-consistent field U_i. Due to the static quadrupole deformations the $l = 2$ term is singled out and given special treatment. Because of the empirical behavior of the pairing energy it is assumed that the $l \neq 2$ terms in V_{ij} act only between particles in the same orbit. This restricts l to even values. Thus V_{ij} becomes

$$V_{ij} = v_2(r_i, r_j)\, P_2(\cos\theta_{ij}) + G(r_i, r_j),$$

where G includes all the higher-order l terms in V_{ij}. It is postulated that G is a short-range correlative potential which is responsible for the pairing of nucleons to $J = 0$ in even-even nuclei and for the low energy of $J = 0$ pairs of single-particle states with large orbital angular momenta. In fact, G is postulated to have matrix elements only between two nucleon product states of single-particle wave functions with the same j and opposite m. These states are called conjugate pair states. That is, only matrix elements

$$\langle nlj+,\ nlj- \,|\, G \,|\, n'l'j'+,\ n'l'j'- \rangle$$

are nonzero; + and - stand for m and $-m$. This type of pairing force is similar to that responsible for the existence of superconductivity in some solids, as was pointed out by Bohr, Mottelson, and Pines in 1958.[16] Because of this similarity the nuclear problem may be handled by the same techniques as used in the successful Bardeen- Cooper- Schrieffer (BCS) theory of superconductivity. The complete development of this theory is beyond the purpose of this brief survey; however, the important points of the procedure involve the following ideas.[17]

(a) Only the pairing term $G(r_i, r_j)$ is included in the zero-order Hamiltonian; the P_2 term is treated as a perturbation.

(b) The ground-state wave function for a j subshell is written as

$$\psi_0 = \prod_j \prod_{m>0} (U_j |0j\rangle + V_j |j\,m\rangle\, |\, j\text{-}m\rangle\,) ,$$

where U_j and V_j are real positive constants; $|\,0j\,\rangle$ represents the state with no pairs in the j subshell. Thus U_j^2 is the probability that the j, m conjugate pair is unoccupied and V_j^2 is the probability that it is occupied.

(c) The concept of a quasi particle (j, m) is introduced together with quasi-particle creation and annihilation operators $\alpha^\dagger_{jm}$ and $\beta^\dagger_{jm}$. A quasi particle is a mixture of a nucleon in state j, m and a hole in state j, -m. Here $\alpha^\dagger_{jm}$ and $\beta^\dagger_{jm}$ are given by

$$\alpha^\dagger_{jm} = U_j\, b^\dagger_{jm} - V_j\, b_{j-m} ,$$

$$\beta^\dagger_{jm} = U_j\, b^\dagger_{j-m} + V_j\, b_{jm};$$

$b^\dagger_{jm}$ creates and b_{jm} annihilates a j, m nucleon.

If the nuclear Hamiltonian $\mathcal{H}_{nuc}$ including the G potential is rewritten in terms of this quasi-particle creation and annihilation operator scheme, it turns out that if U_j and V_j are properly defined in terms of the strength of G, the number of nucleons present, and the single-particle (no V_{ij}) energy levels, the resulting Hamiltonian contains no coupling between the quasi-particle states. This greatly simplifies solution of the problem.

The results of such calculations show that instead of there existing a sharp-cutoff Fermi energy below which all nucleon states are filled and above which all are empty, as would be predicted by the ESM, the nucleons are distributed throughout the various single-particle j levels with probabilities given by the V_j^2. This is in many ways equivalent to the effects of configuration mixing as discussed earlier.

IV. THE ATOMIC BEAM METHOD

An atom with electronic magnetic moment $g_J \mu_0 \overline{J}$ and nuclear magnetic moment $g_I \mu_0 \overline{I}$ has energy dependent on an external magnetic field $\overline{H}$, given by

$$\mathcal{H}_{mag} = - g_J \mu_0 \overline{J} \cdot \overline{H} - g_I \mu_0 \overline{I} \cdot \overline{H} .$$

If the magnetic field is large enough so that $\mathcal{H}_{hfs}$ is small compared with $\mathcal{H}_{mag}$, then, as has been discussed earlier, one may write for the energy

$$E_{mag} = - g_J \mu_0 m_J H - g_I \mu_0 m_I H .$$

If H is nonuniform, then a force is exerted on the atom in the z direction given by

$$F_z = - \frac{\partial}{\partial z} E_{mag} = (g_J \mu_0 m_J + g_I \mu_0 m_I) \frac{\partial H}{\partial z} .$$

Because $g_I \approx g_J/2000$, it is a good approximation to write

$$F_z = g_J \mu_0 m_J \frac{\partial H}{\partial z} .$$

Thus atoms with different values of m_J experience a different force when passing through a region of large $\frac{\partial H}{\partial z}$ and hence may be separated.

In the modern atomic beam resonance apparatus, atoms pass through three magnetic field regions in the form of a well-collimated thermal beam. For historical reasons the first and third magnets are labeled A and B and the second or center magnet is called the C magnet. The A and B magnets produce nonuniform fields with large $\frac{\partial H}{\partial z}$. In the so-called "flop-in" device, shown in Fig. IV-1, $\frac{\partial H}{\partial z}$ has the same sign in the A and B magnets. The C magnet, on the other hand, produces a uniform field H_C, which can be varied in magnitude to suit the experiment. A beam is formed by heating the substance of interest inside a suitable oven and allowing a small fraction of the atoms to leave the oven through a slit-shaped hole. With all magnetic fields in the z direction, one can think of the beam as progressing along the positive y axis and the oven slit as being along the x axis. After having passed through the inhomogeneous A magnet field, an atom with a particular m_J value has been deflected from its straight-line

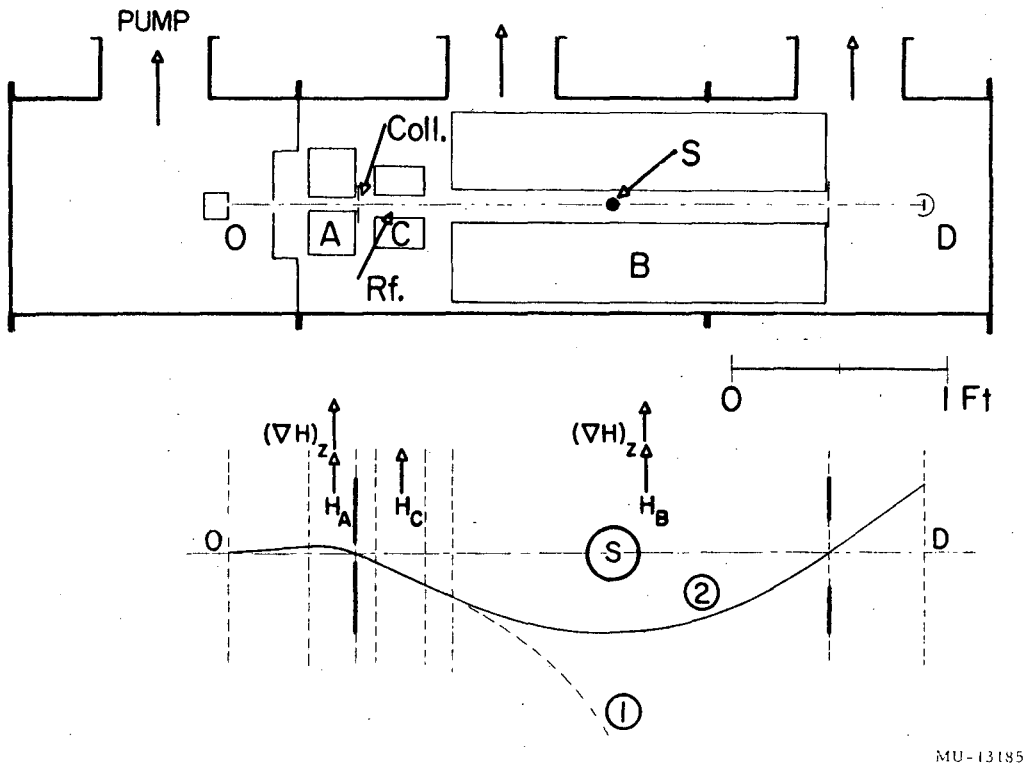

Fig. IV-1. Schematic representation of atomic beam Machine II used in these experiments:

O = Oven

S = Stop wire

D = Detector

1 = Path of nonresonance atoms

2 = Path of resonance atoms .

path by an amount S_A which depends on m_J, $\frac{\partial H_A}{\partial z}$, and the atom's velocity v. No force is exerted in the C region and the atom travels on a straight line until it reaches the B magnet. If in the C region it has been possible to induce the atom to change its state to one with magnetic quantum number $-m_J$, then as it passes through the B magnet field it experiences a deflection S_B opposite to S_A. With proper design, one can have $S_B = - S_A$. Thus, the atom experiences no net deflection after passage through the apparatus, provided the transition $m_J \rightarrow -m_J$ can be carried out in the C region. If m_J remains unchanged, the deflections S_A and S_B add and such atoms do not reach the detector.

An exception occurs in case $m_J = 0$ or v is very large. In these cases, atoms undergo no, or very small, deflections in either the A or B fields and hence reach the detector regardless of whether or not a transition has occurred in the C region. They contribute a large background. These atoms are usually blocked off from reaching the detector by an obstacle placed in the B field whose width is slightly larger than the width of an undeflected beam. Atoms following the flop-in trajectories will pass around this "stop-wire," whereas the $m_J = 0$ or high-velocity atoms will strike it. This increases the signal-to-background ratio for the device.

The detector in the atomic beam device may be a hot surface placed at the focus of the flop-in trajectories; the impinging atoms are ionized and the ion current is collected and measured by an electrometer. This technique works well for the easily ionizable stable alkali atoms, Na, K, Rb, and Cs. Typical resonance signals yield ion currents of $\approx 10^{-11}$ ampere. For radioactive beam detection, the beam is collected on a surface placed at the detector location; the surface is removed after a collection period (typically 5 min) and the collected radioactivity is measured with sensitive counters. Minimum resonance signals yield $\approx$ 10 counts/min, although by careful counting for long periods one can measure signals as low as 1 count/min. A signal of 10 counts/min from an isotope with a half life of 1 hour means that the collecting surface holds about 1500 atoms; this gives an indication of the sensitivity

of the radioactive detection method. Usually with radioactive detection a second surface is exposed to that part of the beam which is not focused; this surface is placed on one side of the center resonance surface and is exposed for the same period. The side-surface radioactivity serves as a monitor of the beam level, and the resonance signal is taken as the ratio of the center activity to the side activity. This method cancels out any fluctuations in the beam intensity which, without such normalization, might appear to be a resonance signal. It has been empirically discovered that a clean sulfur surface has a high collection efficiency which can be uniformly reproduced. In the work here, the sulfur surface is attached to one end of small brass pieces termed "buttons," which slip easily into a loading mechanism at the detection end of the beam device.

The transition $m_J \rightarrow - m_J$ is induced in the C region by the introduction of a small oscillating radiofrequency field, H_{rf}. If the frequency of this rf field matches the Einstein condition $h\nu = | E_1 - E_2 |$ then it is possible to induce the atom to change its state from 1 to 2 or vice versa. In addition to the Einstein condition there are certain selection rules which limit the observation of a particular transition. The device limits consideration to those states 1 and 2 which have opposite m_J values in the large A and B magnetic fields. Furthermore, the transitions are magnetic dipole M(1), and hence must conform to corresponding selection rules. These rules are summarized in the table below. Distinction is made between the two limits (a) $E_{hfs} > E_{mag}$ and (b) $E_{mag} > E_{hfs}$.

	M(1) rule	Machine rule
H_{rf} normal to H_C	(a) $\Delta m_F = \pm 1$ (b) $\Delta m_J = \pm 1$	$m_J(A) = - m_J(B)$, $m_J(a) \neq 0$
H_{rf} parallel to H_C	(a) $\Delta m_F = 0$ (b) $\Delta m_J = 0$	$m_J(A) = - m_J(B)$, $m_J(A) \neq 0$

Transitions with $\Delta m = \pm 1$ are called π transitions, those with $\Delta m = 0$, σ transitions. Note that the σ transition at high H_C (b), is not observable, since the M(1) rule requires $\Delta m_J = 0$, which violates the machine rule. The rules above assume that the atom interacts with a

single rf quantum while passing through the C region. For atoms with odd half-integral J states this is all that is required, since the transition $m_J(A) = \pm 1/2$ to $m_J(B) = \mp 1/2$ is always available; there is no $m_J = 0$ state. For atoms with integral $J > 0$, however, it is not always possible to satisfy the M(1) rules and the machine rule while interacting with a single rf quantum. Thus, the simplest machine-allowed transition for such an atom is the $m_J(A) = \pm 1$ to $m_J(B) = \mp 1$, which requires that two M(1) transitions occur in the C region. This double-quantum transition may require two different rf frequencies corresponding to the energy intervals $m_J = +1$ to $m_J = 0$ and $m_J = 0$ to $m_J = -1$, depending on whether the intervals are equal or not.

In the general atomic beam resonance experiment, one is interested in obtaining values for the quantities I, a, b, g_I, and g_J. In experiments on radioactive atoms, usually g_J is known from work on stable isotopes of the same element and it is considered known in the discussion that follows. The normal procedure is to measure the unknowns in the order I, a and b, g_I. This order has the virtue that one can proceed at all times from a region where possible transition frequencies are well known into one where new information will be learned. Thus to measure I one sets the C field to a low value so that limit (a) is complied with and the Zeeman levels within a hyperfine F level are equally spaced by $g_F \mu_0 H_C$. Since $g_I \approx \frac{g_J}{2000}$, g_F is given very nearly (see Eq. II.24) by

$$g_F = g_J \frac{F(F+1) + J(J+1) - I(I+1)}{2F(F+1)} .$$

Thus observation of a resonance at frequency

$$\nu = g_F \frac{\mu_0}{h} H_C \tag{IV.1}$$

immediately implies a value of I, provided one knows the value of F and H_C H_C is measured by the observation of a resonance in a calibration beam of atoms whose constants are already known, thus

$$H_C = \frac{\nu_c}{g_{F_c}} \frac{h}{\mu_0} ,$$

so that

$$g_F = \frac{\nu}{\nu_c} g_{F_c} \tag{IV.2}$$

where the subscript c refers to the calibration isotope. F is restricted, of course, to the values I+J down to $|I-J|$ in integer steps, and the machine selection rules usually limit consideration to only a few of these. There is always a spin-dependent low-field transition available within the maximum F level, F = I+J.

Having measured I, one continues to observe the $\Delta F = 0$, $\Delta m_F = \pm 1$ transition until its frequency begins to depart from the linear relationship, Eq. IV.1. At this point one is beginning to gain information about the zero-field hyperfine intervals, because as H_C is increased, $\mathcal{H}_{mag}$ begins to mix zero field states of the same m_F, but of F's differing by ±1. Thus, the two levels connected by H_{rf} begin to curve, and this curvature manifests itself as a shift in frequency from the linear low-field expression. Since the hyperfine intervals are linear combinations of a and b, measurement of the frequency shift yields information on a and b. The extraction of a and b from the frequency vs C-field data is done by computer routine. The routine, HYPERFINE, fits calculated frequencies to observed frequencies and magnetic fields by varying any number of the unknown quantities a, b, g_I, and g_J. The fit is a least-squares one and the best values and their errors are computed. Having obtained preliminary values for a and b from HYPERFINE, one can use them as input to another program which calculates transition frequencies and their uncertainties at any value of H_C. One then does a new experiment at the highest H_C commensurate with acceptable uncertainty in the calculated transition frequency. Typically, with radioactive atoms, one can tolerate an uncertainty in frequency of 5 to 20 times the expected line width of the resonance. Thus at each step in field one can expect to decrease the uncertainty in a and b by about 1/5 to 1/20.

When the uncertainty in a and b has been reduced to the point that the corresponding uncertainties in the zero-field hyperfine intervals are tolerable, one can abandon the $\Delta F = 0$, $\Delta m_F = \pm 1$ transition that has been followed to a moderate to high magnetic field (a few hundred gauss), and search at near zero H_C for $\Delta F = 1$ hyperfine transitions. The

frequencies of such transitions, apart from a small correction due to the nonzero value of H_C, are direct measurements of the hyperfine intervals, and serve to determine the final values of a and b. Increased precision in a and b can then be achieved only through reduction of the resonance line width.

Direct measurement of g_I is hampered by its smallness compared with g_J, nonetheless in the high-field limit it is possible to observe transitions corresponding to $\Delta m_J = 0$ and $\Delta m_I = \pm 1$ provided two or more rf fields are present in the C region. The g_I-dependent frequency is then

$$\nu_i = g_I \frac{\mu_0}{h} H_C \quad .$$

The second rf frequency is necessary to satisfy the machine selection rule, which is violated by $\Delta m_J = 0$. In some cases two different allowed transitions form a doublet whose separation depends only on g_I. Otherwise, g_I can be treated as a free parameter in the fit of all observed frequencies and magnetic fields; this will require a great many observations in order to obtain the precision of a single direct measurement. When g_I has not been measured directly for the isotope under study, but has been, measured for some other isotope of the same element whose a constant is known, one uses the proportionality between the g_I's and a's to determine the unknown g_I, using Eq. II.19.

V. RESEARCH ON ^{110}In

A. Production of the Isotope

Neutron-deficient radioactive isotopes of indium (Z = 49) may be easily produced by bombardment of silver (Z = 47) targets with α particles (Z = 2, N = 2) accelerated in a cyclotron; the silver nucleus absorbs an α particle and emits several neutrons. The process is written Ag(α, kn)In, where k is the number of neutrons emitted; k varies with the incident α energy and may range from 1 to 6 as E_α runs from ≈ 25 MeV to ≈ 100 MeV.

In this work it was desired to produce and measure the spin I of ^{110}In, which has a half life of 66 min. Because there are two stable Ag isotopes, ^{107}Ag 52% abundant and ^{109}Ag 48% abundant, ^{110}In may be produced in two ways:

$$^{107}\mathrm{Ag}\ (\alpha, \mathrm{ln})^{110}\mathrm{In} \quad \text{for} \quad E_\alpha \approx 11 \text{ to } 25 \text{ MeV},$$

$$^{109}\mathrm{Ag}\ (\alpha, 3\mathrm{n})^{110}\mathrm{In} \quad \text{for} \quad E_\alpha \approx 25 \text{ to } 45 \text{ MeV}.$$

The silver targets were 0.010-in.-thick foils and were bombarded in the 88-inch cyclotron at the Lawrence Radiation Laboratory. Because the targets contained two Ag isotopes and were thick enough to slow the α beam to below threshold for the (α, kn) reactions, several other radioactive In isotopes were produced besides ^{110}In. Table V-I lists those produced and their half lives. Only those activities with half lives greater than 1 min are listed.

A summary of the cyclotron bombardment data and resulting activity for the runs discussed here is listed below.

Run	E_α (MeV)	Integrated cyclotron beam current (μA-h)	Bombardment time (h)	Oven activity (R/h)
819	25	30.0	1.5	.8 @ 6"
845	45	83.0	4.5	80. @ 4"
846	45	55.0	2.7	40. @ 5"-6"

Ghoshal[18] has studied the (α, kn) reaction yields versus E_α for k = 1, 2, and 3. His data show that for a thick target with $E_\alpha \approx 25$ MeV

Table V-I. Indium isotope production.

Process	E_α (MeV)	Half life
$^{107}Ag\ (\alpha, 1n)\ ^{110}In$		66 min
$^{107}Ag\ (\alpha, 1n)\ ^{110m}In$		4.9 h
	11 to 25	
$^{109}Ag\ (\alpha, 1n)\ ^{112}In$		14 min
$^{109}Ag\ (\alpha, 1n)\ ^{112m}In$		21 min
$^{107}Ag\ (\alpha, 2n)\ ^{109}In$		4.3 h
$^{107}Ag\ (\alpha, 2n)\ ^{109m}In$		1.3 min
	15 to 35	
$^{109}Ag\ (\alpha, 2n)\ ^{111}In$		2.81 days
$^{109}Ag\ (\alpha, 2n)\ ^{111m}In$		≈10 min
$^{107}Ag\ (\alpha, 3n)\ ^{108}In$		58 min
	25 to 45	
$^{109}Ag\ (\alpha, 3n)\ ^{110}In$		66 min
$^{109}Ag\ (\alpha, 3n)\ ^{110m}In$		4.9 h

only the $k = 1$ and $k = 2$ processes occur to an appreciable extent. Thus only one activity with half life of the order of 1 hour, ^{110}In, should be produced by bombardment with 25-MeV α's. At higher $E_\alpha \approx 45$ MeV, the $k = 1$ and $k = 3$ processes produce ^{110}In and the $k = 3$ process also produces ^{108}In, whose half life is so close to that of ^{110}In that the two may not be distinguishable by decay analysis. The $k = 3$ process, however, does produce a great deal more ^{110}In than the $k = 1$.

After production of the isotopes in the cyclotron it was necessary to perform a chemical separation of the In from the Ag target. In order to protect personnel from the high level of radiation the chemical separation was carried out inside a LRL junior cave, which provided 2 in. of lead shielding. The target was dissolved in ≈ 10 ml of a hot concentrated nitric acid solution which contained ≈ 50 mg of dissolved stable In carrier. After dissolution, concentrated ammonium hydroxide was added slowly, a drop at a time, until the milky precipitate indium hydroxide was formed. The precipitate was consolidated by centrifugation and the solution poured off. The indium hydroxide was washed in water and recentrifuged; it was then dissolved in a minimum of dilute hydrochloric acid. About 500 mg of powdered manganese was added and additional hydrochloric acid was introduced while shaking until the manganese had reduced the dissolved indium and it floated to the surface as a sponge. It was important that the hydrochloric acid not be too strong or the indium sponge might partially redissolve after the reduction. To prevent this possibility the solution was diluted with water as soon as the reaction was completed. The sponge was then removed and dried before being loaded into the oven for insertion into the beam machine.

B. Formation of the Atomic Beam

The electronic ground state of In is $(5p)^2P_{1/2}$, with a g_J of about $-2/3$. The nearby fine-structure state $^2P_{3/2}$ is separated by 2212 cm^{-1} and has $g_J \approx -4/3$. Typical oven temperatures for production of a useful beam was $\approx 1300°C$; at this temperature approximately 20% of the beam atoms were in the $^2P_{3/2}$ state. Investigations with beams of stable $^{113,115}In$, detected by surface ionization on a hot iridium wire, showed that resonances in the $^2P_{3/2}$ state were much

stronger than those in the $^2P_{1/2}$ (by about 5 to 10 times). This is because, despite the low population of the $^2P_{3/2}$ state, its larger g_J allows stronger focusing of the atoms by the atomic beam device. Because of this all radioactive resonances observed were in the excited $^2P_{3/2}$ state.

A carbon oven was used and was heated by electron bombardment to the desired temperature. The carbon slits were set to a width of ≈ 0.004 in. Typical electron bombardment power ranged from 120 to 200 watts.

C. Measurement and Results

To measure the spin of ^{110}In the technique described in Sec. III was used. Observations of the Zeeman transition in the hfs level with $F = I + J$ were carried out at three C-magnet fields. The magnetic field was kept low so that the frequency of the transition was given by Eq. IV.1. Figure V-1 shows the results of a spin search (Run 819) carried out at a field of about 2.2 gauss. Although the error on each point is rather large due to the low counting rates (maximum of 2.4 counts/min above background) the $I = 2$ signal is significantly above the background level, as indicated by the points at $I = 1$ and $I = 3$. A small signal was expected at $I = 7$ due to the presence in the beam of 4.9-hr ^{110m}In, whose spin was established by Marino.[19]

The identification of the $I = 2$ signal as arising from ^{110}In is based on the following argument. The bombardment energy for Run 819 was $E_\alpha = 25$ MeV; at this energy only the (α, kn) reactions with $k = 1$ or 2 occur to any appreciable extent.[18] Thus the only expected activity with half life ≈ 1 h is that due to ^{110}In. If a button exposed at the $I = 2$ frequency shows an enhanced radioactivity which decays with a half life of ≈ 1 h, then one may reasonably assign the spin to ^{110}In.

To implement this identification a special $I = 2$ button was exposed, at the end of Run 819, for a longer period than those buttons contributing to Fig. V-1; this provided a high counting rate which would allow a decay analysis. The decay of this button (button NH) was compared with the decay of a normalization button (MW); recall that the normalization button receives a large sample of the unfocused beam.

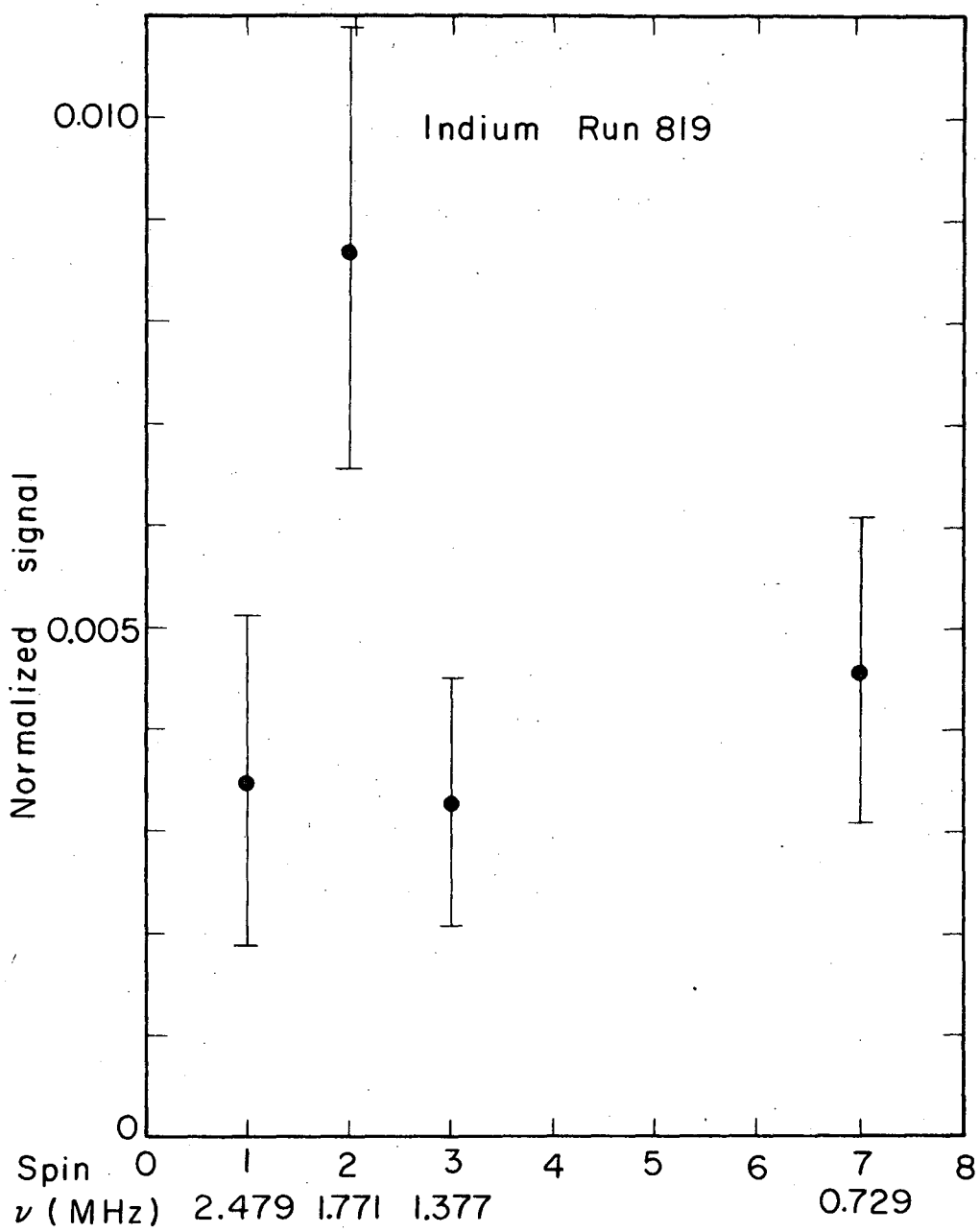

XBL674-2748

Fig. V-1. Indium Run 819 spin search at ≈ 2.2 gauss.

Immediately after collection NH counted ≈ 15 counts/min; at the same time MW counted ≈ 259 counts/min. The decay of these two buttons was compared in the following manner.

If there is a number, k, of activities with half lives T_j in the atomic beam, then the activity on a resonance button exposed at a frequency ν which focuses the $j = 1$ activity is given by

$$A(t) = r_1(\nu) \exp[-t(\ln 2)/T_1] + \sum_{j=1}^{k} a_j \exp[-t(\ln 2)/T_j]$$

where $A(t)$ is the total activity and $r_1(\nu)$ the amplitude of the resonant T_1 activity, and the summation includes the background level of all activities given by the exponential decays of the amplitudes a_j. The normalization activity N decays according to

$$N(t) = \sum_{j=1}^{k} n_j \exp[-t(\ln 2)/T_j] .$$

It is clear that the background decay in $A(t)$ is simply proportional to $N(t)$; that is,

$$\sum_{j=1}^{k} a_j \exp[-t(\ln 2)/T_j] = fN(t) ,$$

where f is some constant. If f were known and the decay curves $N(t)$ and $A(t)$ were known, then one could easily extract the resonant activity as

$$r(t) = r_1(\nu) \exp[-t(\ln 2)/T_1] = A(t) - fN(t).$$

It is easy to determine f when T_1 is the shortest of the T_j. One simply picks f so that the two curves $A(t)$ and $fN(t)$ agree over the region $t >> T_1$ (usually $t \geqslant 3T_1$ is sufficient). The above technique was used to extract from button NH that portion of its activity due to the $K = 2$ signal. Table V-II gives the pertinent data.

In this procedure f was determined by a least-squares matching of $A(t)$ and $fN(t)$ over the last three points ($t \geqslant 257$ min). Figure V-2 shows a semilogarithmic plot of $r(t)$ vs t. A least-squares computer fit of the function $r_1 \exp[-t(\ln 2)/T_1]$ to the $r(t)$ points yielded the results

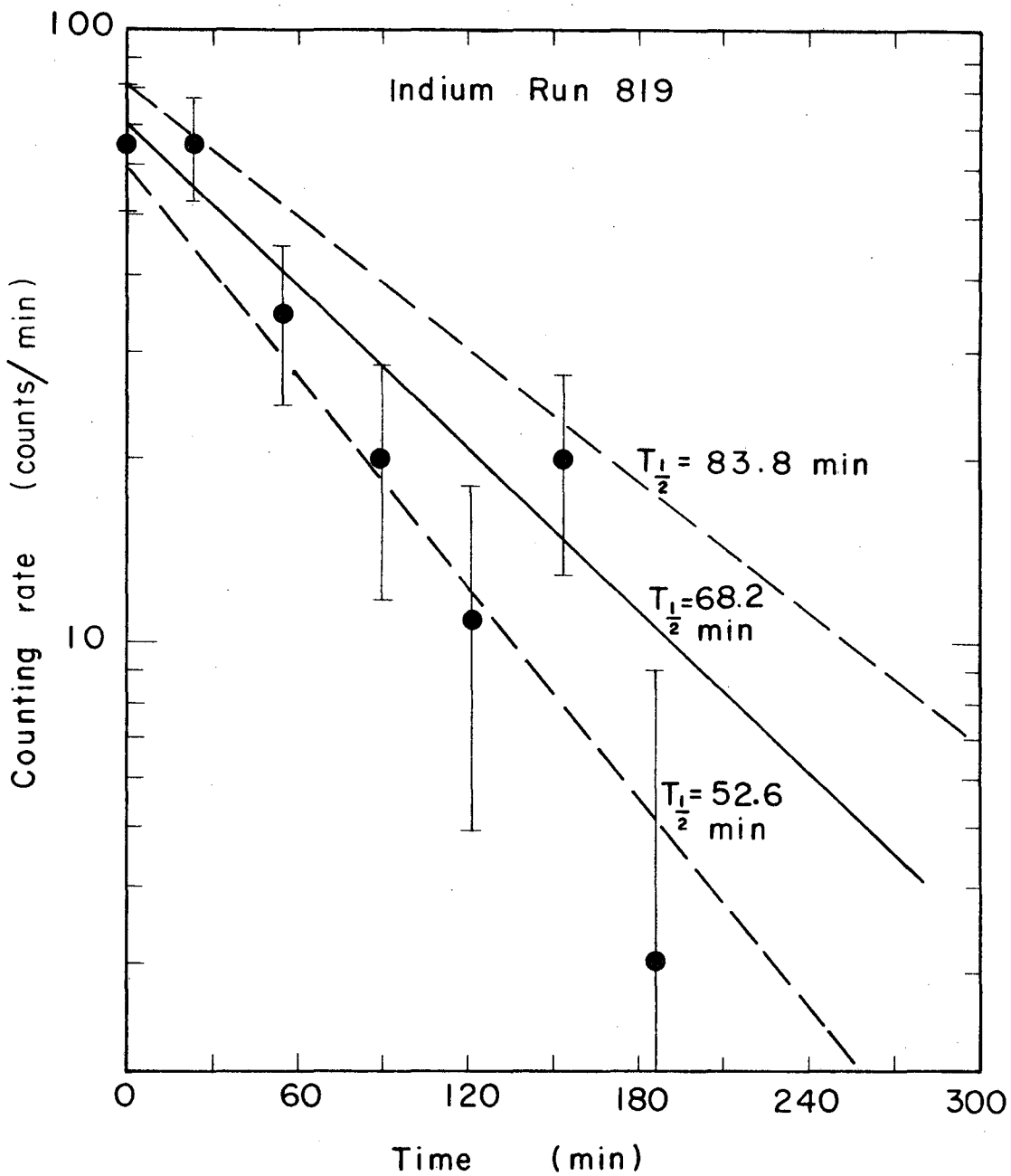

XBL 674-2749

Fig. V-2. Decay of enhanced activity on button NH of indium Run 819. The solid line is a least-squares computer fit to the data; the dashed lines indicate the error in the fit.

Table V-II. Extraction of resonance activity r(t) from comparison of decays of Run 819 buttons NH and MW

t (min)	Counts/min					
	A(t)	δA(t)	N(t)	δN(t)	r(t)	δr(t)
0.0000	15.2300	1.0954	258.9000	7.2553	6.5470	1.5955
23.0000	13.5500	0.8079	208.9533	7.3768	6.5421	1.2458
54.0000	9.1633	0.6306	170.2764	4.7819	3.4526	0.9899
89.0000	6.6633	0.5607	138.0304	4.1753	2.0340	0.8365
122.0000	4.8300	0.5033	111.2000	3.3985	1.1005	0.7097
154.0000	5.2300	0.5163	95.8000	3.1638	2.0170	0.6738
187.0000	3.1966	0.4459	86.2600	4.0798	0.3036	0.6003
219.0000	4.0966	0.4784	77.7620	2.9626	1.4886	0.5956
257.0000	3.1966	0.3153	69.6379	4.0799	0.8611	0.4596
320.0000	1.8079	0.2049	60.1388	2.8916	-0.2089	0.3476
389.0000	1.0300	0.2054	33.1333	1.1170	-0.0812	0.2543

$$T_1 = 68.2 \pm 15.6 \text{ min},$$

$$r_1 = 7.1 \pm 1.1 \text{ counts/min}.$$

This analysis lends strong support to the assignment of I = 2 to the 66-min ^{110}In.

Further evidence in support of the assignment of I = 2 comes from the results of Run 845. Figure V-3 shows a plot of the resonance signal vs the rf frequency at a C-magnet field of 2.62 gauss. The vertical line labeled ν_∞ indicates the predicted frequency (see Eq. IV.1) for I = 2 in the $^2P_{3/2}$ electronic state, assuming that the hfs intervals are infinite (extreme low-field approximation).

The lines at $\nu_\infty + \delta\nu_\infty$ and $\nu_\infty - \delta\nu_\infty$ represent the uncertainty in this predicted frequency due to the error (≈ 0.12 gauss) in calibration of the C-magnet field. A small positive shift of the observed line from ν_∞ is a consequence of the finite value of the hfs intervals.

Figure V-4 shows a similar resonance plot at a field of 10.25 gauss obtained during Run 846. Here the shift from ν_∞ is increased over that of Run 845, as was expected at the increased magnetic field.

At the end of Run 846 again a special decay button (DR) was exposed in order to obtain further evidence for identification of the resonance activity. This button's decay was compared with that of a normalization button (DS) exposed to the unfocused beam. The analysis was the same as used for Run 819 above. The radio frequency during the exposure of DR was 8.251 MHz, i.e., the peak of Fig. V-4.

Table V-III shows the decay data and extraction of the resonance activity for DR compared with DS.

Figure V-5 shows a semilogarithmic plot of the points r(t) vs t of Table V-III. A least-squares fit of $r_1 \exp[-t(\ln 2)/T_i]$ to the points yielded

$$T_1 = 70.1 \pm 2.6 \text{ min},$$

$$r_1 = 278.4 \pm 8.8 \text{ counts/min}.$$

It should be pointed out that the incident α energy for the bombardments of Runs 845 and 846 was ≈ 45 MeV. Thus ^{108}In with a half life of ≈ 58 min was undoubtedly produced by the (α, 3n) process. Because

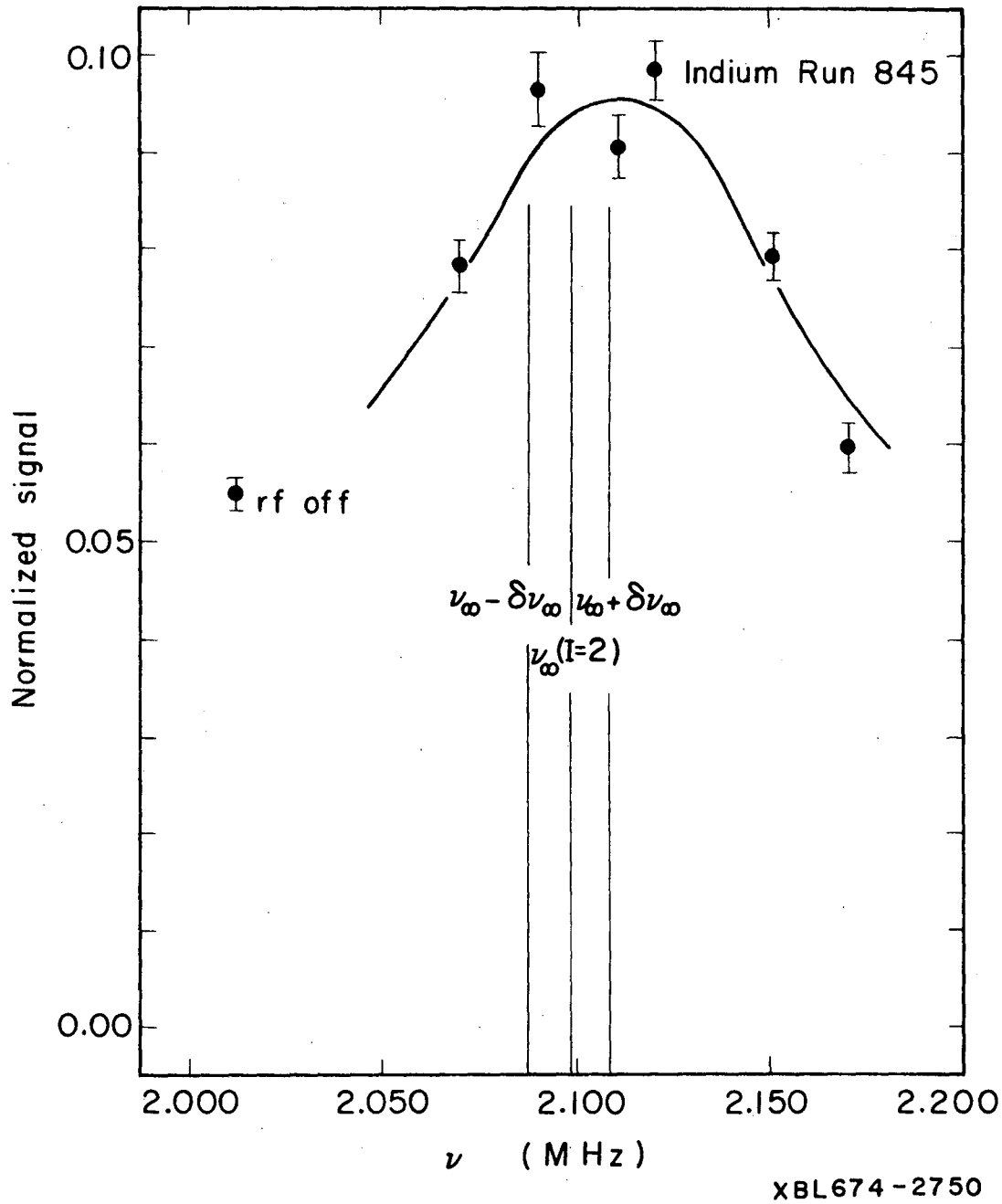

Fig. V-3. Indium Run 845 resonance at ≈ 2.6 gauss. The transition is (F = 3.5, M = - 1.5) ⟷ (F = 3.5, M = - 3.5).

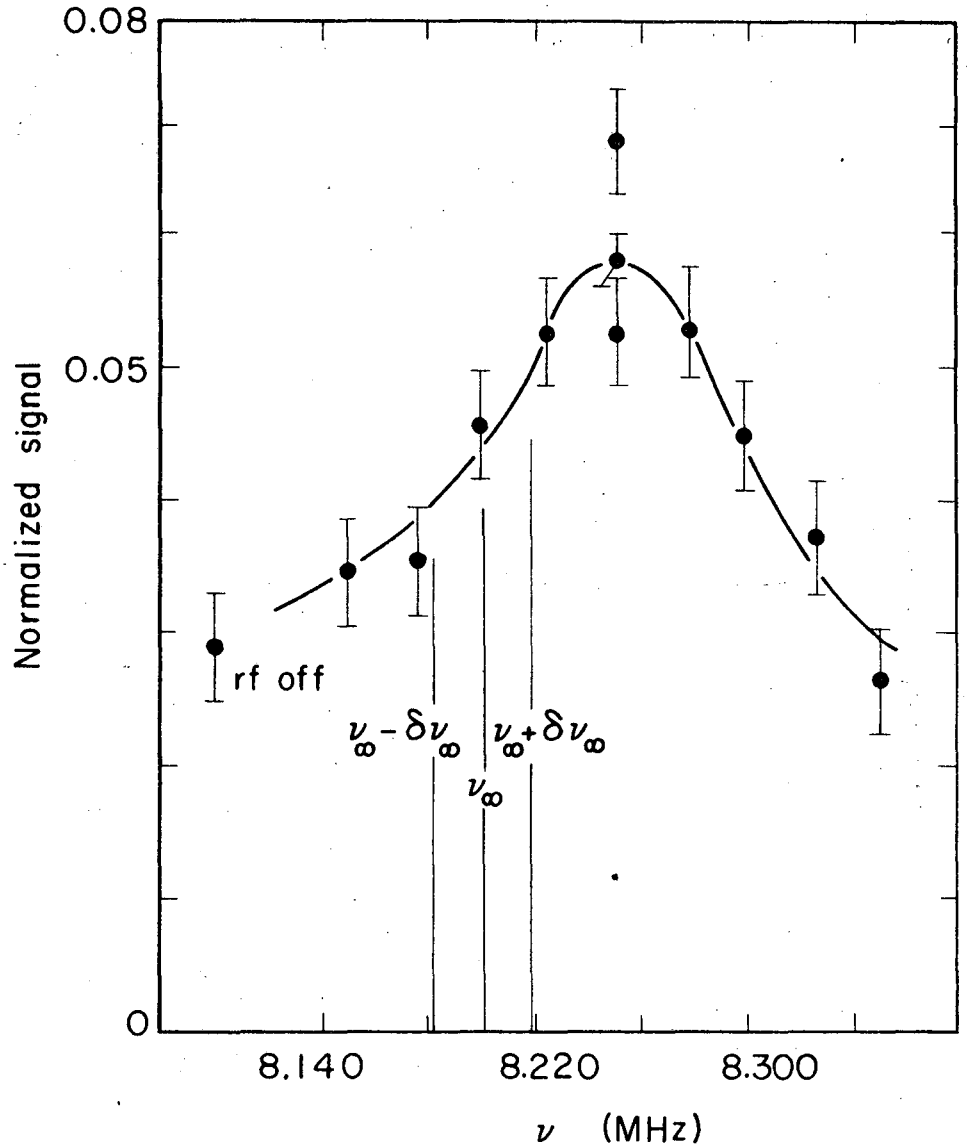

Fig. V-4. Indium Run 846 resonance at ≈ 10.25 gauss. The transition is (F = 3.5, M = - 1.5) ⟷ (F = 3.5, M = - 3.5).

XBL674-2751

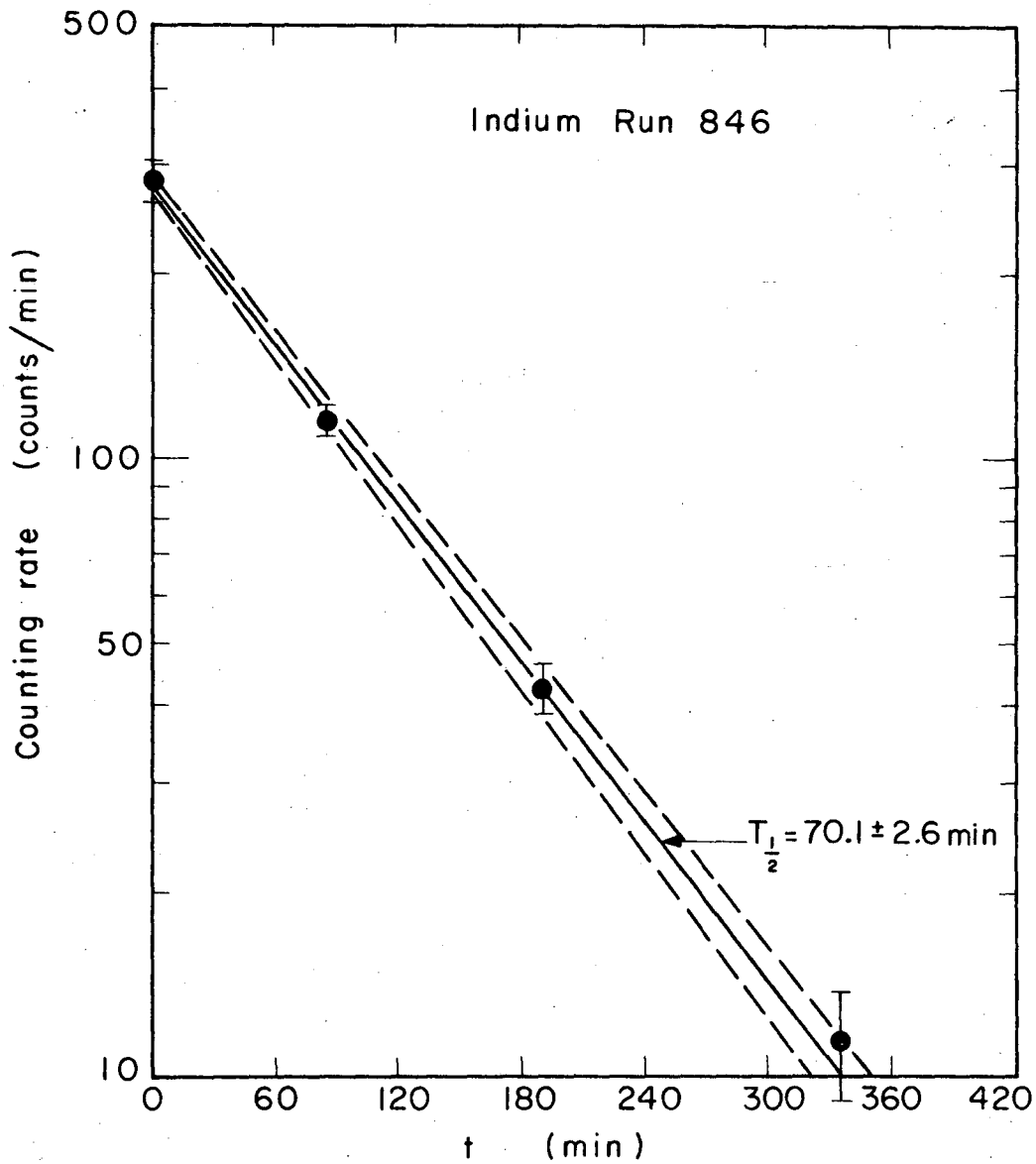

Fig. V-5. Decay of enhanced activity on button DR of indium Run 846. The solid line is a least-squares computer fit to the data; the dashed lines indicate the error in the fit.

XBL674-2752

Table V-III. Extraction of resonance activity r(t) from comparison of decay of Run 846 buttons DR and DS.

t (min)	Counts/min					
	A(t)	δA(t)	N(t)	δN(t)	r(t)	δr(t)
0.0	493.9200	4.9814	7985.9148	42.1882	281.3483	9.4746
86.0	239.6200	3.4785	4680.2311	31.6228	115.0400	5.8894
190.0	120.3200	1.7514	2915.9514	25.1493	42.7022	3.4651
335.0	61.5700	1.2644	1884.4506	14.5403	11.4090	2.3011
788.0	21.7450	0.7758	831.4717	16.0790	- 0.3873	1.2147
966.0	16.3206	0.4740	604.2282	8.4958	0.2370	0.8002
1237.0	12.1700	0.4257	439.1889	4.7538	- 0.4795	0.6244
2392.0	6.9400	0.2783	249.5374	7.1396	0.2977	0.4192
3290.0	4.8683	0.2631	207.7401	3.5736	- 0.6613	0.3484

of the uncertainty (≈ 10%) in the determination of the half lives of ^{108}In and ^{110}In, one cannot conclusively state that the decay analysis of Run 846 identifies the resonance as due only to ^{110}In. The possibility exists that ^{108}In also has I = 2 and that the resonances of Runs 845 and 846, Figs. V-3 -V-4, are combinations of ^{108}In and ^{110}In signals. Thus although the fit $T_1 = 70.1 \pm 2.6$ min favors a half life of ≈ 66 min over one of ≈ 58 min, one must regard the results of 845 and 846 only as confirming the existence of a 1-h activity (or activities) with I = 2, and rely on the decay analysis of Run 819, Table V-II and Fig. V-2, as establishing that at least ^{110}In has I = 2.

D. Interpretation of Results

^{110}In has an odd-odd nucleus with Z = 49 and N = 61; thus it has one proton hole short of and 11 neutrons beyond the closed major shell Z = 50 or N = 50. The proton hole is in the $1g_{9/2}$ subshell, as indicated by the observed ground-state spin I = 9/2 for all the odd-mass indium isotopes ^{109}In through ^{117}In. The configuration of the last 11 neutrons in ^{110}In may be taken as that for ^{109}Cd, which has Z = 48 and N = 61; ^{109}Cd has been observed to have I = 5/2. The 11 neutrons are distributed with five in the $2d_{5/2}$ and six in the $1g_{7/2}$ subshell. Thus the ^{110}In spin I = 2 probably arises from the coupling of a $1g_{9/2}$ proton hole and a $2d_{5/2}$ neutron hole. The coupling rules for odd-odd nuclei given in Section III may be applied. Since $g_{9/2}$ and $d_{5/2}$ both are cases in which j = l+1/2, the weak particle-particle (same as hole-hole) rule predicts I = 9/2+5/2 = 7 or I = 9/2 - 5/2 = 2. The theory is ambiguous because of the nearness in energy of these two spin states; however, the spin of 4.9-h ^{110m}In has been observed by Marino[19] to be I = 7. The theory then makes the assignment of I = 2 to the 66-min ground state ^{110}In.

VI. RESEARCH ON ^{121}Sn

A. Production of the Isotope

Radioactive ^{121}Sn with a half life of 27 h may easily be produced by irradiation of 33% abundant ^{120}Sn in the core of a nuclear reactor. The process, written ^{120}Sn (n, γ) ^{121}Sn, involves the absorption of a thermal neutron by the ^{120}Sn nucleus and emission of one or more γ rays. The cross section for the ^{120}Sn (n, γ) ^{121}Sn reaction is ≈ 0.14 barn. One-gram samples encapsulated in quartz were irradiated for 3-day periods in the General Electric reactor at Vallecitos, California. Many other activities are produced from unenriched Sn by the (n, γ) process on the other even-mass Sn isotopes. However, calculations show and observation confirms that for a 3-day irradiation the cross sections, abundances, and half lives are such that 27-h ^{121}Sn is the overwhelming activity present during the first week after irradiation. After this period the residual activity is primarily due to ^{113}Sn, with a 118-day half life. Immediately after irradiation the ^{121}Sn activity is some 200 times that from ^{113}Sn.

The flux in the General Electric reactor, $\approx 1 \times 10^{14}$ neutrons/cm^2/sec, produced ≈ 0.5 curie per gram of Sn metal. ^{121}Sn is a low-energy β^- emitter, and consequently shielding and handling problems were minimal.

Since the ^{121}Sn was produced in metallic form in the unactivated stable Sn, no chemical separation or addition of carrier material was required before the sample was introduced into the beam device.

B. Properties of the Atomic Beam

The electronic configuration of the ground state of Sn is $5s^2 5p^2$. This configuration yields the five electronic states listed in Table VI-I below. Also included are the separations from the ground $^3P_0$ state, the percentage of the atomic beam (at 1400°C) present in each state, and the electronic g factor, g_J. It is impossible to deflect the $^3P_0$ atoms in our beam device, and all work reported here was carried out in the excited $^3P_1$ state.

The atomic beam was produced by electron bombardment of a tantalum oven containing a carbon crucible and lid. The Sn was placed inside the crucible, and the beam exited by way of a carbon snout,

Table VI-I. Sn beam properties.

State	Energy (cm^{-1})	% of beam atoms in state	g_J(Ref. 20)
$^3P_0$	0.0	52.7	0
$^3P_1$	1691.8	34.8	-1.50110(7)
$^3P_2$	3427.7	12.4	-1.44878(9)
$^1D_2$	8613.0	0.131	-1.05230(8)
$^1S_0$	17162.6	≈ 0	0

≈ 3/8-in. long, which passed through the tantalum wall and projected beyond the main body of the oven ≈ 1/4-in. The end of the snout just passed through the loop of the electron filament; thus the snout end was kept hot to insure that good excitation of the $^3P_1$ state occurred and that no Sn would collect inside and block passage from the oven. The snout end had a 0.004-in. slit sawed in it to form the source slit for the atomic beam.

Typical electron bombardment power was 160 to 200 watts. This produced side-button normalization signals of 300 to 900 counts/min after 5 min of collection. Resonance signals ranged from 20 to 80 counts/min.

C. Spin Measurement

The nuclear spin I of ^{121}Sn was measured by observation of rf transitions between low-field Zeeman levels in the hfs state with $F = I + J$. Because $J = 1$, a single transition changing m_F by ±1 in the C field does not satisfy the machine selection rule $m_J(A) = - m_J(B)$. However, as was shown in Sec. IV, at low field the Zeeman levels are equally spaced by an amount $h\nu$, where

$$\nu = g_F \frac{\mu_0}{h} H_C .$$

Because the levels are equally spaced, by suitable adjustment of the rf field intensity, it is possible to induce transitions yielding $\Delta m_F = \pm 2$. One of these transitions corresponds at the high field of the A and B magnets to the transition $m_J = \pm 1 \rightarrow m_J = \mp 1$, thus satisfying the machine selection rule for observation of a flop-in signal. Such double quantum transitions at frequency ν may be observed with decreasing intensity as H_C is increased until the low-field approximation of equal-level spacing is violated by several resonance line widths.

Figure VI-1 shows the results of a spin search at $H_C = 1.25$ gauss. The large signal at $I = 3/2$ is approximately 3.5 times the background level indicated by the two points labeled "r.f. off." The small signal at $I = 5/2$ is due to the low-frequency wing of the 0.130-MHz full width at half maximum $I = 3/2$ resonance.

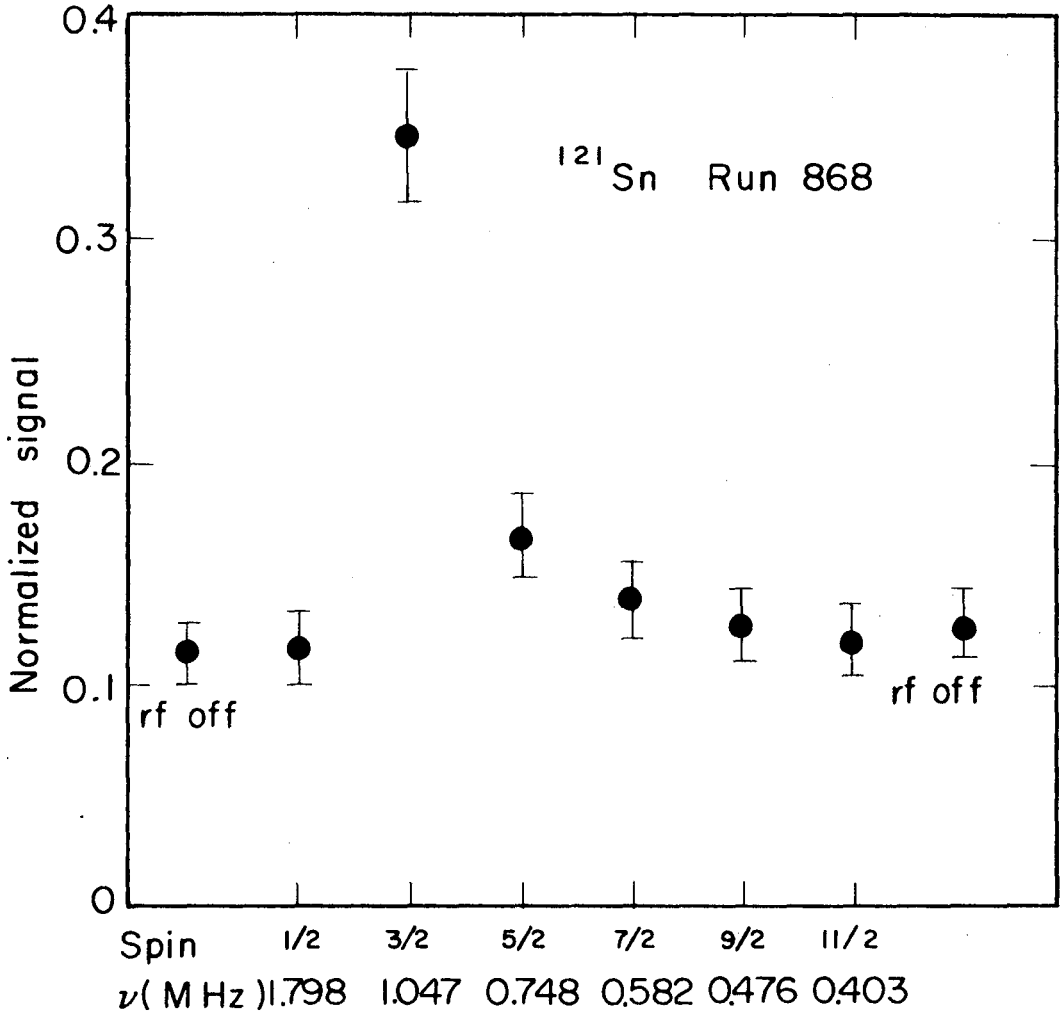

XBL674-2753

Fig. VI-1. ^{121}Sn Run 868 spin search at 1.25 gauss.

The $I = 3/2$ signal was identified as due to 27-h ^{121}Sn by following the decay of the resonance button radioactivity for several days to establish its characteristic half life. Figure VI-2 shows a semi-logarithmic plot of the decay. For the first 4 days the points fall on or near the line for straight 27-h decay; after this the rate of decay slows, indicating approach to that of the prominent residual activity, 118-day ^{113}Sn. The overwhelming activity on the $I = 3/2$ button, and indeed in the entire sample, was 27-h ^{121}Sn.

D. hfs Measurements and Results

Several different types of rf resonances were observed in ^{121}Sn at various magnetic fields in order to obtain values for the magnetic dipole and electric quadruple interaction constants a and b. These types are summarized in Table VI-II.

Figure VI-3 shows an energy-level diagram for the ^{121}Sn $^3P_1$ hyperfine states in a magnetic field extending to 190 gauss. Indicated by vertical lines are the states connected by observed resonances. The solid lines indicate single-frequency Type I or III resonances; the dashed lines indicate two-frequency Type II or IV resonances.

Table VI-III lists all the observational data. The resonances are listed in the order in which they were observed. For a Type I resonance the frequency listed is twice the applied rf frequency, since two quanta were required to make the transition.

As with all atomic beam research, the philosophy used here was to proceed as much as possible from regions of rf frequency and C-magnet field where resonances had been observed into regions where they had not. Observations of new resonances allowed extrapolation to higher magnetic field or to another type of transition, each time narrowing the error in a and b.

The Type I resonance which had been used to measure I (because it is independent of a and b at low field) was followed up in magnetic field to approximately 35 gauss (resonance 892A1); at this field the signal-to-background ratio had dropped to 0.5 whereas, at low field, it had been approximately 3.5. It was expected that this would occur because of the breakdown of the low-field approximation of equal Zeeman

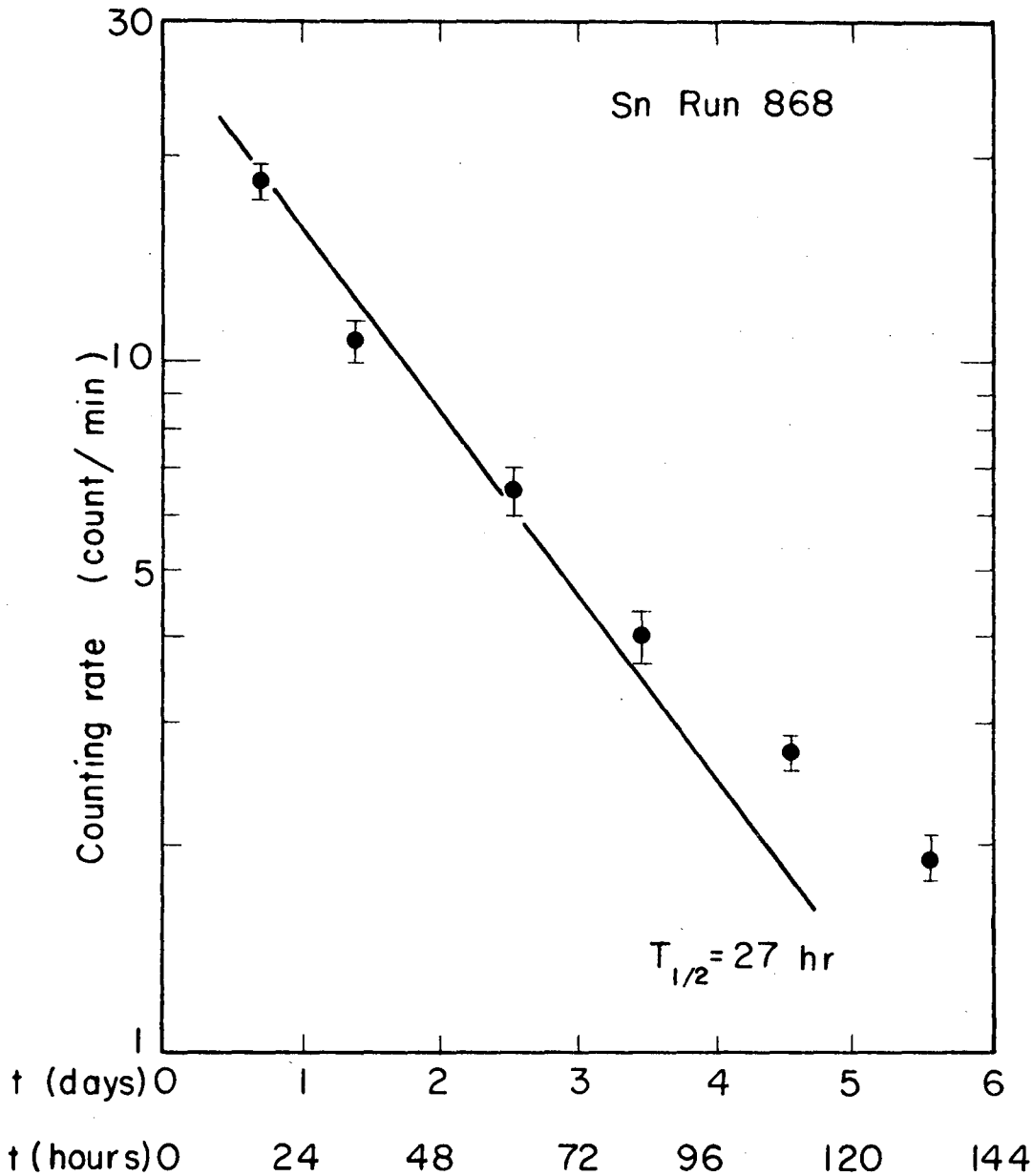

XBL674-2754

Fig. VI-2. Decay of activity on I = 3/2 button IG from ^{121}Sn Run 868.

Table VI-II. Types of resonance observed.

Type	Quantum Numbers: Level 1	Level 2	Level 3	rf Requirements	Comments
I	F, M_F		$F, M_F \pm 2$	one signal at $\nu = [E(1)-E(3)]/2h$	Double quantum transition vanishes as field is increased
II	F, M_F	$F, M_F \pm 1$	$F, M_F \pm 2$	two signals at $\nu_{12} = [E(1) - E(2)]/h$ and $\nu_{23} = [E(2)-E(3)]/h$	Two single-quantum transitions in cascade
III	F, M_F	$F \pm 1, M_F \pm 1$		one signal at $\nu = [E(1)-E(2)]/h$	Single quantum transition
IV	F, M_F	$F \pm 1, M_F \pm 1$	$F \pm 2, M_F \pm 2$	Same as Type II	Same as Type II

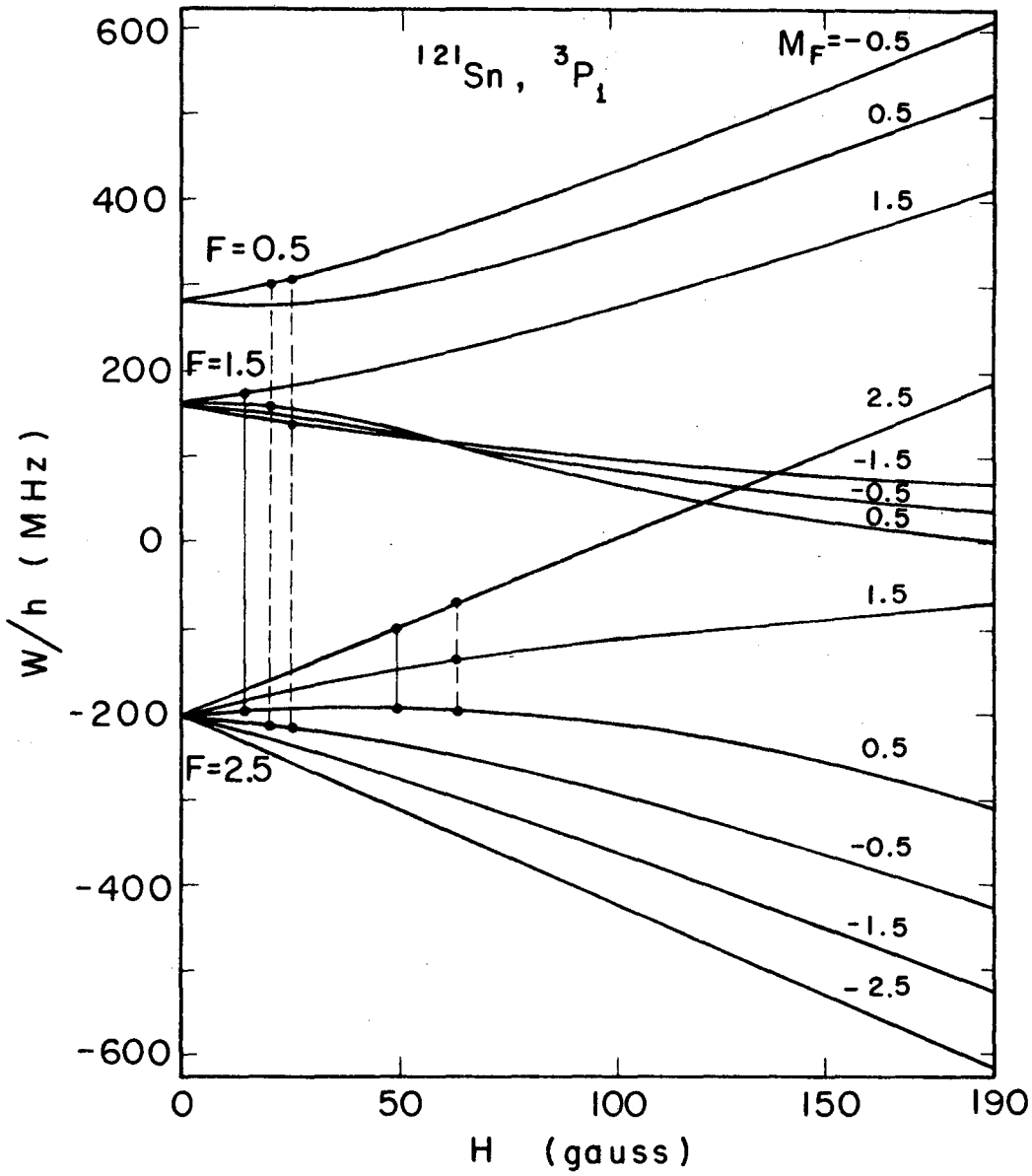

XBL674-2755

Fig. VI-3. Energy-level diagram for the $^3P_1$ hfs levels of 27-h ^{121}Sn. The diagram is drawn for hfs constants a, b < 0.

level spacing. Figure VI-4 shows resonance 871D2; this is a Type I resonance at approximately 17.3 gauss.

Because the Type I resonance was unobservable at fields much above 35 gauss, the Type II technique, involving superposition of two rf fields in the C region, was developed to allow observation of Zeeman resonances at higher magnetic fields. The technique required rf fields at frequencies matching the two energy intervals which make up the Type I double-quantum interval--that is, one frequency corresponding to the $(F=5/2,\ M=3/2) \longleftrightarrow (F=5/2,\ M=1/2)$ interval and one corresponding to the $(F=5/2,\ M=5/2) \longleftrightarrow (F=5/2,\ M=3/2)$ interval. With the rf field intensities properly set, one then in effect has atoms making the Type I double-quantum transition $(F=5/2,\ M=1/2) \longleftrightarrow (F=5/2,\ M=5/2)$; however, two different frequencies were required to connect these levels with the intermediate $M=3/2$ level at fields above approximately 35 gauss.

The operation of the Type II and Type IV two-frequency resonance technique can be understood qualitatively by considering an arbitrary three-level system, as shown in Fig. VI-5. It is desired to cause an atom in state A to make the transition to state C by superimposing the two rf fields at frequencies ν_1 and ν_2. It must be emphasized that in the experiments described here a single conductor carried the two rf signals ν_1 and ν_2 into the C-magnet field; thus they were superimposed in the space through which the beam passed. With P_1 the probability that an atom will make the transition B to C or C to B, one can write for an atom starting in state A the following:

Transition	Normalized probability
(a) $A \rightarrow B \rightarrow C$	$P_1 P_2 / [P_1(P_1+P_2) + 2(1-P_1)^2]$
(b) $A \rightarrow B \rightarrow A$	$P_1^2 / [P_1(P_1+P_2) + 2(1-P_1)^2]$
(c) $A \rightarrow A \rightarrow A$	$2(1-P_1)^2 / [P_1(P_1+P_2) + 2(1-P_1)^2]$.

Only two-step processes have been considered, since they are the simplest which give the desired effect $(A \rightarrow B \rightarrow C)$, and because it is possible by adjusting the rf field intensities to severely limit higher-step processes. It is desired to maximize the probability for occurrence

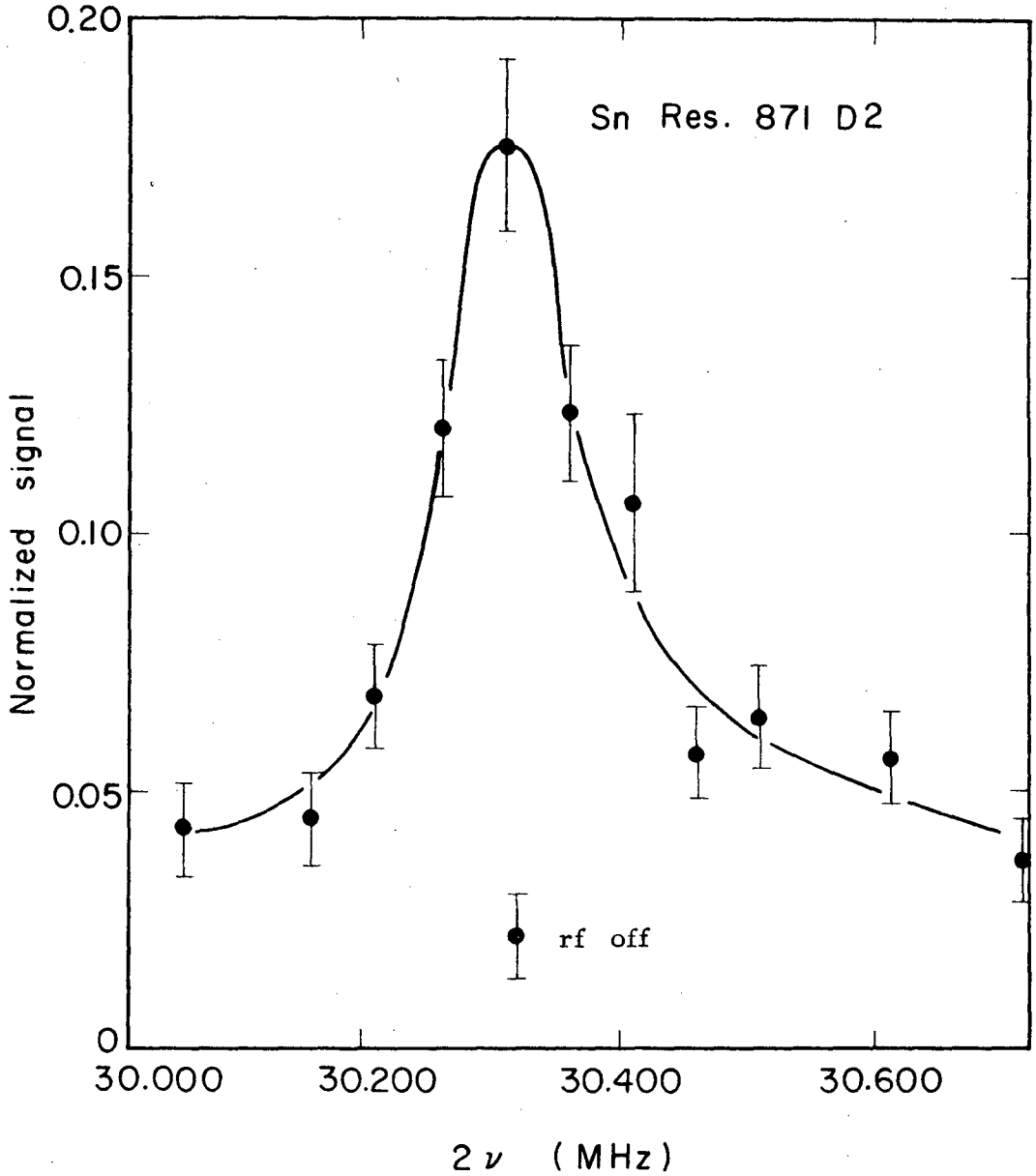

XBL674-2756

Fig. VI-4. ^{121}Sn Type I resonance 871D2 at 17.3 gauss. The levels connected are (F = 2.5, M = 2.5) and (F = 2.5, M = 0.5).

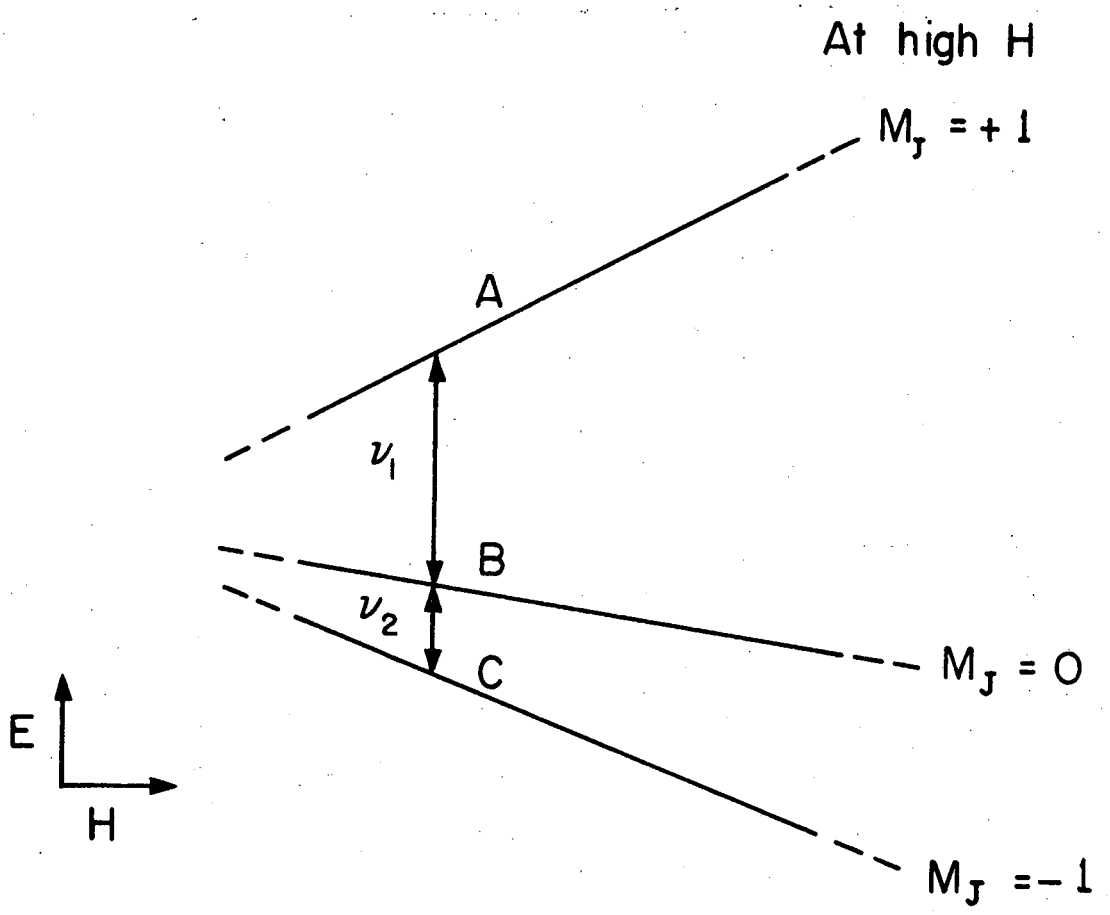

Fig. VI-5. Three-level system.

XBL674-2757

of transition (a), since it is the only two-step process observable. If one assumes that $P_1 = P_2$ then it is easy to show that the (a) process has a maximum probability of 1/2 when $P_1 = 1$; (b) and (c) then have probabilities 1/2 and 0. Hence under ideal conditions one can expect 1/2 of the atoms starting in state A to end in state C when emerging from the rf region. Similarly 1/2 of the atoms starting in C will end in A.

The implementation of the two-frequency technique required two rf generators, rf power amplifiers, a means of measuring the two frequencies, and a device for mixing the two signals before transmission into the C-magnet field.

One generator was set to the predicted frequency ν_1 for one of the transitions, say A$\leftrightarrow$B, and the other was varied until a signal corresponding to the B$\leftrightarrow$C transition was detected. This resonance was traced out with ν_1 held fixed; once the peak of the B$\leftrightarrow$C resonance was determined, ν_2 was set there and ν_1 was varied to locate the peak of the A$\leftrightarrow$B resonance. One could then set ν_1 at its peak value and recheck the location of the peak of the B$\leftrightarrow$C resonance by varying ν_2. This process of hopping back and forth from one resonance to the other, holding one generator at the fixed frequency of its resonance peak while varying the other, could be carried out until the peak frequencies no longer changed; at this point one had located the frequencies of the A$\leftrightarrow$B and B$\leftrightarrow$C transitions at the particular magnetic field setting and could proceed to a higher field, using the new data to predict new starting values for ν_1 and ν_2. In practice it was found that one could locate the two peak frequencies uniquely with only one or two sweeps of each resonance.

Figure VI-6 shows the Type II two-frequency resonances 892DC and 892DD observed at 24.3 gauss. At this field the two transitions $(F_1=5/2, M_1=5/2)\leftrightarrow(F_2=5/2, M_2=3/2)$ and $(F_1=5/2, M_1=3/2)\leftrightarrow(F_2=5/2, M_2=1/2)$ are separated in frequency by approximately 1 MHz.

The Type II resonances were followed up in magnetic field to approximately 90 gauss (894DA and 894DB). These observations narrowed the error in the predicted frequency for the low-field Type III

hyperfine transition ($F_1=3/2$, $M_1=3/2$)$\leftrightarrow$($F_2=5/2$, $M_2=1/2$) so that a search for it became practical. This is a single-quantum transition at low magnetic fields, and it was observed in Run 897 at fields of 0.9 and 1.3 gauss. Figure VI-7 shows resonance 897A1. The resonance was observed twice to insure that it had the predicted dependence on magnetic field.

The $F=3/2 \leftrightarrow F=5/2$ hyperfine interval has the dependence on a and b given by Eq. II.15 which yields

$$[E_{hfs\ (3/2)} - E_{hfs\ (5/2)}]/h = -2.5a - 1.25b.$$

The Type III observations fixed the left-hand side of the above at 362.280±0.040 MHz, thus yielding one equation in a and b. Independent knowledge of a and b however, was not sufficient at this stage to predict the $F=3/2$ to $F=1/2$ hfs interval with enough precision to allow observations connecting states in these levels. Hence the Type II resonances were pursued up to 183 gauss to reduce the predicted uncertainty in the $3/2 \leftrightarrow 1/2$ interval. Figure VI-8 and VI-9 show the Type II resonances 900BA and 900BB obtained at 183 gauss.

The $F=3/2$ to $F=1/2$ interval was measured by observation of a series of low-field Type IV resonances—the 901 resonances listed in Table VI-III. These two-frequency resonances were observed by using one rf field connecting the 5/2 F level to the 3/2 F level and another connecting the 3/2 to the 1/2. Figure VI-10 shows the rf circuit used for Run 901. The hybrid junction allowed approximately 50 db isolation of the ν_1 circuit from the ν_2 circuit while mixing the two rf signals. Figure VI-11 and VI-12 show the resonances 901BA and 901BB obtained at 2.5 gauss.

Having measured the two hfs intervals, $5/2 \leftrightarrow 3/2$ and $3/2 \leftrightarrow 1/2$, a and b were uniquely determined in magnitude. A computer fit (by the routine HYPERFINE) of calculated frequencies to the 32 observed frequencies varying a and b yielded the results listed in Table VI-IV together with the χ^2 of the fits.

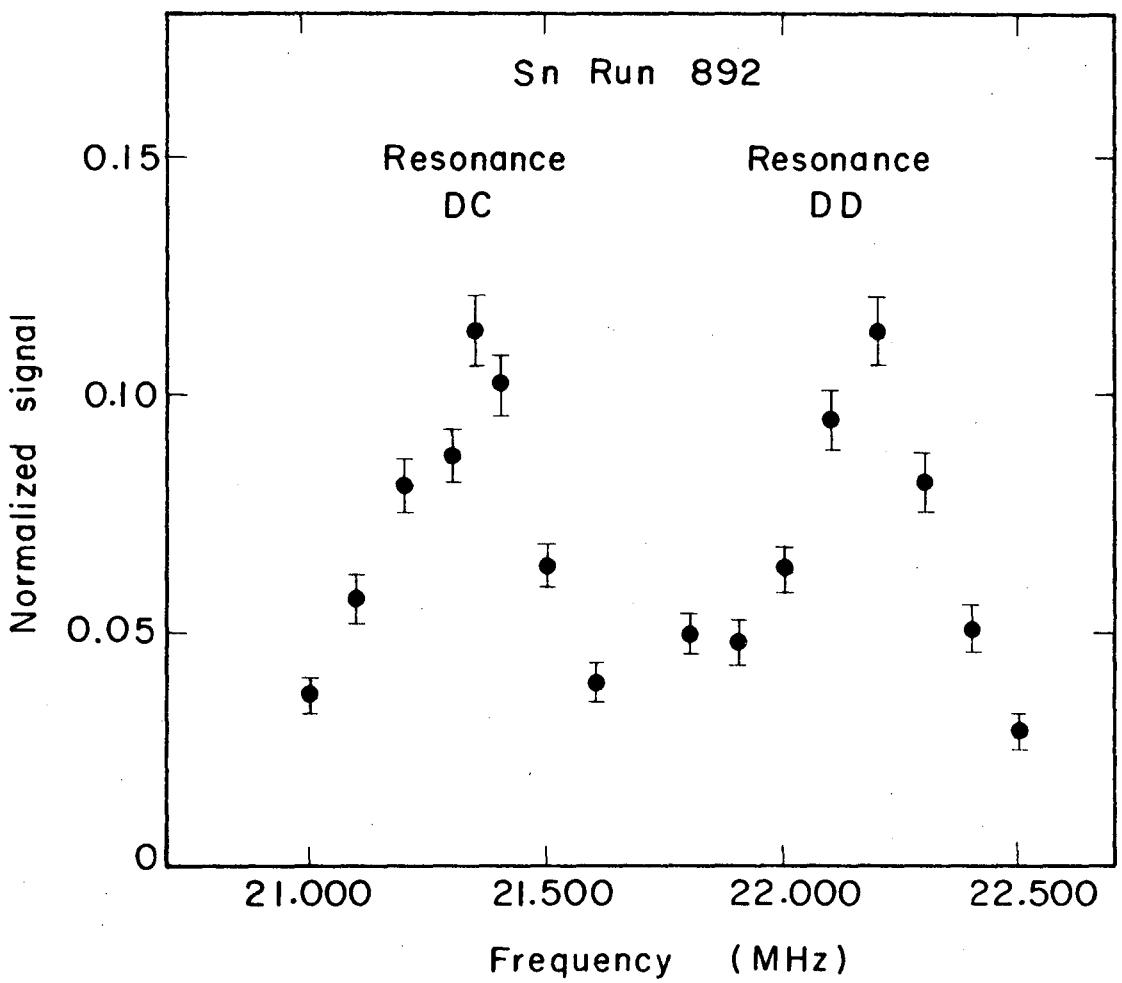

XBL674-2758

Fig. VI-6. ^{121}Sn Type II resonances 892DC and 892DD at 24.3 gauss. The levels connected in DC are (F = 2.5, M = 1.5) and (F = 2.5, M = 0.5), those in DD are (F = 2.5, M = 2.5) and (F = 2.5, M = 1.5).

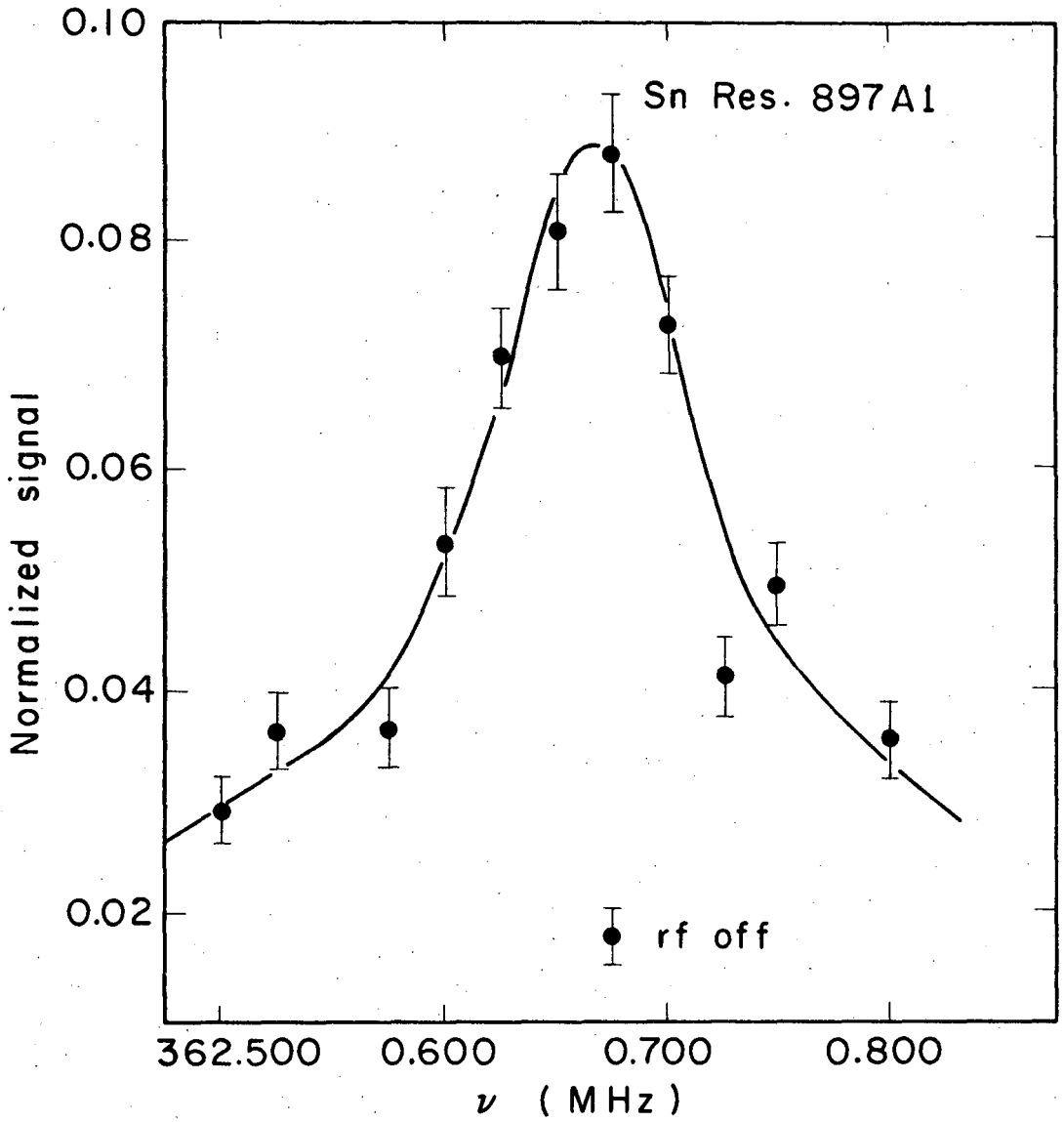

Fig. VI-7. ^{121}Sn Type III hyperfine-transition resonance 897A1 at 0.9 gauss. The levels connected are (F = 1.5, M = 1.5) and (F = 2.5, M = 0.5).

XBL674-2759

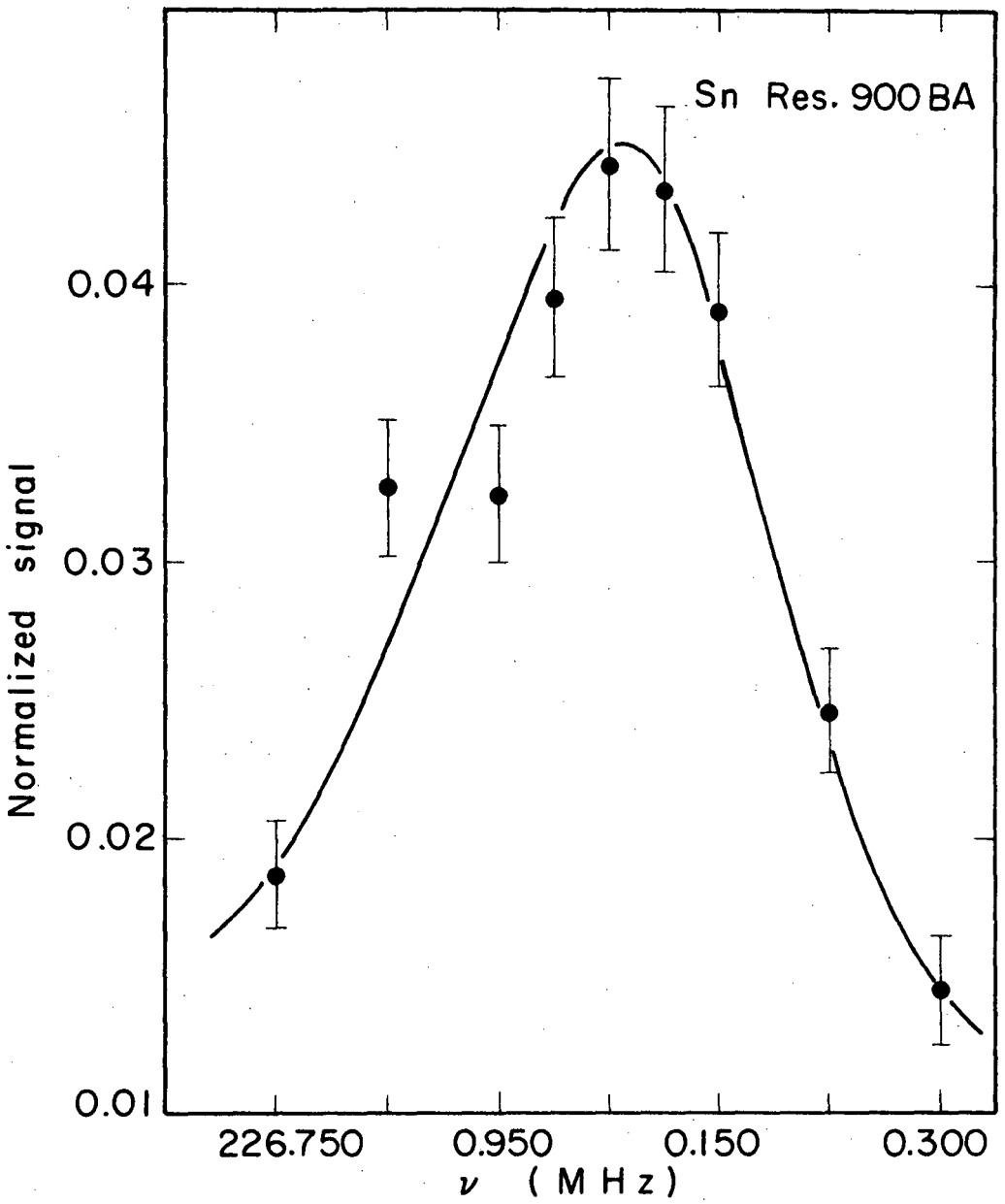

XBL674-2760

Fig. VI-8. ^{121}Sn Type II resonance 900BA at 183 gauss. The levels connected are (F = 2.5, M = 1.5) and (F = 2.5, M = 0.5).

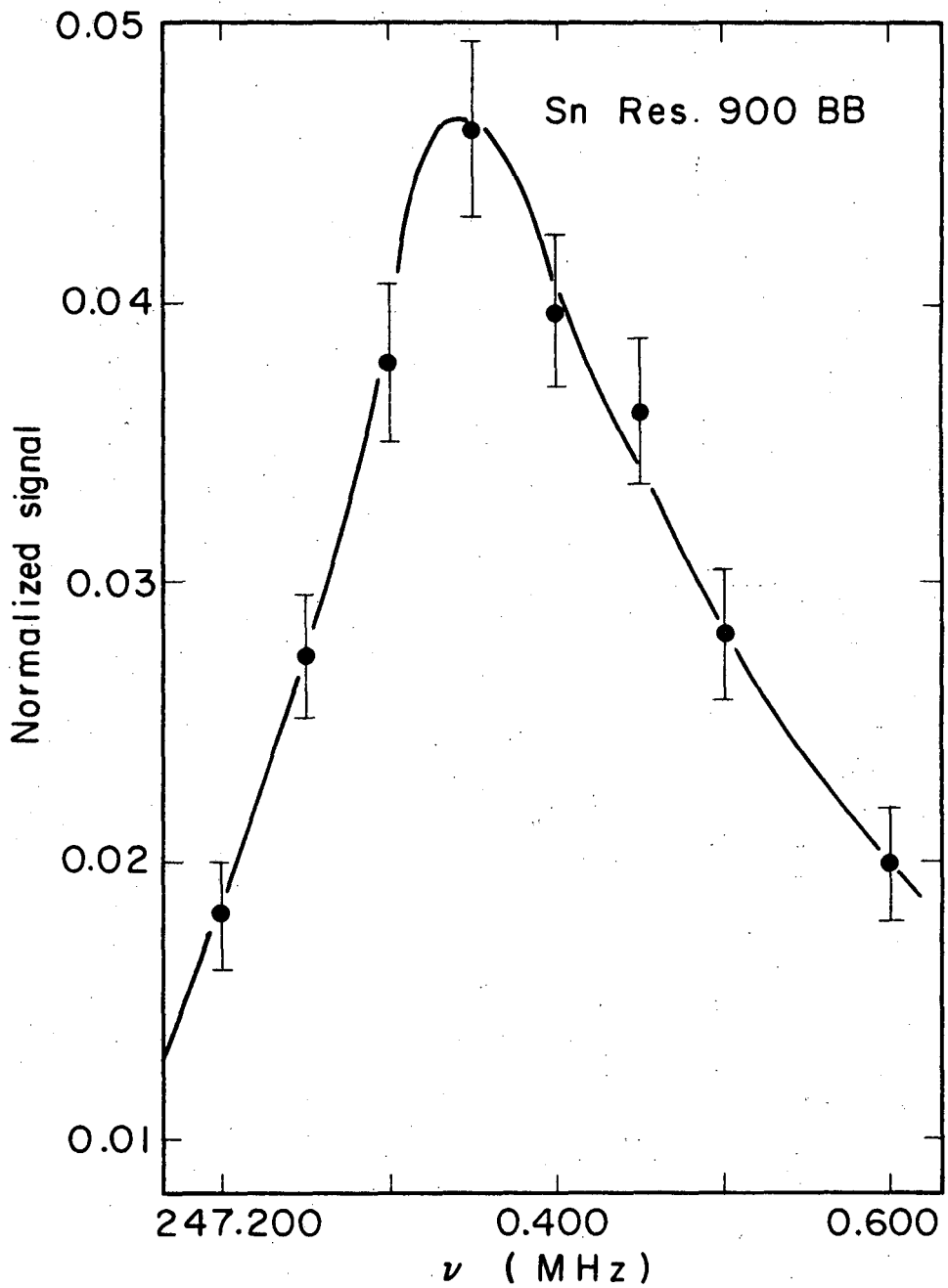

XBL674-2761

Fig. VI-9. ^{121}Sn Type II resonance 900BB at 183 gauss. The levels connected are (F = 2.5, M = 2.5) and (F = 2.5, M = 1.5).

Table VI-III. Observations on ^{121}Sn (32 observations).

	Calibration isotope data			C-Magnet field (gauss)		^{121}Sn Resonances								
Res. No.	Name	Frequency (MHz)	Freq. error (MHz)	H	ΔH	Res. type	F_1	M_1	F_2	M_2	Frequency (MHz)	Freq. error (MHz)	$\nu_{obs} - \nu_{calc}$ (MHz)	Weight factor
868A4	CS133	0.4380	0.0250	1.2515	0.0714	I	5/2	5/2	5/2	1/2	2.0600	0.0500	-0.04984	58.5
871A1	CS133	0.9890	0.0200	2.8247	0.0571	I	5/2	5/2	5/2	1/2	4.7040	0.0500	-0.07754	83.5
871B1	CS133	2.0130	0.0180	5.7449	0.0513	I	5/2	5/2	5/2	1/2	9.7600	0.0500	-0.03855	96.3
871C1	CS133	3.9230	0.0150	11.1796	0.0426	I	5/2	5/2	5/2	1/2	19.2360	0.2000	-0.10045	21.9
871D2	CS133	6.0730	0.0180	17.2783	0.0510	I	5/2	5/2	5/2	1/2	30.3100	0.0300	-0.04311	103.7
872A1	CS133	6.9750	0.0180	19.8310	0.0509	I	5/2	5/2	5/2	1/2	35.0300	0.0600	-0.03342	79.7
876A2	CS133	8.8560	0.0180	25.1431	0.0508	I	5/2	5/2	5/2	1/2	45.0500	0.0600	-0.00462	77.2
891C1	RB85	2.3731	0.0300	5.0645	0.0638	I	5/2	5/2	5/2	1/2	8.7000	0.1500	0.07716	28.9
891D3	RB85	14.2894	0.0400	29.9127	0.0818	I	5/2	5/2	5/2	1/2	54.5000	0.2000	0.25485	15.3
892A1	RB85	16.7301	0.0300	34.8861	0.0609	I	5/2	5/2	5/2	1/2	64.0500	0.1330	-0.00215	30.8
892DC	RB85	11.5600	0.0500	24.3052	0.1032	II	5/2	3/2	5/2	1/2	21.3500	0.1000	0.07818	53.1
892DD	RB85	11.5600	0.0500	24.3052	0.1032	II	5/2	5/2	5/2	3/2	22.2000	0.0750	0.01026	62.5
894AA	RB85	15.5459	0.0200	32.4779	0.0407	II	5/2	3/2	5/2	1/2	28.8250	0.0800	0.01462	127.4
894AB	RB85	15.5459	0.0200	32.4779	0.0407	II	5/2	5/2	5/2	3/2	30.4500	0.0500	-0.01429	233.1
894BA	RB85	21.7466	0.0300	44.9888	0.0599	II	5/2	3/2	5/2	1/2	40.7500	0.0500	-0.00460	168.9
894BB	RB85	21.7466	0.0300	44.9888	0.0599	II	5/2	5/2	5/2	3/2	43.9750	0.0750	0.03993	99.0
894CA	RB85	31.9065	0.0400	64.9741	0.0775	II	5/2	3/2	5/2	1/2	60.9750	0.0500	-0.01922	109.2
894CB	RB85	31.9065	0.0400	64.9741	0.0775	II	5/2	5/2	5/2	3/2	67.5000	0.0500	0.04901	85.6
894DA	RB85	45.0974	0.0250	90.0202	0.0465	II	5/2	3/2	5/2	1/2	88.8000	0.2000	-0.09901	23.2
894DB	RB85	45.0974	0.0250	90.0202	0.0465	II	5/2	5/2	5/2	3/2	100.2000	0.1000	-0.03509	70.8
897A1	RB85	0.4312	0.0300	0.9231	0.0642	III	3/2	3/2	5/2	1/2	362.6750	0.0300	-0.00017	597.0
897B1	RB85	0.6282	0.0300	1.3445	0.0641	III	3/2	3/2	5/2	1/2	362.8500	0.0400	-0.00913	417.3
900AA	RB85	70.1277	0.0300	134.9826	0.0520	II	5/2	3/2	5/2	1/2	148.5400	0.0750	-0.00731	86.5
900AB	RB85	70.1277	0.0300	134.9826	0.0520	II	5/2	5/2	5/2	3/2	167.1550	0.0500	0.00642	107.3
900BA	RB85	98.8927	0.0300	182.9667	0.0482	II	5/2	3/2	5/2	1/2	227.0750	0.0750	0.03134	77.3
900BB	RB85	98.8927	0.0300	182.9667	0.0482	II	5/2	5/2	5/2	3/2	247.3650	0.0600	0.03542	93.8
901AA	RB85	0.9185	0.0300	1.9650	0.0641	IV	1/2	-1/2	3/2	1/2	121.2250	0.0400	0.01042	344.5
901AB	RB85	0.9185	0.0300	1.9650	0.0641	IV	3/2	1/2	5/2	-1/2	363.6200	0.0300	0.00915	377.3
901BA	RB85	1.1718	0.0200	2.5056	0.0427	IV	1/2	-1/2	3/2	1/2	121.5150	0.0400	-0.01491	442.2
901BB	RB85	1.1718	0.0200	2.5056	0.0427	IV	3/2	1/2	5/2	-1/2	363.9550	0.0300	-0.00494	608.2
901CA	RB85	0.9035	0.0250	1.9329	0.0534	IV	1/2	-1/2	3/2	-3/2	123.3250	0.0600	0.03547	91.2
901CB	RB85	0.9035	0.0250	1.9329	0.0534	IV	3/2	-3/2	5/2	-1/2	361.5000	0.0150	0.00304	1507.6

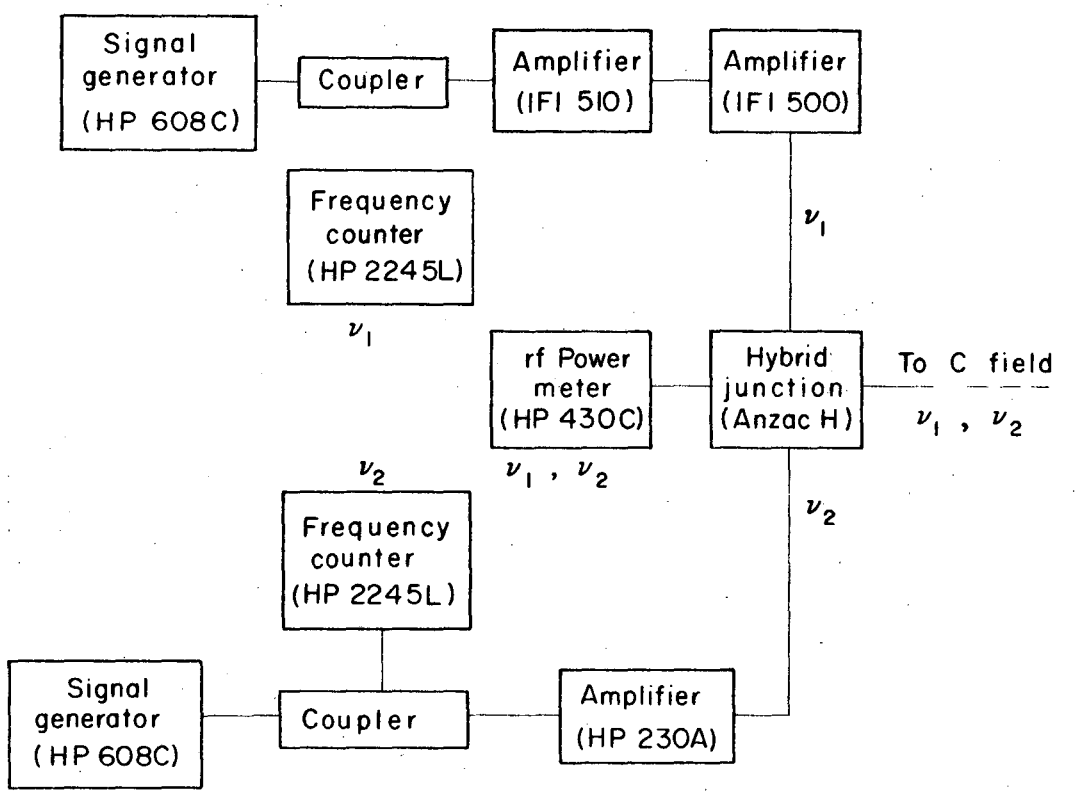

XBL674-2762

Fig. VI-10. The rf circuit for Run 901.

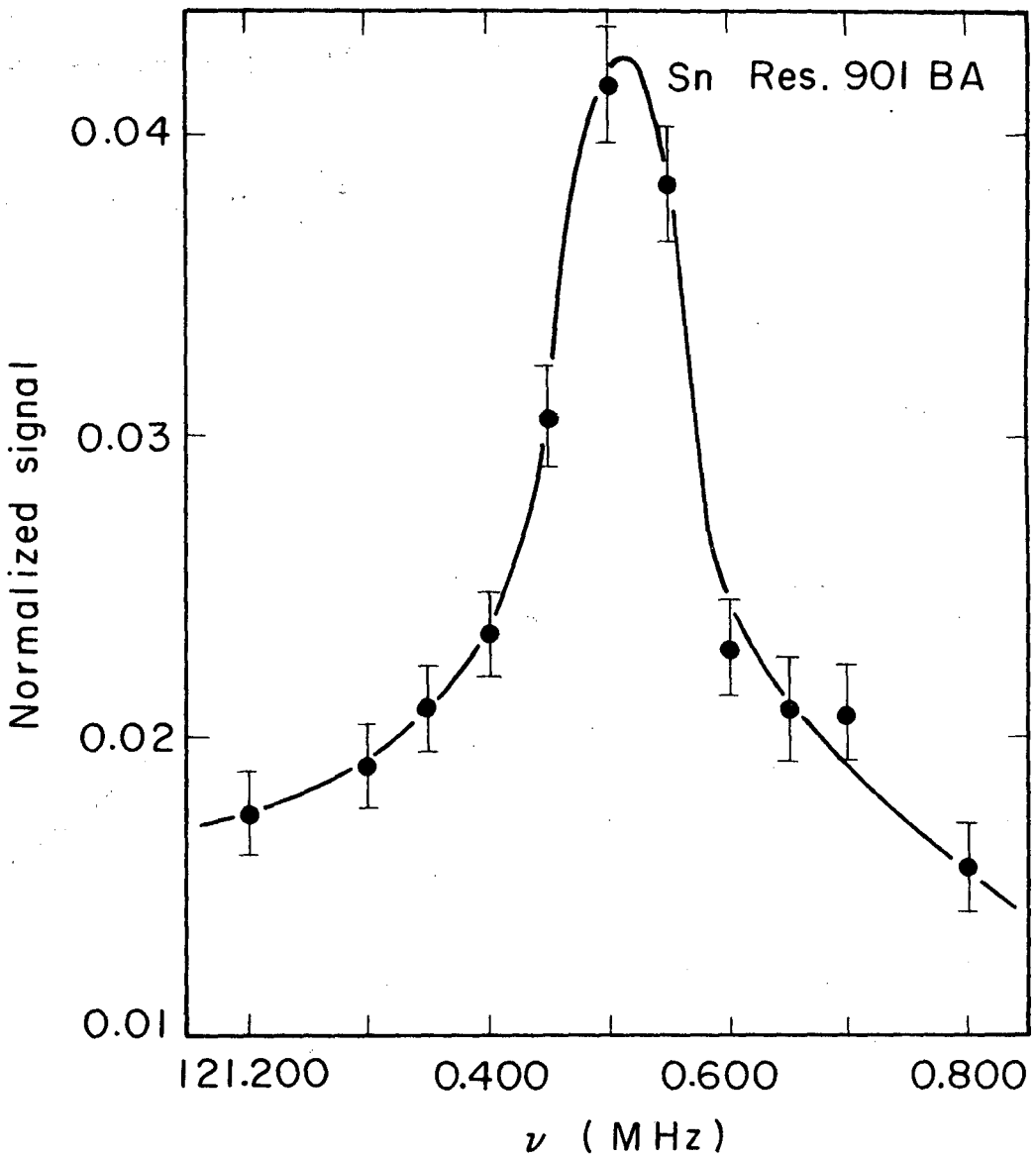

XBL674-2763

Fig. VI-11. ^{121}Sn Type IV hyperfine-transition resonance 901BA at 2.5 gauss. The levels connected are (F = 0.5, M = - 0.5) and (F = 1.5, M = 0.5).

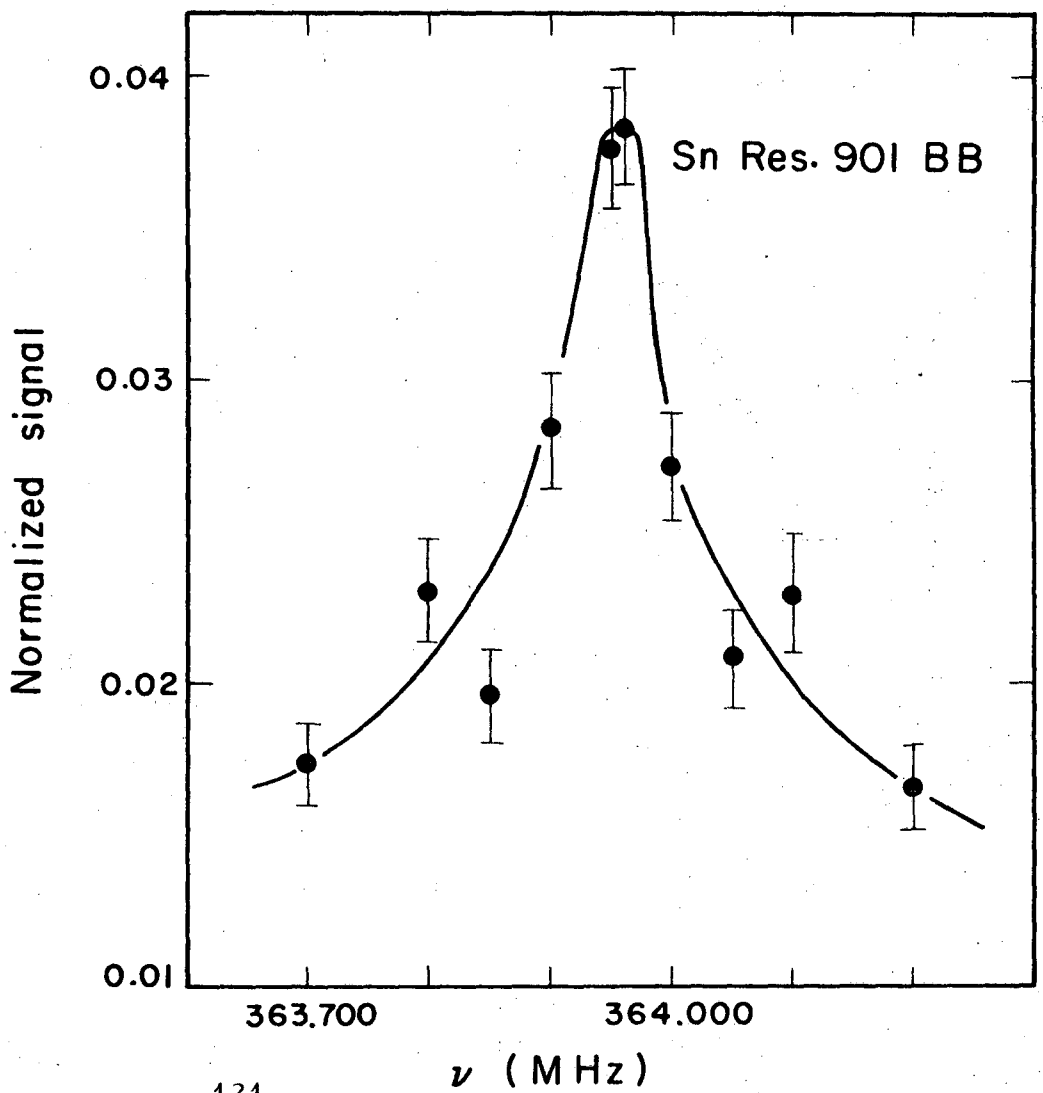

Fig. VI-12. ^{121}Sn Type IV hyperfine-transition resonance 901BB at 2.5 gauss. The levels connected are (F = 1.5, M = 0.5) and (F = 2.5, M = - 0.5).

XBL674-2764

Table VI-IV. Results for 21-h ^{121}Sn (32 observations).

a (MHz)	b (MHz)	μ_I (nm)	χ^2
+128.726(8)	+32.373(12)	-0.699(7)	4.72
-128.726(8)	-32.374(12)	+0.699(7)	4.06

The numbers in parenthesis indicate the error in the last figure, and in the case of a and b represent one standard deviation. The magnetic moments were calculated by using Eq. II.19 and the magnetic moment and hyperfine structure constant a for stable ^{119}Sn with I = 1/2. These quantities were measured by Proctor[21] and by Childs and Goodman[22]. The values used were

$$\mu_I(^{119}\mathrm{Sn}) = -\ 1.04611(84)\mathrm{nm}$$

$$A(^{119}\mathrm{Sn}) = +\ 578.296(4)\ .$$

The error in μ_I for ^{121}Sn is taken as 1% to allow for a possible hfs anomaly, although Goodman and Childs calculate very small anomalies ($\lesssim$ 0.04%) comparing ^{115}Sn, ^{117}Sn and ^{119}Sn. No diamagnetic correction has been made.

The difference in the χ^2 for the two sign combinations is not pronounced enough to definitely choose one or the other. It is known from Childs and Goodman measurement of a positive sign for a in the $^3P_1$ state of ^{115,117,119}Sn and the known negative sign of $^{115,117,119}\mu_I$ that a and μ_I should have opposite signs.

E. Origin of the a Constant

The existence of a finite magnetic dipole interaction constant for the odd-mass Sn isotopes is of interest because in the simple nonrelativistic treatment the magnetic field of the atomic electrons at the nucleus given by H_e, Eq. II.9, should be identically zero in the $5p^2\ ^3P_1$ electronic state. This can be seen easily by substituting numerical values into the formula below[23] for the H_e in a $l^n\ ^{2S+1}L_J$ Hund's-rule state (maximum S and L consistent with the exclusion principle):

$$H_e = \frac{-2\mu_0}{(J+1)} \langle r^{-3} \rangle \left\{ \frac{K}{2} + \frac{(2L - n^2)}{n^2(2L-1)\ (2l-1)\ (2l+3)} \left[L(L+1)K - \frac{3K(K-2)\ L(L+1)}{2} \right] \right\},$$

where

$$K = J(J+1) + L(L+1) - S(S+1)\ .$$

There are two possible sources for a nonvanishing a in this case; they are relativistic effects, and configuration mixing by the Coulomb interaction e^2/r_{ij} between electrons.

The contribution of relativity to the a was calculated by using the effective operator technique of Sandars[9] described in Sec. II.5. The $^3P_1$ state is not mixed by $\mathcal{H}_{fs}$ with any of the other multiplets in the p^2 configuration, since it is the only one with $J = 1$. This is borne out by the equality of the measured $^3P_1$ $g_J = -1.50111(7)$ (Ref. 20) to that calculated for pure LS coupling $g_J = -1.50116$. Thus, the BDLSC correction to a should be zero for this state. The remaining relativistic contribution, a^r, was calculated by using the effective operator $H^1_{hfs\ eff}$ of Eq. II.29 and the formulas in the appendix, and is given by

$$a^r = a^r_{01} + a^r_{12} + a^r_{10} ,$$

where a^r_{01} is the contribution due to the term in $\bar{I}$, a^r_{12} that due to the $(\bar{s}\, C^2)^1$ term, and a^r_{10} that due to the $\bar{s}$ term in Eq. II.29. In calculating a^r the value of the fine-structure splitting constant $\xi = 2171.5\ cm^{-1}$ determined by Childs and Goodman[20] and Eq. II.20 with $Z_{eff} = 46$ was used to determine $\langle r^{-3} \rangle$. The results are summarized:

$$a^r_{01} = 201.6\ \text{MHz} ,$$
$$a^r_{12} = -238.7\ \text{MHz} ,$$
$$a^r_{10} = -11.0\ \text{MHz} ,$$
$$\overline{\phantom{a^r = -48.1\ \text{MHz}}}$$
$$a^r = -48.1\ \text{MHz} .$$

The above calculation was carried out with $\mu_I = +0.700$ nm, and is in agreement with that of Childs and Goodman[22] for a^r in the $^3P_1$ state of ^{117}Sn where the only difference is $I = 1/2$ and $\mu_I = -1.00$ nm.

The difference between the observed $a = -128.7$ MHz and a^r is assumed to be due to the effects of configuration interaction; labeling this difference a^c, one has $a^c = a - a^r = -80.6$ MHz. Thus, configuration interaction effects are supposed to be responsible for about 2/3 of the observed a in the $5\ p^2\ ^3P_1$ state of Sn.

The configuration interaction e^2/r_{ij} can only mix in other $^3P_1$ multiplets arising from configurations other than $5s^2\ 5p^2$ provided they have the same (even) parity. Such states include those in the continuum, and it is not clear how fast the resulting infinite sums converge

in the expression for a^c. This, plus ignorance of the many radial integrals involved, makes calculation of a^c extremely difficult.

F. J-Mixing Corrections to hfs Constants

The effect of second-order hfs interactions on the $^3P_1$ a and b constants due to the nearby $^3P_2$ levels was calculated by using the technique of Woodgate[5] described in Sec. II.B. The radial integrals were those used in the calculation of a^r. The results were extremely small shifts in a and b below the limits of experimental error. The shift in a is -60 Hz for the dipole-dipole interaction ($k_1 = k_2 = 1$ in Eq. II.22) and a positive moment $\mu_I = 0.7$ nm, whereas the dipole-quadrupole shift ($k_1 = 2$, $k_2 = 1$) is +19 Hz. The shift in b due to the dipole-dipole interaction is only -53 Hz.

G. The Nuclear Quadrupole Moment

It is possible to determine the nuclear quadrupole moment Q from the observed b by using Eq. II.14, provided one can evaluate q_J for the $5p^2\ ^3P_1$ state. This can be done by using a formula (similar to that giving H_e) for q_J in Hund's rule L S term with n equivalent electrons (or holes). The expression is[23]

$$q_J = \pm \left[\frac{3K(K-1) - 4L(L+1)\ J(J+1)}{(2L-1)\ (J+1)\ (2J+3)} \right] \left[\frac{(2l-n^2)}{n(2l-1)\ (2l+3)} \right] \langle r^{-3} \rangle ,$$

where

$$K = J(J+1) + L(L+1) - S(S+1) .$$

The positive sign is used with n equivalent electrons and the negative sign with n equivalent holes, where $n < 2l + 1$. Substitution of $n = 2$, $l = L = S = J = 1$ yields

$$q_J = \frac{1}{5} \langle r^{-3} \rangle .$$

Substitution of q_J, using the value of $\langle r^{-3} \rangle$ determined from Childs and Goodman's value of ξ, and the observed value of $b = \pm 32.374$ MHz into Eq. II.14 yields

$$Q = \pm 0.087 \times 10^{-24}\ \text{cm}^2 .$$

A relativistic calculation, using Eq II.28 with $k = 2$ and the expressions in Appendix 1, yielded

$$q_J = 0.219\ \langle r^{-3} \rangle .$$

This yields

$$Q = \pm 0.079 \times 10^{-24}\ \mathrm{cm}^2 .$$

The effects of relativity are thus ≈ 10%.

It is difficult to assign an error to Q, since configuration interactions are known to contribute a large part to q_J in many cases and they have not been included in the calculations above. Sternheimer has shown[24-26] that q_J may differ by as much as 50% from the single-configuration value in some cases. Thus, it is probably safe to say that $|Q| = 0.08 \pm 0.04 \times 10^{-24}\ \mathrm{cm}^2$.

H. Interpretation of the Nuclear Spin and Moments

The nuclear spin I = 3/2 for the ground state of 27-h ^{121}Sn is consistent with a simple shell-model assignment of an odd neutron to the $2d_{3/2}$ subshell. ^{119}Sn is known to have I = 1/2 in the ground state, but it has a nearby (0.024-keV) 250-day metastable state, very probably with I = 3/2. The possible odd-neutron shell-model configurations for ^{121}Sn together with two suggested by Noya et al.[12] for ^{119}Sn are listed below:

Isotope	$2d_{5/2}$	$1g_{7/2}$	$3s_{1/2}$	$2d_{3/2}$	$1h_{11/2}$
^{119}Sn(I=1/2)	6	8	1	0	4
	6	8	1	2	2
^{121}Sn(I=3/2)	6	8	2	1	4
	6	8	0	1	6
	6	8	0	3	4

Some experiments carried out by Cohen and Price[27] involving (d, p) and (d, t) reactions on the stable Sn isotopes indicate that each of the three configurations above must be considered to be present (plus probably some others) in the ^{121}Sn ground-state wave function. Cohen and Price were able to measure the quantities V_j^2 of Sec. III, which give the probability of finding a neutron in the state j for the even-mass Sn isotopes 116 through 124; $(2j+1) \cdot V_j^2$ is just the average number of neutrons in the j subshell; this quantity is given below based on their results for ^{120}Sn and ^{122}Sn.

Average number of neutrons in shell-model states					
Isotope	$2d_{5/2}$	$1g_{7/2}$	$3s_{1/2}$	$2d_{3/2}$	$1h_{11/2}$
^{120}Sn(I = 0)	5.22	7.12	1.22	2.20	4.20
^{122}Sn(I = 0)	5.16	7.36	1.38	2.36	5.64

The above table indicates that a large number of shell-model configurations would have to be mixed in the nuclear wave function to successfully predict the properties of Sn nuclei. T. T. S. Kuo et al.[28] have dealt with this problem by using the quasi-particle transformation to diagonalize a shell-model Hamiltonian with a residual pairing interaction, and have successfully predicted the transition from I = 1/2 for ^{119}Sn to I = 3/2 for ^{121}Sn.

The Schmidt value for the magnetic moment of a $d_{3/2}$ neutron is + 1.15 nm; the value calculated by T. T. S. Kuo et al. is 0.99 nm, and is in better agreement with the observed value of ±0.699 nm for ^{121}Sn. It is difficult to imagine how this odd-neutron nucleus with I = 3/2 could possibly have a negative magnetic moment despite the complexities of the nuclear wave function. Thus, although the measurements discussed in Sec. VI.D do not distinguish between a positive and negative moment, it is felt that its sign is positive, and consequently that the hfs constants a and b are negative.

The ^{121}Sn nuclear quadrupole moment Q = - 0.08(4) barn (assumes b negative) may be successfully reproduced by the single-particle formula Eq. III.5, provided one assigns an effective g_l of + 1 to the odd j = 3/2 neutron (i.e., treat it as if it were a proton). This effective positive charge for the odd neutron is consistent with the value of 1.35 used by Kuo to reproduce the observed electric quadrupole transition probabilities in the even-mass Sn isotopes. Assigning such a charge to the neutron is an effective way of accounting for the polarization of the charged proton core by the odd neutrons. The calculated value of Q is then -0.085 barn. The quadrupole moment of the 250-day ^{119m}Sn observed by Boyle et al.[29] is also -0.08(4) barn.

VII. RESEARCH ON ^{88}Rb

A. Production of the Isotope

Radioactive ^{88}Rb with a half life of 18 min is easily produced by neutron irradiation of the 28% abundant naturally occurring ^{87}Rb. Two reactors were used to produce ^{88}Rb for these experiments. Most of the irradiations were done in the General Electric Test Reactor at Vallecitos, California, and the samples were flown by helicopter the approximately 20 miles to Berkeley; this took about one half life. The most recent experiments, however, have used samples irradiated in the new Triga Mk III reactor, recently placed in operation on the UC campus. Although the flux of the Triga is estimated to be $\approx 1/5$ that of the GE reactor, one half life is saved between removal from irradiation and the beginning of the experiment. No loss of signal intensity was observed after changing to the campus reactor.

^{87}Rb was irradiated in 100-mg samples of RbF salt. The RbF was dried thoroughly and encapsulated in quartz vials for delivery to the reactor. The fluorine contributed no significant activity to the sample, since only 11-sec ^{20}F was produced and had decayed away by the time the experiment began. The principal activities produced besides the ^{88}Rb were ^{86}Rb with an 18.6-day half life and probably ^{134m}Cs with a 2.9-h half life. ^{86}Rb is produced from neutron capture by 72% abundant ^{85}Rb, and ^{134m}Cs was expected to be produced from 100% abundant ^{133}Cs, which may have been present as an impurity in the RbF sample.

That the observed signals in the experiments described here were due to ^{88}Rb and not to some other activity was established by a decay analysis of all buttons exposed during each run. In addition, an especially careful decay analysis of the type described in Sec. V.C was carried out for the peak button (AD) of the resonance observed in Run 879. Figure VII-1 shows a plot of the decay of the resonance activity on button AD; also shown is the least-squares computer fit to the points, which yielded a half life of 17.5±2.4 min.

In general, it was observed that during the first 45 min after irradiation the 18-min ^{88}Rb was the predominant activity present, about 3 to 10 times the long-lived background activities.

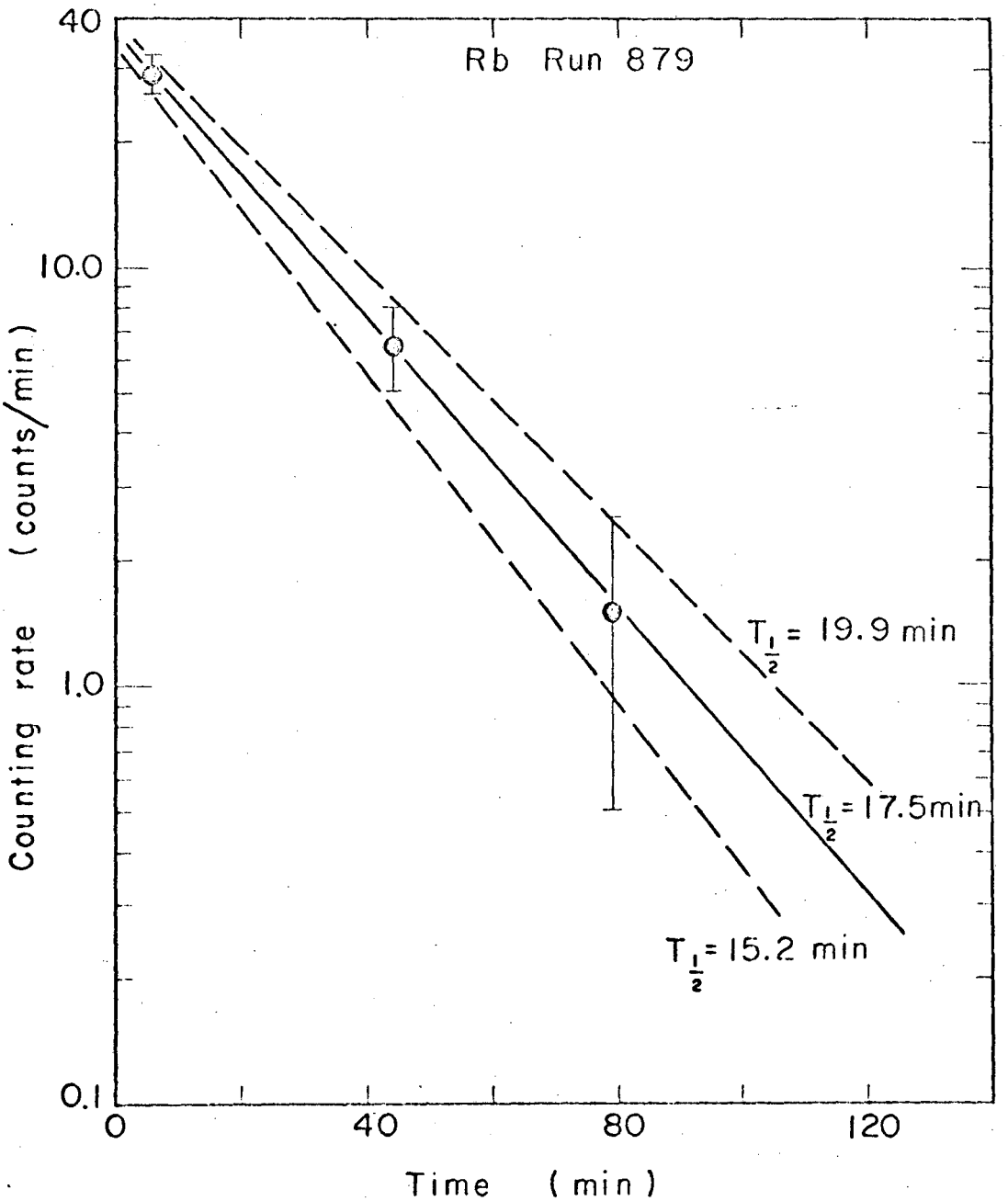

XBL674-2765

Fig. VII-1. Decay of enhanced activity on button AD of ^{88}Rb Run 879. The solid line is a lease-squares computer fit to the data; the dashed lines indicate the error in the fit.

B. Formation of the Atomic Beam

Upon delivery of the sample to the laboratory it was immediately opened and loaded into a tantalum oven together with some freshly made filings of calcium metal. An excess of Ca was used, usually 1.5 to 2 times the RbF in volume. The RbF and Ca were mixed in the oven before it was sealed and loaded into the atomic beam machine.

Once in the beam machine the oven was heated initially by electron bombardment and finally by radiation from a nearby tungsten filament. The electron bombardment served to heat the oven quickly so that the chemical reaction $Ca + 2\,RbF \rightarrow CaF_2 + 2\,Rb\uparrow$ could be initiated; once it had begun, only the radiation from the filament was required to sustain it.

As a monitor of the atomic beam intensity a hot-wire surface ionization detector and electrometer were used to observe the stable ^{85}Rb atoms coming from the oven; this was in addition to the usual radioactive monitoring by the side buttons, and was used primarily to establish that the reaction above had begun and, by observation of rf resonances in the ^{85}Rb atoms, to check the setting of the C-magnet field throughout the experiment.

The electronic state of Rb is (5s) $^2S_{1/2}$ with $g_J = -2.0$. This allows observation of strong flop-in signals because of the large change of atomic magnetic moment as m_J changes sign.

C. hfs Measurements and Results

Earlier work by Ehlers and Shugart[30] had established a nuclear spin $I = 2$ for ^{88}Rb by observation of the low-field $\Delta F = 0$ rf transition. Their measurements extended up in magnetic field to 15.05 gauss, and are included as the first four of the observations listed here.

To establish continuity with the earlier observations, the first of the new Runs (879) was carried out at 14.87 gauss, and thenceforth the field was increased steadily until the error in the calculated a from the computer fit to the data was small enough to warrant searching for a $\Delta F = 1$ hyperfine transition.

Figure VII-2 shows an energy-level diagram for hfs levels of ^{88}Rb for $a > 0$ ($\mu_I > 0$). The $\Delta F = 0$ "across the board" transition which was

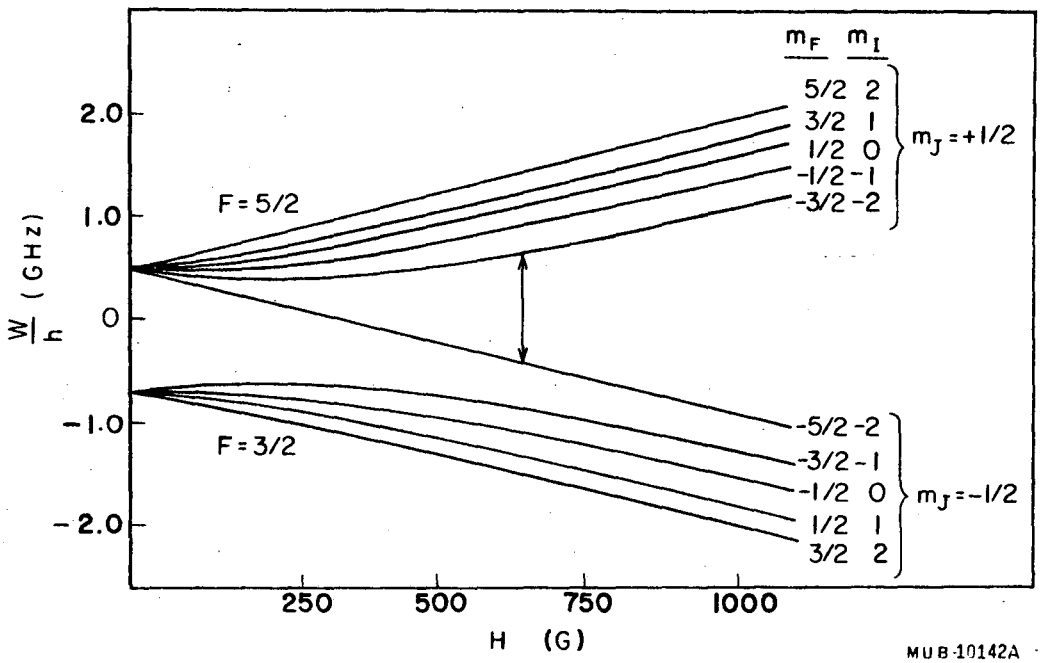

Fig. VII-2. Energy-level diagram for ^{88}Rb drawn with a > 0.

followed up in field is indicated. Table VII-I summarizes the observations made at all magnetic fields. Two observations were made at ≈ 120 gauss (Run 888 and Run 908) with the C-magnet field in opposite directions to test for possible biasing of the data by a direction-dependent shift in the resonance peaks. Figures VII-3 and VII-4 show resonance plots from Runs 888 and 908. The signal represents the ratio of the short-half-life activity on the center resonance button to that on the side normalization button exposed to the beam at the same time. The amount of short-half-life activity on each button was obtained by taking the difference between its counting rate immediately after exposure to the atomic beam and its counting rate at a much later time, after the 18-min ^{88}Rb had decayed away.

$\Delta F = 1$ transitions connecting the $F = 5/2$ and $F = 3/2$ hfs levels were observed in Runs 914, 916, and 922. Each of the observable $F = 1$ transitions has a unique dependence on the C-magnet field strength. The change in frequency of the $(F_1 = 5/2,\ M_1 = 5/2) \longleftrightarrow (F_2 = 3/2,\ M_2 = 3/2)$ resonance between Runs 914 and 916, where the magnetic field changed by 0.47 gauss, served to confirm the assignment of these quantum numbers to this resonance.

Figure VII-5 shows a resonance plot obtained from Run 922. This resonance is an unresolved doublet at the magnetic field of this run ($H_C = 1.883$ gauss), and measures the interval $(F_1 = 3/2,\ M_1 = \pm 1/2) \longleftrightarrow (F_2 = 5/2,\ M_2 = \mp 1/2)$; at this field the two components of this doublet are separated by less than 1 kHz, or about 1/50 of the resonance line width. This particular resonance is the most auspicious one of all the possible $\Delta F = 1$ transitions for fixing the hfs splitting, because at low fields it is very nearly independent of magnetic field and hence should have a line width approaching the limit for the beam device. It is the most significant of all the measurements made, as is reflected by the large weight assigned to it in the computer fit (Table VII-I).

The results of the computer fit to the data of Table VII-I by the routine HYPERFINE are listed below:

Table VII-I. Observations on ^{88}Rb (14 observations).

	Calibration isotope data			C-Magnet field (gauss)		^{88}Rb Resonances							
Run No.	Name	Frequency (MHz)	Freq. error (MHz)	H	ΔH	F_1	M_1	F_2	M_2	Frequency (MHz)	Freq. error (MHz)	$\nu_{obs} - \nu_{calc}$ (MHz)	Weight factor
415[a]	RB85	2.1500	0.0200	4.5902	0.0425	5/2	-3/2	5/2	-5/2	2.6000	0.0750	0.0055	160.9
526[a]	RB85	3.5000	0.0250	7.4559	0.0529	5/2	-3/2	5/2	-5/2	4.2250	0.0750	-0.0124	152.5
540[a]	RB85	5.1840	0.0150	11.0129	0.0316	5/2	-3/2	5/2	-5/2	6.3000	0.1000	-0.0015	96.7
547[a]	RB85	7.1060	0.0150	15.0489	0.0314	5/2	-3/2	5/2	-5/2	8.7000	0.1000	0.0224	96.6
879	RB85	7.0200	0.0100	14.8688	0.0209	5/2	-3/2	5/2	-5/2	8.5500	0.0400	-0.0208	570.1
884	RB85	19.2620	0.0150	40.0063	0.0302	5/2	-3/2	5/2	-5/2	24.2000	0.0500	-0.0121	346.2
887	RB85	37.1400	0.0150	75.0321	0.0286	5/2	-3/2	5/2	-5/2	48.6500	0.0750	-0.0274	164.5
888	RB85	61.5950	0.0150	120.0166	0.0266	5/2	-3/2	5/2	-5/2	85.2875	0.0500	-0.0232	327.1
908	RB85	61.5650	0.0150	119.9633	0.0266	5/2	-3/2	5/2	-5/2	85.2875	0.0500	0.0240	327.2
896	RB85	109.6300	0.0100	199.9802	0.0156	5/2	-3/2	5/2	-5/2	167.5750	0.0750	0.0002	167.6
914	RB85	0.7050	0.0250	1.5087	0.0534	5/2	3/2	3/2	3/2	1188.7000	0.3000	0.0782	10.2
914	RB85	0.7050	0.0250	1.5087	0.0534	5/2	5/2	3/2	3/2	1189.5000	0.3000	0.0352	9.6
916	RB85	0.9250	0.0150	1.9788	0.0320	5/2	5/2	3/2	3/2	1190.6000	0.3000	0.0796	10.5
922	RB85	0.8800	0.0160	1.8827	0.0342	5/2	1/2	3/2	-1/2	1186.0900	0.0200	-0.0008	2499.0

a. From earlier work of Ehlers and Shugart (Ref. 30).

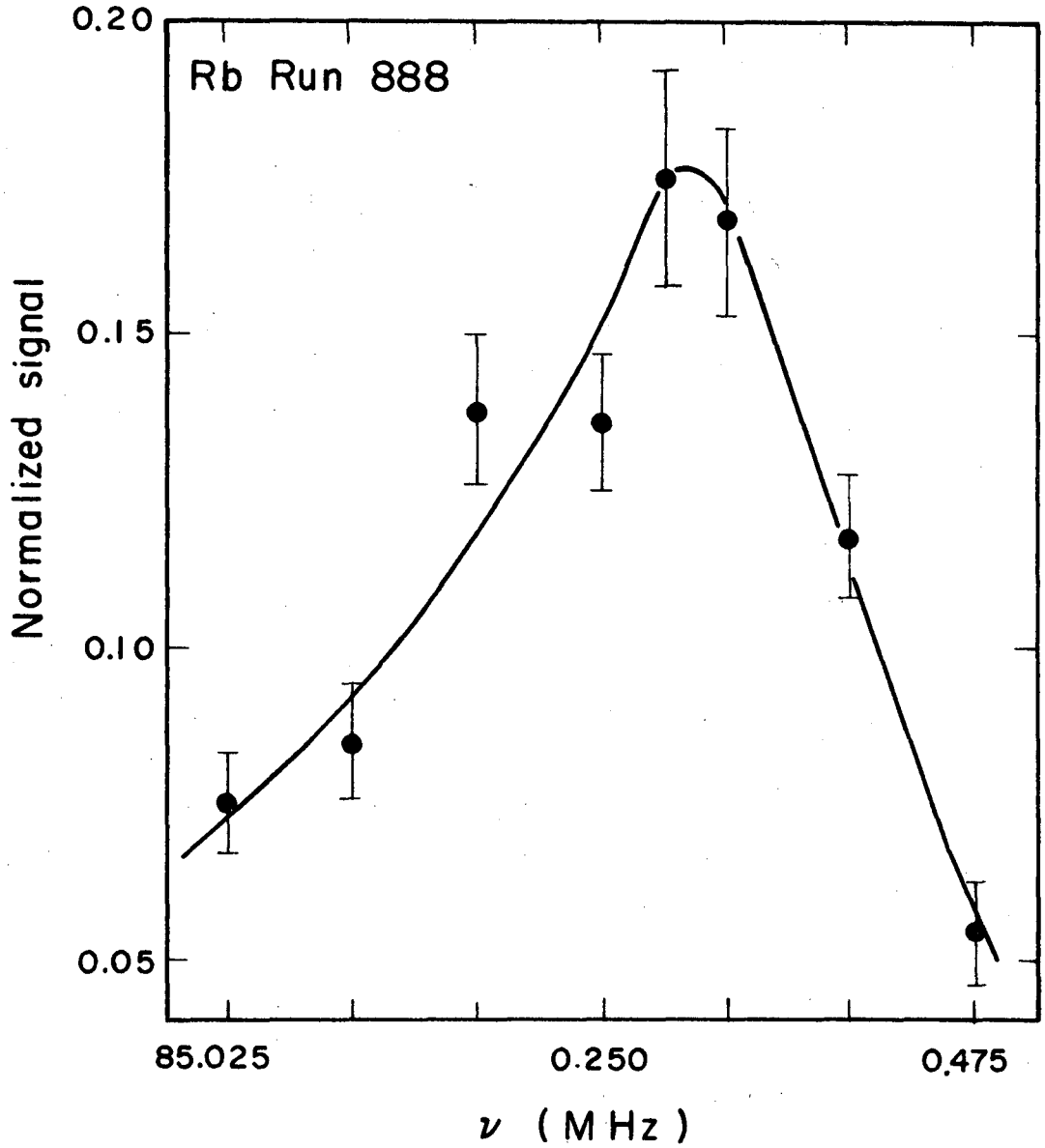

XBL674-2766

Fig. VII-3. ^{88}Rb Run 888 resonance at 120 gauss. The transition is (F = 2.5, M = - 1.5) ⟷ (F = 2.5, M = - 2.5) with the C field in the normal direction.

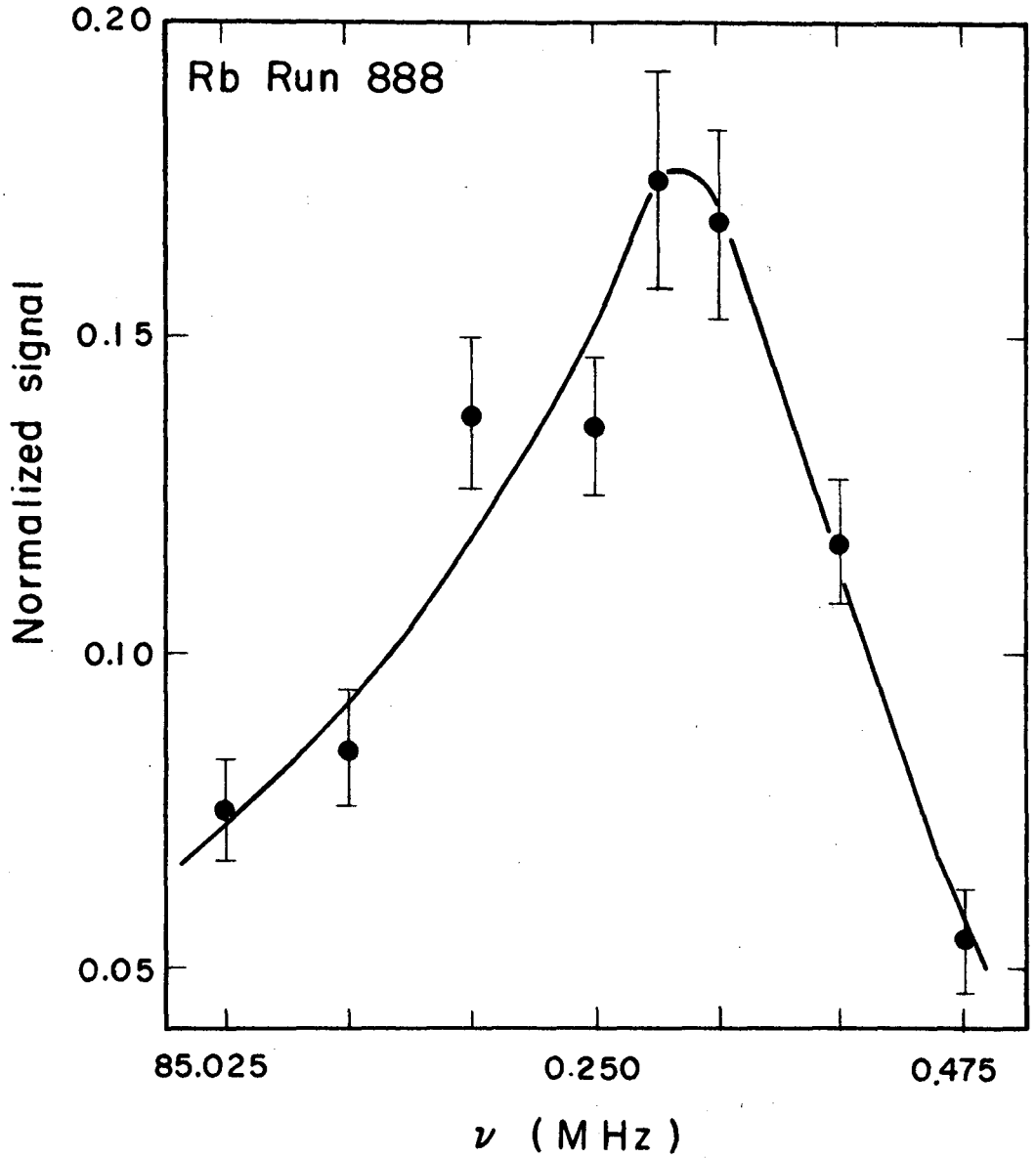

XBL674-2766

Fig. VII-3. ^{88}Rb Run 888 resonance at 120 gauss. The transition is (F = 2.5, M = - 1.5) ⟷ (F = 2.5, M = - 2.5) with the C field in the normal direction.

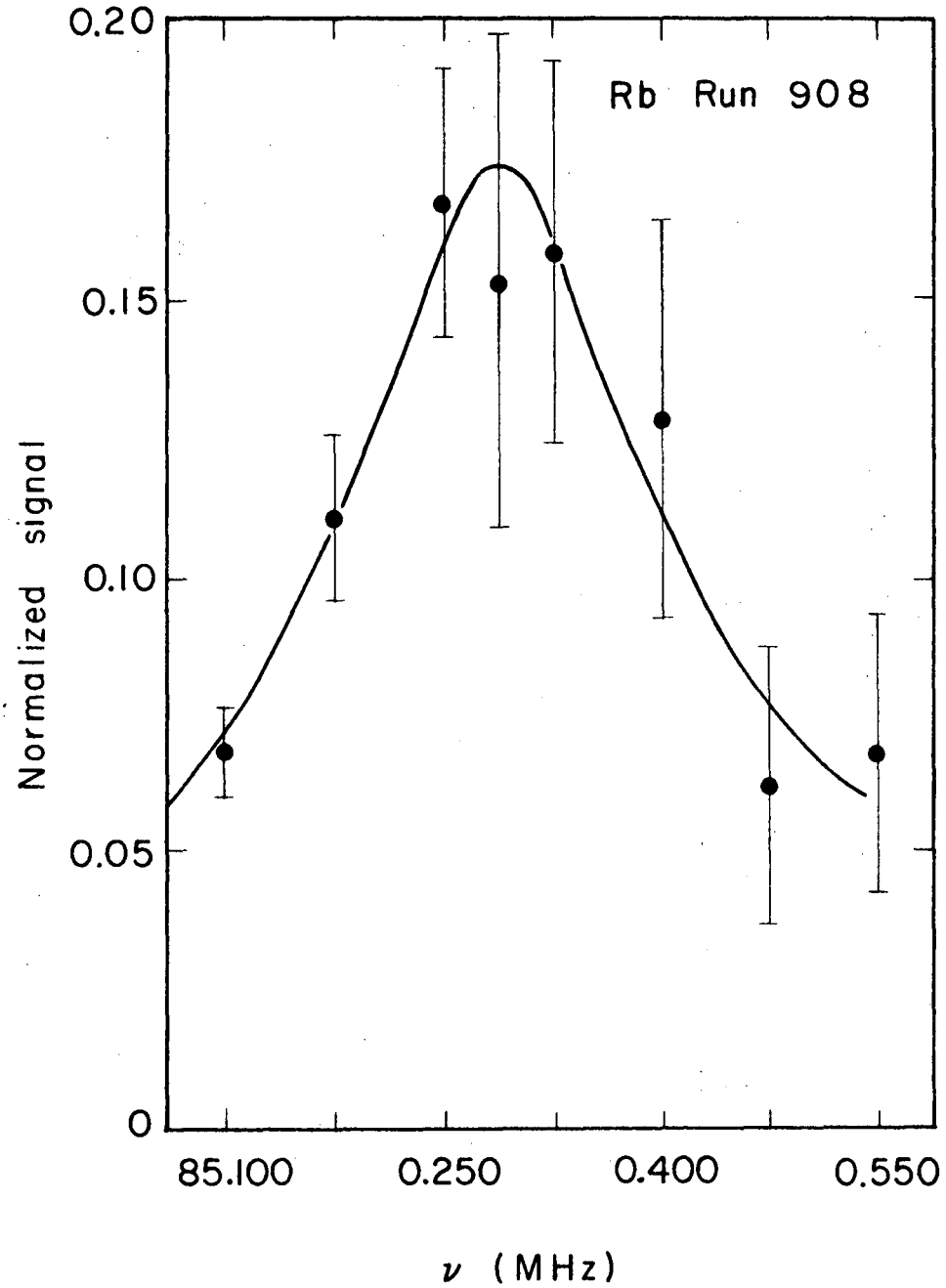

XBL674-2767

Fig. VII-4. ^{88}Rb Run 908 resonance at 120 gauss. The transition is (F = 2.5, M = - 1.5) ⟷ (F = 2.5, M = - 2.5) with the C field in the reversed direction.

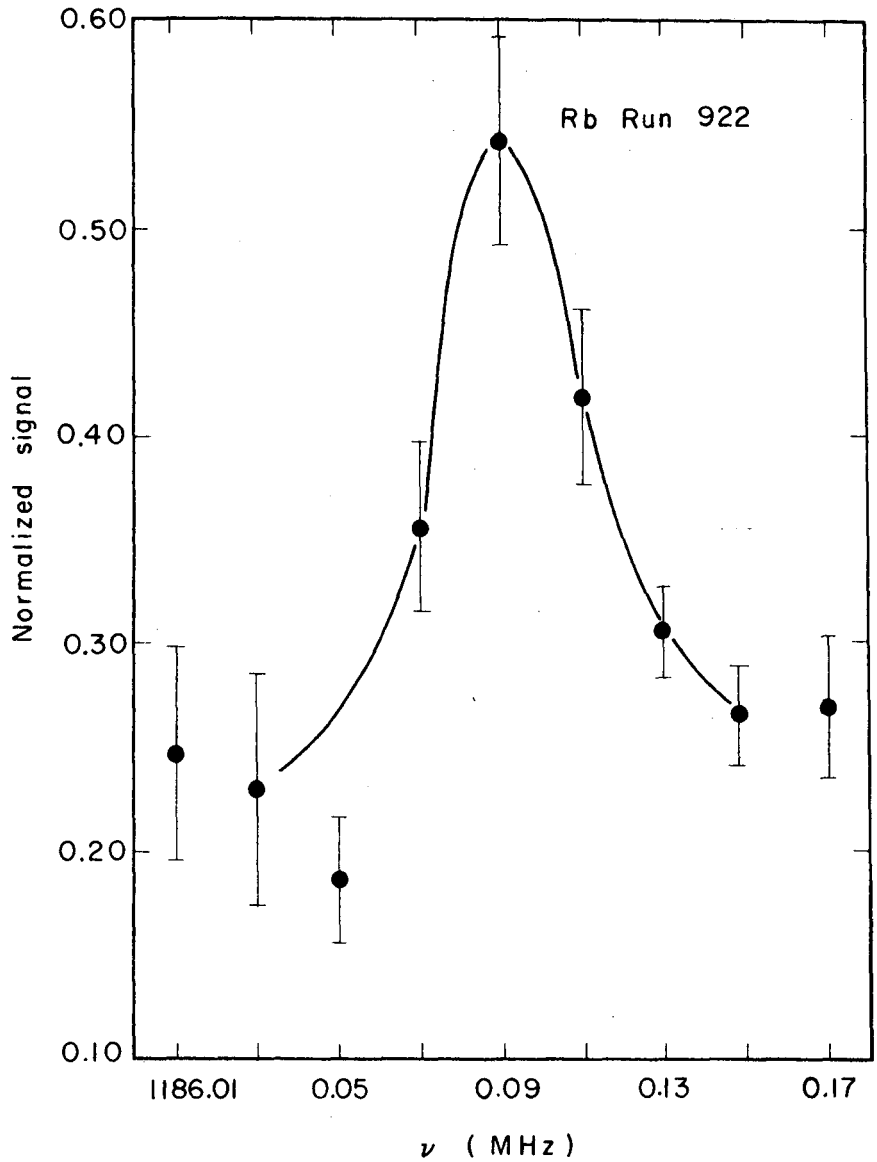

Fig. VII-5. ^{88}Rb Run 922 field-independent hyperfine-transition resonance at 1.9 gauss. The transition is (F = 2.5, M = ± 0.5) ⟷ (F = 1.5, M = ∓ 0.5).

XBL674-2768

^{88}Rb Results

$|a| = 474.432 \pm 0.006$ MHz, $|\mu_I| = 0.506 \pm 0.005$ nm,

$$\left.\begin{array}{l} \chi^2 = 1.00 \text{ for } \mu_I > 0 \\ \chi^2 = 2.50 \text{ for } \mu_I < 0 \end{array}\right\} \text{ 14 observations.}$$

The error in $|a|$ is 1 standard deviation from the mean. The magnetic moment was determined by comparison of the a constants of ^{88}Rb and ^{85}Rb, using Eq. II.19 and the known g_I of ^{85}Rb. The values used were[31]

$$g_I\,(^{85}\text{Rb}) = 2.93700 \times 10^{-4} \text{ (Bohr magnetons)},$$

$$a\,(^{85}\text{Rb}) = 1011.910797 \text{ MHz}.$$

The error listed for μ_I (^{88}Rb) is 1% to include effects of a possible hfs anomaly. No diamagnetic correction has been made.

D. Interpretation of the Nuclear Magnetic Moment

The ^{88}Rb nucleus contains 37 protons and 51 neutrons. The single odd neutron beyond the major closed shell at $N = 50$ most probably occupies the $2d_{5/2}$ subshell. The nine odd protons are not so unambiguously placed, however. It is possible that they may be distributed in a number of ways among the $2p_{3/2}$, $1f_{5/2}$, $2p_{1/2}$, and $1g_{9/2}$ subshells. A simple proton configuration which yields the observed spin $I = 3/2$ for ^{87}Rb placed three in the $2p_{3/2}$ and the remaining six in the $1f_{5/2}$ subshells. Assuming that the same proton configuration exists in ^{88}Rb, the observed spin of $I = 2$ must arise from the coupling of an odd $2d_{5/2}$ neutron with an odd $2p_{3/2}$ proton hole. This is in agreement with the weak particle-hole coupling rule given in Sec. III, which predicts $I = 3$ or 2.

It is possible to calculate μ_I (^{88}Rb) by using Eq. III.4 and the observed magnetic moments of ^{91}Zr ($Z = 40$, $N = 51$, $I = 5/2$) and ^{87}Rb ($Z = 39$, $N = 50$, $I = 3/2$). The values used were $\mu_I(^{91}\text{Zr}) = -1.3$ nm and $\mu_I(^{87}\text{Rb}) = +2.8$ nm, and were taken from Ref. 32. The calculated value for $\mu_I(^{88}\text{Rb})$ is then -0.7 nm, which is in fair agreement with the observed value of ±0.5 nm provided one takes the negative sign.

The results of the experiments described in Sec. VII.B do not distinguish between the two possible signs for $\mu_I(^{88}Rb)$; the factor of 2.5 between χ^2 of the computer fits for positive and negative μ_I, which favors assignment of the + sign, is not considered at all conclusive. It is barely possible that further experiments could definitely decide the sign of μ_I, but this seems doubtful in view of the limitations in resonance line width ($\approx$ 50 kHz) set by the beam machine in its current state and the short half life of the isotope.

It should be pointed out that it is extremely difficult to calculate a positive magnetic moment of the proper magnitude by using Eq. III.4 and observed magnetic moments for any of the other proton configurations, including those which do not predict the spin properly. The same holds when one assumes that the odd neutron occupies the $1g_{7/2}$ subshell; all predict either an extremely small positive moment, +0.04 nm, or negative magnetic moments ranging from -0.7 to -2.8 nm. It would seem that theory strongly requires that μ_I be negative.

ACKNOWLEDGMENTS

It would have been impossible to carry out the research described here without the help and encouragement of a great many people. I wish to pay special thanks to Professor Howard A. Shugart for lending his fantastic experimental ability and unfailing good advice toward the completion of this work. Special thanks go also to Dr. Vernon J. Ehlers, Dr. Paul Vanden Bout, and Professor Antoni Dymanus for invaluable discussions and advice, and particularly for our collaboration on the ^{88}Rb work, which is in no way a one-man project. A special debt is owed to Professor William A. Nierenberg for his early advice and for his making all this possible by founding the Atomic Beam Group at Berkeley. Thanks go also to many of the personnel of the Lawrence Radiation Laboratory, particularly the health chemists and 88-inch cyclotron people, who helped with this work. I am grateful for the contributions of my fellow graduate students and for the patience and diligence of Dana J. Vance and Pat Yarnold in the arduous job of radioactive counting.

Finally, I wish to thank my parents for their great contributions to my education and my wife, Trish, for her sympathy, understanding, and patience.

This work was supported by the U. S. Atomic Energy Commission.

APPENDIX

1. Relativistic Correction Factors

The $P^{(k_s k_l)k}$ of Eq. II.28 for $k=1$ and 2 are given[9] by:

$$P^{(10)1} = \frac{4\mu_0}{3(2l+1)}\sqrt{\frac{6}{(2l+1)}}\,[\,l(l+1)^2 F_{++} - l^2(l+1)F_{--} - l(l+1)F_{+-}\,]\,,$$

$$P^{(12)1} = \frac{2\mu_0(l+1)}{(2l+1)(2l+3)(2l-1)}\sqrt{\frac{5l(2l+3)(2l-1)}{3(l+1)(2l+1)}}$$

$$\times\,[\,-4l(l+1)(2l-1)F_{++} + 4l(l+1)(2l+3)F_{--} - (2l+3)(2l-1)F_{+-}\,]\,,$$

$$P^{(01)1} = \frac{4\mu_0}{(2l+1)}\sqrt{\frac{l(l+1)}{2(2l+1)}}\,[\,2l(l+1)F_{++} + 2l(l+1)F_{--} + F_{+-}\,]\,,$$

$$P^{(02)2} = \frac{e}{(2l+1)}\sqrt{\frac{l(l+1)}{(2l+3)(2l-1)(2l+1)}}\,[\,(l+2)(2l-1)R_{++} + (l-1)(2l+3)R_{--} + 6R_{+-}\,]\,,$$

$$P^{(13)2} = \frac{-3e}{5(2l+1)}\sqrt{\frac{14(l+2)(l-1)l(l+1)}{(2l+3)(2l+1)(2l-1)}}\,[\,(2l-1)R_{++} - (2l+3)R_{--} + 4R_{+-}\,]\,,$$

$$P^{(11)2} = \frac{-6e}{5(2l+1)}\sqrt{\frac{l(l+1)}{(2l+1)}}\,[\,-(l+2)R_{++} + (l-1)R_{--} + 3R_{+-}\,]\,,$$

where the F's and R's are given by

$$F_{jj'} = \frac{-2}{\alpha a_0\,(K+K'+2)}\int_0^\infty (PQ' + QP')\,r^{-2}dr\,,$$

$$R_{jj'} = \int_0^\infty (PP' + QQ')\,r^{-3}\,dr.$$

The + or - signs are written for j and j' according to whether they are $l \pm 1/2$; $K = -(j+1/2)$ for $j = l + 1/2$, and $K = j + 1/2$ for $j = l - 1/2$.

P and Q are the relativistic radial wave functions, and α and a_0 are the fine-structure constant and Bohr radius.

The F's and R's may be determined by using $\langle r^{-3} \rangle$ from Eq. II.20 multiplied by an approximate correction factor obtained from tables in the back of Ref. 4. The appropriate factors are listed below according to the notation of Ref. 4.

Integral	Factor
F_{--}	$-F''$
F_{++}	$-F'$
F_{+-}	$-G$
R_{--}	R''
R_{++}	R'
R_{+-}	S

The various $\langle r^{-3} \rangle$ of Eq. II.29 are given[9] by:

$$\langle r^{-3} \rangle_{01} = \frac{1}{(2l+1)^2} \left[2l(l+1) F_{++} + 2l(l+1) F_{--} + F_{+-} \right] ,$$

$$\langle r^{-3} \rangle_{12} = \frac{1}{3(2l+1)^2} \left[-4l(l+1)\ (2l-1)\ F_{++} + 4l(l+1)\ (2l+3)\ F_{--} - (2l+3)\ (2l-1)\ F_{+-} \right] ,$$

$$\langle r^{-3} \rangle_{10} = \frac{4}{3} \frac{l(l+1)}{(2l+1)^2} \left[(l+2)\ F_{++} - l F_{--} - F_{+-} \right] .$$

2. Constants Used in the Analysis of the Measurements (Refs. 21, 22, 31).

$\mu_0/h = 1.399613$ MHz/G

$M_p/m_e = 1836.1$

^{85}Rb $g_J = -2.0023319$

$\mu_I = 1.34817$ nm

$g_I = 2.93700 \times 10^{-4}$

$a = 1011.910813$ MHz

^{133}Cs $g_J = -2.0025417$

$\mu_I = +2.5641$ nm

$g_I = 3.98994 \times 10^{-4}$

$a = 2298.1579425$ MHz

^{119}Sn $g_J = -1.50110$

$\mu_I = -1.04611$ nm

$g_I = -11.394 \times 10^{-4}$

$a = +578.296$ MHz

REFERENCES

1. Brian R. Judd, Operator Techniques in Atomic Spectroscopy (McGraw-Hill, New York, 1963).
2. C. Schwartz, Theory of Hyperfine Structure, Phys. Rev. 97, 380 (1955).
3. B. R. Judd, Hyperfine Interaction Lecture Notes, Abstracts Supplement, 7th "Brookhaven" Conference on Molecular Beams and Atomic Resonance, Fysiska Institutionen, University of Uppsala, Uppsala, Sweden (1964) (unpublished).
4. H. Kopfermann, Nuclear Moments (Academic Press, New York, 1958).
5. G. K. Woodgate, Hyperfine Structure and Nuclear Moments of Samarium, Proc. Roy. Soc. (London) A293, 117 (1966).
6. Norman F. Ramsey, Molecular Beams (Oxford University Press, London, 1956).
7. H. A. Shugart, Eigenvalue and Least-Squares Techniques Used by the Atomic Beam Group, Lawrence Radiation Laboratory, May 1964 (unpublished).
8. I. P. Grant, Relativistic Self-Consistent Fields, Proc. Roy. Soc. (London) A262, 555 (1961).
9. P. G. H. Sandars and J. Beck, Relativistic Effects in Many Electron Hyperfine Structure, I. Theory, Proc. Roy. Soc. (London) A289, 97 (1965).
10. L. W. Nordheim, Beta-Decay and the Nuclear Shell Model, Phys. Rev. 78, 294 (1950).
11. R. J. Blin-Stoyle, Theories of Nuclear Moments (Oxford University Press, London, 1957).
12. H. Noya, A. Arima, and H. Horie, Nuclear Moments and Configuration Mixing, Suppl. Progr. Theoret. Phys. (Kyoto) 8, 33 (1958).
13. C. Schwartz, The Ground State of Odd-Odd Nuclei, Phys. Rev. 94, 95 (1954).

14. M. H. Brennan and A. M. Bernstein, j-j Coupling Model in Odd-Odd Nuclei, Phys. Rev. 120, 927 (1960).

15. Auriol Bonney (Lawrence Radiation Laboratory), unpublished lecture notes.

16. A. Bohr, B. R. Mottelson, and D. Pines, Possible Analogy Between the Excitation Spectra of Nuclei and Those of the Superconducting Metallic State, Phys. Rev. 110, 936 (1958).

17. M. A. Preston, Physics of the Nucleus (Addison-Wesley, Reading, Mass., 1962).

18. S. N. Ghoshal, Excitation Curves of (α, n); $(\alpha, 2n)$; $(\alpha, 3n)$ Reactions on Silver, Phys. Rev. 73, 417 (1948).

19. L. L. Marino, W. B. Ewbank, W. A. Nierenberg, H. A. Shugart, and H. B. Silsbee, Spins of Indium-109, Indium-110m, and Indium-111, Phys. Rev. 111, 286 (1958).

20. W. J. Childs and L. S. Goodman, Electronic g Factors of the p^2 Configuration in GeI and SnI, Phys. Rev. 134, A66 (1964).

21. W. G. Proctor, On the Magnetic Moments of Tl^{203}, Tl^{205}, Sn^{115}, Sn^{117}, Sn^{119}, Cd^{111}, and Pb^{207}, Phys. Rev. 79, 35 (1950).

22. W. J. Childs and L. S. Goodman, Magnetic Hyperfine Structure of the $^3P_1$ and $^3P_2$ Metastable States of $Sn^{115, 117, 119}$, Phys. Rev. 137, A35 (1965).

23. R. Marrus and W. A. Nierenberg, On Atomic Beams, in Proceedings of the International School of Physics "Enrico Fermi", XVII, 118 (1960).

24. R. Sternheimer, On Nuclear Quadrupole Moments, Phys. Rev. 84, 244 (1951).

25. R. Sternheimer, Effect of the Atomic Core on the Nuclear Quadrupole Coupling, Phys. Rev. 95, 736 (1954).

26. R. Sternheimer, Effect of the Atomic Core on the Nuclear Quadrupole Coupling, Phys. Rev. 105, 158 (1957).

27. B. L. Cohen and R. E. Price, Nuclear Structure Studies in the Tin Isotopes, Phys. Rev. 121, 1441 (1961).

28. T. T. S. Kuo, E. U. Baranger, and M. Baranger, A shell-Model Calculation of the Odd-Mass Tin Isotopes, Nucl. Phys. 79, 513 (1966).

29. A. J. F. Boyle, D. St. P. Bunbury, and C. Edwards, The Isomer Shift in Sn^{119} and the Quadrupole Moment of the First Excited State, Proc. Phys. Soc. (London) 79, 416 (1962).

30. V. J. Ehlers and H. A. Shugart, Nuclear Spin of Rb^{88}, Bull. Am. Phys. Soc. II 5, 503 (1960), Abstract only.

31. P. Vanden Bout, unpublished memo listing current "best" alkali g_J, μ_I, g_I, $\Delta\nu$, and a values (Oct. 1965).

32. G. H. Fuller and V. W. Cohen, Nuclear Moments -- Appendix 1 to Nuclear Data Sheets (Nuclear Data Project, Oak Ridge National Laboratory, Oak Ridge, Tennessee, March 1965).

This report was prepared as an account of Government sponsored work. Neither the United States, nor the Commission, nor any person acting on behalf of the Commission:

A. Makes any warranty or representation, expressed or implied, with respect to the accuracy, completeness, or usefulness of the information contained in this report, or that the use of any information, apparatus, method, or process disclosed in this report may not infringe privately owned rights; or

B. Assumes any liabilities with respect to the use of, or for damages resulting from the use of any information, apparatus, method, or process disclosed in this report.

As used in the above, "person acting on behalf of the Commission" includes any employee or contractor of the Commission, or employee of such contractor, to the extent that such employee or contractor of the Commission, or employee of such contractor prepares, disseminates, or provides access to, any information pursuant to his employment or contract with the Commission, or his employment with such contractor.